HENRYK GEORGE PISARSKI (B. Sc.)

CORROSION FATIGUE OF AN ALUMINIUM ALLOY

Thesis submitted for the degree of

Doctor of Philosophy

October 1974

CORROSION FATIGUE OF AN ALUMINIUM ALLOY

Synopsis

The corrosion fatigue behaviour of a high strength weldable aluminium-zinc-magnesium alloy (Hiduminium 48) has been investigated under different loading conditions. Further studies were carried out in two regions of the weld heat affected zone.

The influences of cycling frequency and waveform shape on crack growth rate in salt water were related to a single parameter, the stress intensity rise time. Long stress intensity rise times enhanced environmental fatigue crack growth rate, while short rise times reduced environmental influence.

The relationship between crack growth rate and stress intensity amplitude (ΔK) was not linear but followed a two-stage process in which the transition from the first to the second stage was affected by environment and yield strength. Decreases in yield strength increased the ΔK factor at which the transition occurred while increase in environmental severity reduced the transition.

Crack growth rates in the heat affected zone were up to one order of magnitude slower than in the parent material. However by using the factor $\Delta K/Kc-Kmin$ (Q) the different crack growth rates resulting from material toughness and stress ratio effects were normalised to a single design curve. Use of the Q factor showed that in the heat affected zone the

influence of salt water on crack growth rate was independent of stress ratio.

The mechanism of fatigue crack growth was dependent on ΔK and environment. Under low stress intensity factors growth was associated with cleavage-like step wise growth, which was enhanced by the presence of salt water. At medium values of ΔK, in air, growth was controlled by a ductile striation mechanism. In both the parent material and heat affected zone at high ΔK crack growth was predominantly by microvoid coalescence. The occurrence of this mechanism was also independent of the environment used.

CONTENTS

LIST OF SYMBOLS USED

a	Crack length
B	Specimen thickness
da/dN	Crack growth rate
E	Young's modulus
G	Strain energy release rate
K, ΔK	Stress intensity factor, amplitude of K during fatigue
I, II and III	Subscripts to K or G – crack opening mode
K_{Ic}	Critical plane strain stress intensity factor
Kc	Plane strain/plane stress K
K_Q	K corresponding to 2% crack extension
K*	Equivalent energy K
Kmax	Maximum K during fatigue cycle
Kmin	Minimum K during fatigue cycle
L	Specimen span
m	Metre
mm	Millimetre, 10^{-3} metres
nm	Nanometre, 10^{-9} metres
N	Cycles or Newton
P	Load
P*	Pseudo elastic load
ΔP	Fatigue load amplitude
Q	ΔK/(Kmax – Kmin)

R	Stress ratio
Vg	Crack opening displacement at the mouth of a crack
W	Specimen width
Y	Compliance of K calibration function
γ	Surface energy
δ	Crack tip opening displacement
υ	Poisson's ratio
σ	Stress
σ_{ys}	Yield or proof stress
σ_{uts}	Tensile strength

Composition and strength of aluminium alloys referenced

2024-T3	3.8-4.9 Cu/ 0.3-0.9 Mn/ 1.2-1.8 Mg/ 0.25 Zn/ 290 MN/m^2[*] / 6.3 mm[**]
7075-T6	1.2-2.0 Cu/ 0.3 Mn/ 2.1-2.9 Mg/ 5.6-5.1 Zn/ 0.18-0.35 Cr/ 476 MN/m^2[*] / 3.2-6.3 mm[**]
T651	420 MN/m^2[*] / 6.3-12.6 mm[**]
7079-T6	0.4-0.8 Cu/ 0.1-0.3 Mn/ 2.9-3.7 Mg/3.4-4.8 Zn/ 0.1-0.25 Cr/ 448 MN/m^2[*] / 1.0-6.3 mm[**]
T651	448 MN/m^2[*] / 6.3-25.4 mm[**]
7178-T6	1.6-2.4 Cu/ 2.4-3.1 Mg/ 6.3-7.3 Zn/ 0.18-0.35 Cr/ 503 MN/m^2[*] / 1.1-6.3 mm[**]
DTD 5070A	~2.5 Cu/~1.5 Mg/ (~1.2 Ni)/~400 MN/m^2[*] /
DTD 683	~1.3 Cu/~0.4 Mn/~2.7 Mg/~5.8 Zn/~530 MN/m^2[*]

* = Yield stress (0.2% offset) MN/m^2

** = Maximum plate thickness, mm

1. INTRODUCTION

With the economic need to fabricate engineering structures quickly and efficiently the application of fusion welding processes have become indispensable. In many cases where high strength to weight ratio is required the use of aluminium alloys has fulfilled this need. However when the strength of these alloys is increased, by work hardening or use of precipitation hardening alloys, welding can become difficult and results in the degradation of the parent material properties. Aluminium-zinc-magnesium alloys have been developed to overcome these problems. The achievement of good welding and strength properties have thus increased the potential engineering use of this type of alloy. Typical applications have been girder bridges, light weight armour, cryogenic storage vessels, transport containers and electricity power line pylons. However, the full potential of this type of alloy has not been fully exploited so far, and among the reasons for this has been the lack of design data. Little published data on the fatigue characteristics has been available apart from some work on programme loading in which cumulative life was measured[106]. In view of this and also of the need to investigate some of the basic characteristics of the relationship between environment and fatigue loading a study was made of the corrosion fatigue behaviour of this alloy in terms of its crack propagation performance using a fracture mechanics approach.

In the thesis that follows a review is initially made of the mechanics of fracture using a linear elastic fracture mechanics approach. This approach is extended into the field of fatigue crack propagation in which various propagation theories together with the mechanisms of fatigue are discussed. The important influences of corrosion environments and the manner in which stress corrosion can be superimposed on fatigue are considered. However these factors cannot be considered in isolation from the stress environment, therefore the influences of frequency, waveform and stress ratio are discussed.

The experimental part of the work begins by considering the influence of loading conditions, in a relatively inert air environment, mainly to provide a basis for comparison with the corrosion fatigue tests. These tests are carried out in the parent material and also in two regions of a weld heat affected zone. The influence of stress environments involving stress ratio, frequency and waveform variations are studied together with the influence of corrosive environments, water and salt water, to determine their significance on fatigue crack propagation rate. In this way the major factors affecting the growth of defects in a welded structure can be quantitatively described so as to provide useful engineering design data. In parallel with this work experiments are also directed towards the understanding of some of the mechanisms involved in fatigue and corrosion fatigue crack extension.

2. THE MECHANICS OF FRACTURE

2.1 Introduction to Fracture Mechanics

Benefit of fracture mechanics

In recent times the use of fracture mechanics techniques
has assumed an important role in the design of structures
against failure by fast fracture. The fracture mechanics
philosophy is based on the assumption that all structures con-
tain defects and it aims to determine the size of defect likely
to cause failure. It is clear that if an allowable defect size
for a structure is determined, safety and economic benefits
result because realistic specifications can be drawn up so
that prior to the operation of a structure dangerous defects
can be identified and removed. Defects below a critical size
can then be tolerated in a structure without the danger of
failure. Another important benefit of fracture mechanics has
been the ability to use data produced in the laboratory directly
in design. Critical defect sizes determined from fracture tough-
ness tests in the laboratory on materials which behave linear
elastically up to fracture can be applied directly to the
real structure. Hence there is no need to go to the expense
of full scale testing of structure to produce design data. In
materials which show ductility before fracture the situation
at present is not so straightforward. In this case, general
yielding fracture mechanics has to be used. Suitable data for
defect size determination can only be obtained from empirical
relationships between small scale and large scale tests.

The situation described above applies to structures which are statically loaded; however, fracture mechanics can be extended to include fatigue loading. In these cases, sub-critical defects grow in length by fatigue until they reach a critical size for failure to occur. This means that if a fatigue law is known an assessment of the ~~time period~~ cycles required for the crack to grow from a detectible size, determined by non-destructive methods, to a critical size can be calculated. In this way, the safe life, or the interval between inspection periods, of a structure can be found [1]. Due to various factors which will be described later, linear elastic fracture mechanics analysis can be used to describe crack growth behaviour of most materials as long as high strain low cycle fatigue does not occur.

In structures subject to variable loading the wave forms imposed can be very complex. In the simulation of these load-ings for laboratory work, a rationalisation of their complex form has to be made so that the individual components can be studied. Basically they can be broken down into block loading programmes, where specific mean and alternating loads can be repeated in a known sequence, programmes of specific frequency and wave form shape. Even if the latter do not influence crack propagation very much in a relatively inert environment, such as dry air, wet environments can. Hence there can be a complicated relationship between environment on the one hand and mechanical loading variables such as frequency and waveform on the other.

Once these relationships are understood, a more accurate knowledge of the variables involved in growth of defects in fabricated structures can be gained.

Theory of fracture

The manner in which a crack behaves in a material has been considered by Griffith[2]. He proposed that when crack extension occurs, the decrease in strain energy stored in the material under tension is balanced by the increase in surface energy due to the creation of a new surface. The effect of a crack on the energy of an elastic body was based on Ingliss[3] solution for an elliptical crack. The expression derived for the critical gross section stress fracture (σ_{crit}) for an infinitely wide and thin plate containing an elliptical crack is:-

$$\sigma_{crit} = \left[\frac{2E\gamma}{\pi a}\right]^{\frac{1}{2}} \qquad\qquad _____ (1)$$

Where   E = Young's modulus

γ = surface energy

2a = length of the crack

This equation only applies to materials which obey Hooke's Law, therefore any plasticity effects at the crack tip are neglected.

However all materials exhibit some plastic deformation during fracture and the surface energy term in equation (1) cannot account for this. The work done by plastic deformation during crack extension is large compared with the surface energy. Because of these problems, Irwin[4,5] modified Griffith's equation to take into account the total work consumed per unit area of crack extension. He called this value the strain-energy release rate (G) which reaches a critical value Gc at the point of fracture. The modified Griffith equation then becomes:-

$$\sigma_{crit} = \left[\frac{EGc}{\pi a} \right]^{\frac{1}{2}} \underline{\hspace{2cm}} (2)$$

Now a critical stress intensity term, Kc, can be used to take into account the Young's modulus for the material. Depending on the stress condition the relationship between Gc and Kc is given by:-

$$Kc^2 = EGc \quad \text{for plane stress conditions}$$

$$\text{or} \quad Kc^2 = \frac{EGc}{(1 - \upsilon^2)} \quad \text{for plane strain conditions}$$

Therefore the Griffith-Irwin equation may be re-written as:-

$$\sigma_{crit} = \left(\frac{Kc^2}{\pi a} \right)^{\frac{1}{2}} \underline{\hspace{2cm}} (3)$$

- 6 -

Re-arranging equation (3) to obtain the critical stress intensity for fracture, then:-

$$Kc = \sigma_{crit}(\pi a)^{\frac{1}{2}} \qquad \underline{\qquad\qquad} (4)$$

The calculation of stress fields near cracks was made by Sneddon[6] who used the definition of an Airy stress function proposed by Westergard[7]. Irwin[5] and Williams[8] extended the applicability of the proposed field equations to the case of an isotropic elastic body.

Three crack opening modes have been recognised and these are illustrated in figure 1. The modes are as follows:-

Mode I   - Tensile opening

Mode II   - In-plane shearing

Mode III- Anti-plane shearing

Usually the modes of opening are given as subscripts to G or K. For the Griffith model, Mode I opening is assumed.

The elastic stress fields for mode I opening using the notation given in figure 2 as described by Paris and Sih[9] are given below:-

$$\begin{bmatrix} \sigma_x \\ \tau_{xy} \\ \sigma_y \end{bmatrix} = K_I (2\pi r)^{-\frac{1}{2}} \cos(\theta/2) \begin{bmatrix} 1-\sin(\theta/2)\sin(3\theta/2) \\ \sin(\theta/2)\cos(3\theta/2) \\ 1+\sin(\theta/2)\sin(3\theta/2) \end{bmatrix} \underline{\quad} (5)$$
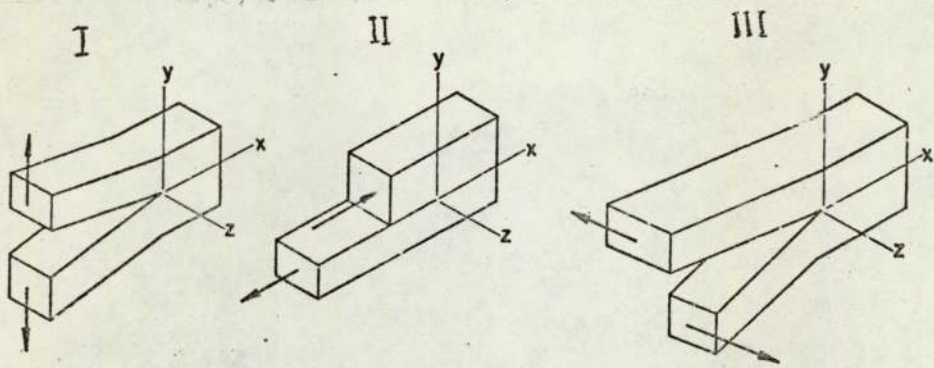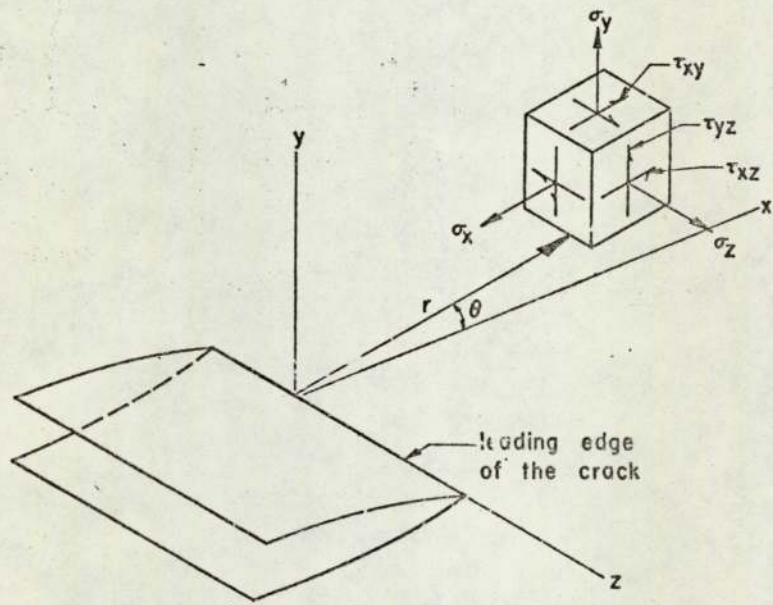
Fig 1   The Basic Modes of Crack Surface Displacements.

Coordinates Measured from the Leading Edge of a Crack and the Stress Components in the Crack Tip Stress Field.

Fig 2

(Figs. 1 and 2 after ref 9)

Plasticity effects

From the above equations it can be seen that for any value of θ the stress fields are a function of $(r)^{-\frac{1}{2}}$. As r tends to zero, the stresses rise to infinity, but this is physically impossible. The equations given in 5 only describe the elastic stress distribution and do not describe the boundary conditions very close to the crack tip. Considering the boundary conditions, the σ_y stress near to the crack tip only rises to a value where the material yields, the σ_x stress falls to zero at the crack tip surface while the development of the σ_z stress depends on whether there are plane strain or plane stress conditions. The value of the σ_y stress depends on the constraint around the volume of yielded material. In a plane stress situation $\sigma_z = 0$ and no constraint exists so the σ_y stress reaches the uniaxial yield stress of the material. The approximate extent of yielding is given by equation 5 where

$$\sigma_y = \sigma_{ys}$$

$$\theta = 0$$

$$r = r_p \quad , \text{ ie the plastic zone radius}$$

then

$$r_p = \frac{1}{2\pi} \left(\frac{KI}{\sigma_{ys}}\right)^2 \underline{\hspace{2cm}} (6)$$

For the plane strain situation there are no zero principal stresses therefore the plastic zone is constrained. For this material to yield the stress must rise to above that for

yield in the uniaxial tension case. This stress can be
determined by using either the Tresca or Von Mises yield
criteria. Using the Tresca criterion, yielding will be given
by the difference of the maximum and minimum principal stresses,
i.e.

$$\sigma_{ys} = \sigma_y - \sigma_z$$

Irwin estimates that in this situation yielding occurs when
σ_y reaches $\sqrt{3}\sigma_{ys}$, therefore the plastic zone radius is
approximately one third smaller than the plane stress situation,
i.e.

$$r_p = \frac{1}{6\pi} \left(\frac{KI}{\sigma_{ys}}\right)^2 \underline{\hspace{2cm}} \quad (7)$$

Because the load carried by the elastic stress distribution
at $r < r_p$ is borne by the plastic zone at σ_y the plastic zone
must extend over a distance w to carry this load. Rice [10]
estimates that w is equal to $2r_p$. As the elastic-plastic
boundary is now at a distance w from the crack tip the elastic
stress distribution is modified; this is illustrated in figure 3.

This model implies that the actual crack length (a) is increased
by an amount r_p to give a notional crack length of $a + r_p$. The
physical manifestation of the notional crack length is a blunting
of the real crack to give a crack tip opening displacement
almost parallel to its initial position. This means that the
actual value of K is raised, then equation 4 becomes

$$KI = \sigma (\pi(a + r_p))^{\frac{1}{2}} \underline{\hspace{2cm}} \quad (8)$$

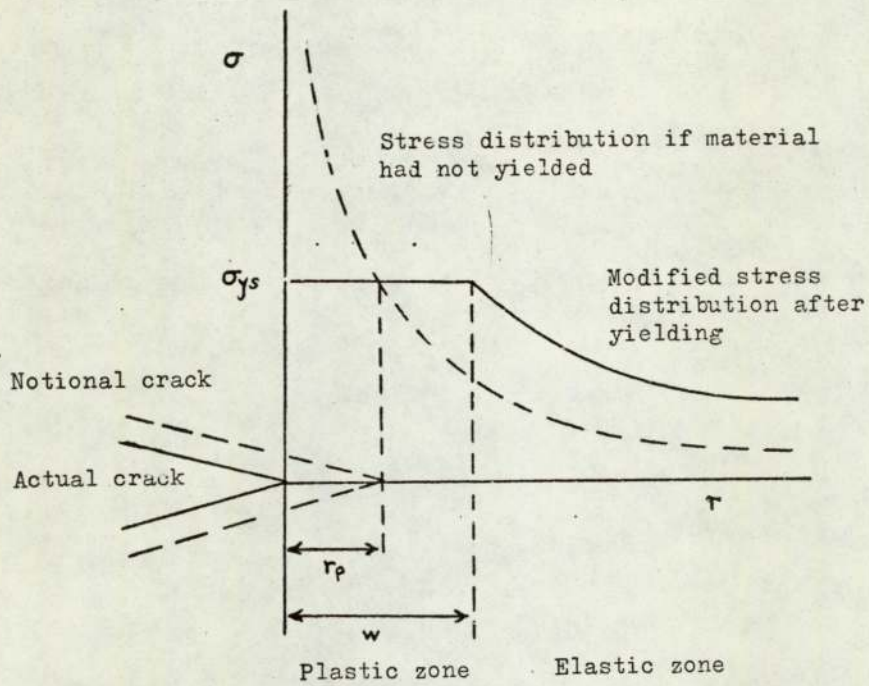From equations 6 and 7 it can be seen that for the case of

Fig 3   Stress distribution ahead of a crack under
         plane stress.

plane stress the increase in Kc is greater than that for plane stress due to the higher value of r_p. The presence of the plastic zone then effectively raises the value of K from that calculated on the basis of crack length only, i.e.

$$K = \sigma (\pi a)^{\frac{1}{2}} \left[1 + \frac{1}{6} \left(\frac{\sigma}{\sigma_{ys}} \right)^2 \right]^{\frac{1}{2}} \quad \text{Plane strain} \quad \text{--- (9)}$$

K calculated on   plastic zone
crack length   correction factor
only

If a working stress of 2/3 yield is substituted in the above equation then the increase in K, above that calculated when the plastic zone correction factor is not included, amounts to just over 3%.

Wells[11] has shown that there is a critical crack tip opening displacement (δ_c) for fracture to occur. δ_c was related to stress intensity by the following equations:

$$\delta_c = \frac{4 Gc}{\pi \sigma_{ys}} = \frac{4 K_c^2}{\pi E \sigma_{ys}} \quad \underline{\hspace{3cm}} \quad (10)$$

In a later paper[12], he modified the above expression for more general applications for conditions below general yielding.

$$Gc = n \sigma_{ys} \delta_c$$

$$Kc = (E \sigma_{ys} \delta_c n/\mu)^{\frac{1}{2}} \quad \underline{\hspace{3cm}} \quad (11)$$

Where $\mu = 1$ and $n = 1$ for plane stress

$\mu = (1 - \upsilon^2)$ and $n = 2$ for plane strain

n is an estimate of triaxial stress factor experienced by the material ahead of the crack tip.

The use of δ_c values above general yielding, although not equivalent to Kc values can be used to compare toughness of various materials. However equation 11 does hold approximately above general yield so long as a plane stress situation exists. Methods of measuring δ_c are given in ref. 105

2.2   Fracture Toughness

The definition of K given in equation 4 holds is only applicable to an infinite plate, that is where the size of the crack is very much smaller than the dimensions of the plate. To allow the applicability of equation 4 to other geometries, a correction factor Y is used. Y is called the compliance function, its value depending on a combination of the geometry and crack length in a structure. For example, in simple structure such as a single edge notch tension sample Y is a polynomial function depending on the crack length to specimen width ratio. A more general definition of K can be written as:

$$K = Y\sigma(a)^{\frac{1}{2}} \qquad\qquad\qquad (12)$$

where σ is the gross section stress

Because the compliance function is a characteristic of a particular structure geometry it is possible to relate a certain value of stress intensity to any other geometry. The Kc of a material is a specific property of that material. Therefore once a Kc determination has been made on a laboratory test specimen, the critical stress, for a specific defect size, for

fast fracture to occur can be found in any other structure, providing that the compliance function for that structure is known. This is why the fracture mechanics approach to design is so useful.

Two general methods are available for the determination of the compliance function, i.e. experimental and mathematical stress analysis techniques. The experimental method involves the measuring of specimen compliance at various crack length to specimen width ratios and has been performed by, among others, Sullivan[13] and more recently by Winters[14]. The mathematical treatment using boundary collocation techniques has been reported by Brown and Srawley[15].

Methods for the determination of the critical stress intensity for fracture or fracture toughness of a material have been described in the literature[9,15,104]. It should be noted that the methods described really only apply to materials which behave linear elastically and for valid toughness values conditions of plane strain must be observed. An equation[15] which gives guide to the thickness (B) of specimen required to maintain plane strain conditions for Mode I opening is given below.

$$B \geq 2.5 \left(\frac{K_{Ic}}{\sigma_{ys}}\right)^2 \qquad \rule{2cm}{0.4pt} \quad (13)$$

If the criterion described by the above equation is not satisfied the specimen will fail under a mixture of plane strain and plane stress conditions resulting in a mixed mode of fracture, i.e. showing shear and tensile fracture. In this case, the value of K_c is specific to that specimen thickness only.

There is some general relationship between yield strength and fracture toughness and the broad relationship between the two is given in figure 4[16]. This is called a Ratio Analysis Diagram and this type of diagram can be of use in the selection of materials for design purposes[16, 17].

2.3   Mechanics of Fatigue Crack Propagation

Under a fatigue loading situation the plastic zone sizes given by equations 6 and 7 do not hold as the zone is experiencing alternating plasticity. During initial loading on the first cycle, a plastic zone forms with its size governed by equations 6 and 7. At maximum load the material ahead of the crack tip has yielded; however, during unloading reversed yeilding occurs and a new plastic zone, characteristic of the load reduction, forms inside the old. The material experiences a total range of twice the yield stress for reversed plasticity to occur. Both Paris[18] and Rice[19] have shown that the size of the reversed plastic zone depends mainly on the load fluctuation and is independent of the maximum load, while mean load is a minor variable. The formation of the fatigue plastic zone using the principle of superposition described by Rice[19] is shown in figure 5. Therefore equations 6 and 7 may be rewritten as follows for the fatigue situation where ΔK is the stress intensity factor range.

$$r_p = \frac{1}{2\pi} \left(\frac{\Delta K}{2\sigma_{ys}}\right)^2 \qquad \text{Plane stress} \qquad (14)$$

$$r_p = \frac{1}{6\pi} \left(\frac{\Delta K}{2\sigma_{ys}}\right)^2 \qquad \text{Plane strain} \qquad (15)$$
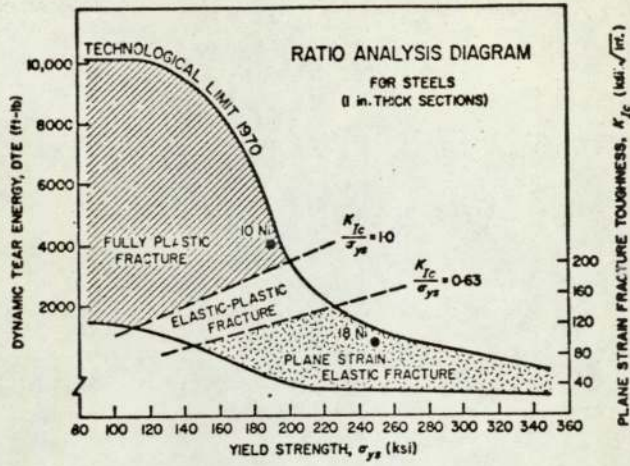
Ratio analysis diagram showing the upper and lower limits of fracture toughness for 1 in. thick steels over the yield strength range from 80 to 360 ksi   The diagram is divided into subregions of fracture behavior as defined by significant K_{Ic}/σ_{ys} ratio lines. Data points are shown for a 10Ni steel (σ_{ys} = 193 ksi) and an 18Ni steel (σ_{ys} = 248 ksi).
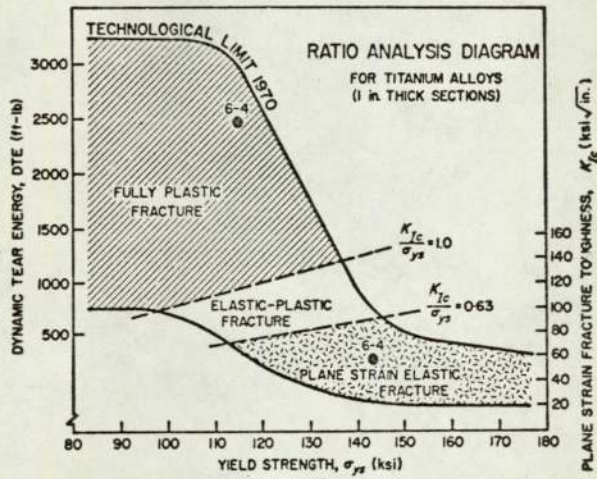
Ratio analysis diagram for 1 in. thick titanium alloys over the yield strength range from 80 to 180 ksi   showing data points for two samples of Ti–6Al–4V (σ_{ys} = 115 and 143 ksi, respectively).
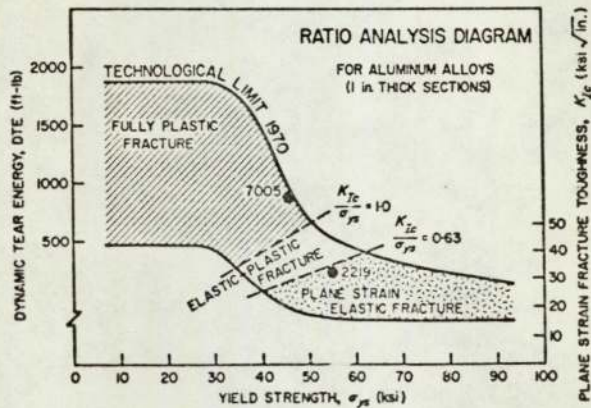
Ratio analysis diagram for 1 in. thick aluminum alloys over the yield strength range from 10 to 90 ksi   showing data points for 7005-T63 (σ_{ys} = 47 ksi) and 2219-T87 (σ_{ys} = 55 ksi).

Fig 4 (after ref 17)

Fig 5 *Plastic superposition for unloading. Adding (b) for load* $-\Delta L$ *with a doubled yield stress to (a) gives the solution (c) resulting after unloading from* L *to* L-ΔL. *Reloading,* L-ΔL *to* L, *restores (a).* (ref 10)
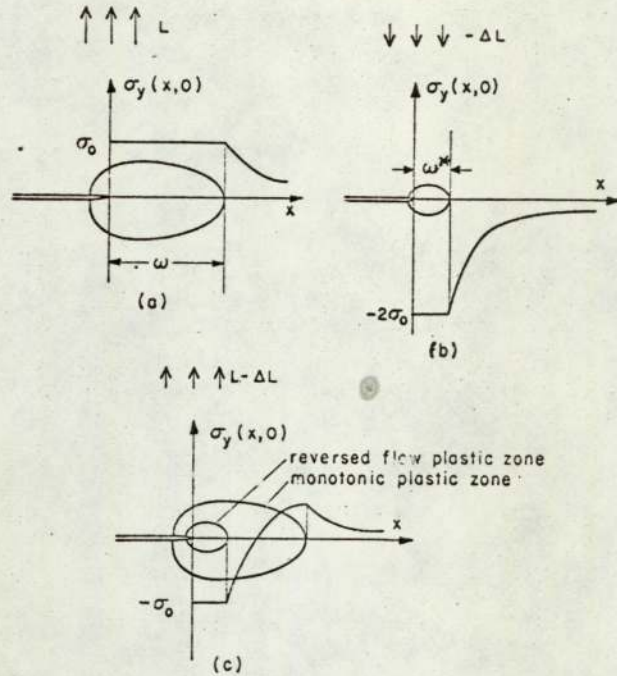
By comparing equations 14, 15 and 6, 7 for the case where the fatigue stress intensity varies from zero to some maximum value ($\Delta K = K$) the cyclic plastic zone size is about one quarter of monotonic plastic zone size.

In the analysis described above the initial crack before fatigue loading is applied is idealized to be a fine stress free saw cut in the material. This method assumes that crack closure does not occur at positive tensile stresses. With a real fatigue crack grown under constant load amplitude conditions the stress intensity factor range ΔK increases with increase in crack length. (This is assuming that the specimen geometry is not of the constant compliance type). This results in an increasing amount of residual tensile plastic deformation left on the fracture surfaces as the crack progresses. Elber[20] has shown that the crack opening displacement in this case is less than that for an idealized crack for the same ΔK. Therefore the real fatigue crack will close before the load reaches zero due to the clamping effect of the previously deformed material. Fatigue crack closure at positive tensile stresses has also been observed by Irving et al[21]. This means that an effective ΔK, less than that calculated using equation 12, operates and the fatigue plastic zone sizes given in equations 14 and 15 are therefore only approximate.

Fatigue crack propagation theories

Fatigue is usually divided into three main stages:

i) crack initiation ii) crack growth iii) failure

Grosskreutz[23] and Plumbridge and Ryder[24] have reviewed
the mechanisms involved in crack initiation. In smooth
specimens subject to tensile loading crack initiation occurs
at a face surface on favourably orientated slip planes in
which the shear stress is greatest. The growth of micro-
cracks along the slip plane is called stage 1 crack growth[25].

The actual process of crack initiation can occur very quickly
and it has been found that smooth specimens of ductile material
are cracked after <10% of their total life[24]. When the
reduction of the ratio of shear to normal stress at the crack
tip occurs the crack propagates normal to the tensile
direction, this is called stage II crack growth[25].

Factors such as corrosive environments, fabrication
defects in practical structures tend to limit the ~~effectiveness~~ extent
of stage I since the crack may already be present in the
structure[1]. Therefore Stage II crack growth stage is
important. Stage II is usually associated with the production
of striations, bursts of fast fracture, microvoid coalescence,
cleavage fracture of intergranular fracture depending on
material, composition and heat treatment.

Although some work has been reported characterizing fatigue
crack growth rate with stress amplitude, one of the first
applications of the elastic stress intensity factor to fatigue
was made by Donaldson and Anderson[1]. They showed that crack
growth rate was a function of ΔK, i.e.

$$da/dN = f \ (\ \Delta K)$$ _____ (16)

Paris and Erdogan[26] examining data from different sources proposed that the crack growth rate could be represented by a fourth power relationship of ΔK, i.e.

$$da/dN = \frac{1}{M} (\Delta K)^4 \qquad \qquad (17)$$

Paris[18] has shown that this equation holds for a variety of different metals. Potentially it is very useful as once the pre-exponent factor is known it is possible to integrate equation 17 to obtain the number of cycles for a crack to grow from say a minimum detectable value to the critical defect size for a structure for fast fracture to occur. Similarly it is possible to produce an inspection schedule for monitoring crack length so that appropriate remedial action can be taken. Paris[18] argued that the exponent in equation 17 is 4 because crack growth rate is primarily dependent on the volume of material plastically deformed ahead of the crack tip. By considering equations 14 and 15 it can be seen that

$$r_p = f (\Delta K)^2$$

but the volume of material V_p for unit crack width is given by

$$V_p = (r_p)^2$$

therefore $\qquad V_p = f(\Delta K)^4 \propto da/dN$

Hence an exponent of 4.

Liu[27] suggested that by considering the stress and strain histories ahead of the crack tip at low values of ΔK the exponent should be 2. Although much argument was produced to

support either Paris' or Liu's propositions further work has shown that the exponent is not a constant. Miller[28] has shown that the exponent for some high strength steels varies from 2.53 to 6.73. Feeney et al[29] showed that in various aluminium alloys the exponent depended on alloy, crack growth and environment. The ranges of exponent they obtain varied from 4 to 33. Subsequent work has shown that the relationship between ΔK and crack growth rate (da/dN) using log/log plots is a sigmoidal one: a schematic representation is shown in figure 6. In region 1, at low crack growth rates, a threshold stress intensity (ΔKth) is observed below which a crack will not propagate. Above ΔKth crack growth is strongly dependent on ΔK. As region II shows a linear relationship between ΔK and crack growth rate can be described by the general Paris equation:-

$$da/dN = C \ (\Delta K)^m \qquad \text{_____ (18)}$$

Region III is where the crack growth rate increases rapidly becoming unstable as fast fracture occurs. If the stress intensity range varies from zero to some maximum value, Kmax fast fracture occurs when Kmax = Kc. For values of Kmin $\neq$ 0 the curve shown in figure 6 is shifted upwards. The term stress ratio, R, is used to characterize the ratio of Kmin to Kmax and its effect on crack growth rate is shown in figure 7[29].

Forman et al [30] have proposed a modification to the Paris equation to take into account the effect of R value. They argue that when Kmax = Kc fast fracture occurs and the crack growth rate is effectively infinite, i.e.
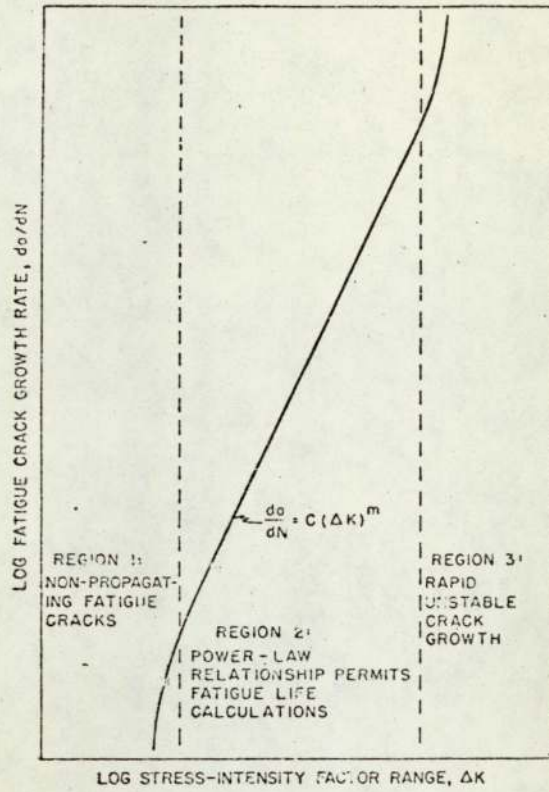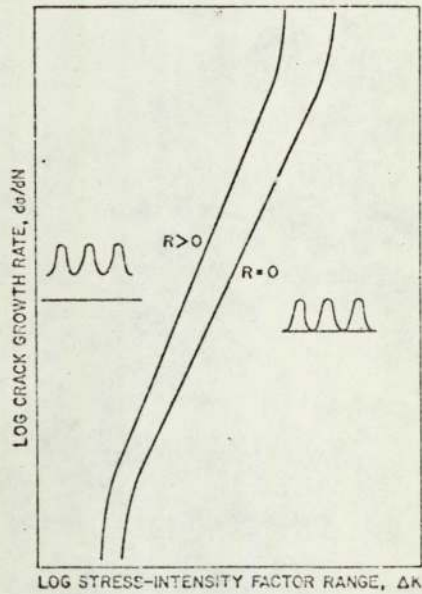
Fig 6 (after ref 29)

Fig 7

$$\lim_{Kmax \to Kc} da/dN = \infty \qquad \text{_____(19)}$$

Because $R = Kmin/Kmax$

and $\Delta K = Kmax - Kmin$

then $Kmax = \Delta K/(1-R)$

Therefore equation 19 for $R \neq 0$ becomes

$$\lim_{\Delta K \to (1-R)Kc} da/dN = \infty$$

Assuming that the correct crack growth equation is given by

Paris' equation but with the addition of a singularity at

$\left[(1-R)Kc - \Delta K\right]$ the new crack growth equation would be

$$da/dN = \frac{C(K)^m}{\left[(1-R)\,Kc - \Delta K\right]} \qquad \text{_____ (20)}$$

Where C and m are experimental constants, and Kc = fracture

toughness.

Forman et al then go on to show that crack growth rates

for different R values can be fairly well normalized to one

curve. Hudson and Scardina[31] and Hartman and Schijve[32]

have been able to verify Forman's equation (equation 20) using

stress ratios from 0 to about 0.8 in various high strength

aluminium alloys. Dubensky[33] was also able to use the

Forman equation satisfactorily except in 2024-T3 at crack growth

rates above 2500 nm/cycle. Although plastic zone size cor-

rections were made for high ΔK's scatter of the results still

remained.

Pearson[34] has argued that because Forman used centrally cracked sheet specimens in which Kc was very high, the maximum K during fatigue would be considerably less than $(1-R)$Kc. A further factor considered was the change in fracture mode from flat to shear fracture which is a characteristic of sheet specimens. The change in fracture mode has been described, by Wilham[35], Newman[36] and Swanson et al.[37]. Pearson testing thick aluminium specimens (12.7mm.) at different R values was unable to correlate his results using Forman's equation. However by replacing the value of Kc in Forman's equation with maximum K obtained during fatigue testing (lim Kmax) at the onset of fast fracture the following equation provided a better fit to the data:

$$ da/dN = \frac{C (\Delta K)^n}{\left[(1 - R) Kc' - \Delta K \right]^{\frac{1}{2}}} \qquad \text{(21)} $$

where $Kc' = \lim Kmax$.

Although Forman's and Pearson's equations do take into account, to some extent, material properties, a fuller attempt has been made by Heald et al[38]. They base their equation on one given by Weertman[39], i.e.

$$ da/dN = \pi/96 \left[(\Delta K)^4 / \sigma_1^2 (KIc^2 - K^2 max) \right] \qquad \text{(22)} $$

although in Weertman's paper the equation is not given in this form. Heald et al point out that the expression takes into account crack growth behaviour where Kmax approaches KIc but the

- 19 -

numerical coefficient $(\pi/96)$ and the exponent of ΔK are not substantiated by experiment. Also the parameter σ_1 is not properly defined by Weertman. Equation 22 is thus modified to the following

$$da/dN = A \left[\frac{(\Delta K)^4}{\sigma_1^2 (Kc^2 - K^2 max)} \right]^n \qquad \underline{\hspace{2cm}} \quad (23)$$

where σ_1 = ultimate tensile strength

Kc = plane stress fracture toughness for a specific

thickness

With this equation, Richards and Lindley[40] were able to show differences in crack growth rate, due to different micro-structures in a carbon steel and the effect of specimen thickness.

Cherepanov and Halmanov[41] using a dimensional analysis approach have been able to derive a fatigue crack growth equation in which only one fatigue variable needs to be determined. By assuming that crack growth occurs by loading during every cycle and that the specific dissipation energy in a material is constant, the following equation is derived:

$$da/dN = -\beta \left[\frac{Kmax^2 - K^2 min}{Kc^2} + \ln \left[\frac{Kc^2 - Kmax^2}{Kc^2 - Kmin^2} \right] \right] \qquad \underline{\hspace{2cm}} \quad (24)$$

Kc = fracture toughness

β = an experimental parameter having the dimensions

of length

This relationship was found to fit a wide variety of crack growth rates for different materials in the published literature. Cherepanov concluded that equation 24 meant that crack growth is governed by the same ~~mechanism~~ parametric relationship in all materials, the mechanism being independent of the micromechanisms of fracture at the crack.

A number of workers have observed that at very low values of ΔK fatigue cracks will not propagate [42,43,44 - Region 1 in figure 6]. This is a similar situation to that of non-propagating cracks observed by Frost[45] although a fracture mechanics approach was not used in this case. The value of ΔK or threshold ΔK below which fatigue cracks will not propagate is designated as ΔKth. Donahue et al[46], assuming the existence of ΔKth have analysed a number of published crack growth results to obtain ΔKth. In their analysis they use COD concept due to Wells[11] and combine it with the Laird plastic

blunting mode of crack extension. They propose that the amount of crack extension is proportional to COD; however, as the lower limiting value of K at ΔKth implies a lower limiting value of COD (δ_{th}) for crack growth, then

$$da/dN = A \ (\delta - \delta_{th}) \qquad \text{------------} \quad (25)$$

where A = a constant

δ = COD

δ_{th} = lower limit of COD $\equiv \Delta K_{th}$

The COD given by Wells is

$$\delta = \frac{4K^2}{\pi \sigma_{ys} E} \qquad \text{------------} \quad (26)$$

By combining equations 25 and 26, the following is obtained:

$$da/dN = \frac{4A}{\pi \sigma_{ys} E} (K^2 - Kth^2) \underline{\hspace{2cm}}(27)$$

In the cases considered by Donahue, $R \approx 0$, therefore
$K = Kmax = \Delta K$. Equation 27 was used to evaluate ΔKth from the
published data. It was found that this equation could predict
crack growth rates for various aluminium, titanium and steel
alloys up to about 2500 nm/cycle. In non-aggressive environments
the constant A was found to be directly proportional to the
ratio of twice the yield stress to Young's modulus and equation
27 becomes:

$$da/dN = 8/\pi \left[K^2/E^2 - Kth^2/E^2 \right] \underline{\hspace{2cm}} (28)$$

The values of ΔKth calculated with the use of equation 27
are rather high being about 10 $MN/m^{3/2}$ for steels and therefore
the accuracy of the equation may be questioned.

Klesnil and Lukáš have also reviewed evidence suggesting
threshold values of ΔK and modify the Paris equation to take
ΔKth into account, i.e.

$$da/dN = C (\Delta K^n - \Delta Kth^n) \underline{\hspace{2cm}} (29)$$

for constant R value, this equation being very similar to
Donahue's equation. However, they show that the value of ΔKth
can be raised above its true value (Katb) by the presence of
a compressive residual stress in the plastic zone resulting
from prior loading. The following expression was found to

describe the apparent threshold stress intensity:

$$\Delta Kth = Katb (Ka / Katb)^b \underline{\hspace{1cm}} (30)$$

where Ka = stress intensity factor preceding the

threshold value

$Katb$ = basic threshold stress intensity factor

independent of the strength of the material

b = material constant dependent on the strength

of the material

These findings may be an explanation for the high values of
ΔKth found by Donahue in which prior loading was not
taken into account.

Pearson[48] has questioned the validity of fatigue
threshold stress intensities as applied to real structures. He
suggests that as fatigue cracks initiate from almost zero
length and grow to failure they must be growing, when very
short, at values of ΔK less than ΔKth. Therefore the value
of Kth determined from through thickness fatigue crack

specimens should not be applied to short cracks in real struc-
tures. Pearson goes on to show that in smooth aluminium
specimens cracks initiated at the interface between surface
inclusions and the matrix or in the inclusions themselves. The
crack growth rates of these cracks in the early stages of growth
were very much faster that those predicted from analyses on
through section cracks. Again the results concerning thresh-
olds must be considered in the light of the work by Klesnil
and Lukáš[47] discussed earlier, concerning apparent and

basic threshold intensities. However, Pearson's results show
that care must be taken in applying values of ΔKth to the
design of structures, as ΔKth may only be a characteristic of
long through section fatigue cracks.

At high values of ΔK where Kmax approaches the limiting
value Kc, fast crack growth rates are observed, i.e. region 3
in figure 6. Clark[49] and later Barsom[50, 51] found that this
fast crack growth transition appeared to be caused by the
superposition of a ductile tear mechanism on the crack exten-
sion. Barsom has shown that the onset of this transition in
various metals occurs at an essentially constant value of crack
tip opening displacement, $\Delta\delta_t$, which is given by the following:

$$\Delta\delta_t = (1 - \nu^2) \frac{(\Delta Kt)^2}{E\sigma_{ys}} \quad\quad\quad (31)$$

where ΔKt is the value of stress intensity range at the
transition. This equation applies to conditions of plane strain
in the specimen. The constant value of $\Delta\delta_t$ was found to be
approximately to 4.06×10^{-2}mm. Apparently equation 31 does not
take into account reversed plasticity as σ_{ys} is not doubled.
Crooker[52] points out that equation 31 can also be given by
the following:

$$Kt = (0.0016E\sigma_{ys})^{\frac{1}{2}} \quad\quad\quad (32)$$

Because this equation does not contain any fracture toughness
parameter and the only real variable for a specific material
composition is σ_{ys}, values of fracture toughness cannot be given
as a design guide to the fast fatigue crack growth transition

- 24 -

in materials. This means that accelerated fatigue crack growth is not amenable to elimination through the selection of high strength/toughness combinations using diagrams such as those shown in figure 4.

Although in some of the work discussed above use was made of the crack tip opening displacement experimental values of $\Delta\delta$ were not measured physically. Therefore this work requires some experimental verification for the fatigue situations. Dover[53] has measured δ during high strain fatigue cycling of a mild steel. Slant mode of crack propagation was observed as the specimens were probably under plane stress conditions. Crack growth rate was found to be related to the amplitude of crack opening displacement, $\Delta\delta$, and for a constant $\Delta\delta$, a constant crack growth rate was obtained. Two values of $\Delta\delta$ were measured $\Delta\delta_{tr}$ the total COD range and δ_{tl} from the hysteresis loop width. For both cases the following type of expression was found to hold:

$$da/dN = A\,(\Delta\delta)^n \hspace{3cm} (33)$$

Where $A = 14.4 \times 10^3$, $n = 3.26$ for $\Delta\delta_{tr}$

and $A = 94$, $n = 1.72$ for δ_{tl} (Units of A in inches)

A comparison was made of the above constants with those obtained by using the constants from a previously determined Paris equation and the theoretical equation below for fatigue was used to calculate $\Delta\delta$:

- 25 -

$$\Delta\delta = \frac{K^2}{2E\sigma_1} \qquad\qquad\qquad\text{(34)}$$

where σ_1 = ultimate tensile strength to take into account

strain hardening behaviour.   Substituting this value of

$\Delta\delta$ in equation 33, the following constants were evaluated:

$$A = 12.1 \quad\text{and}\quad n = 1.65 \quad (\text{Units of A in inches})$$

This compares well with the constant derived in δtl equation.

Therefore in this case the theoretical derivation of δ com-

pares well with the experimentally determined value.

Pelloux[64] proposed a model of COD in which

$\delta = r_p \times e_{ys}$, where e_{ys} = yield strain for the

fatigue situation, reversed yielding occurs.   Therefore the

plastic zone size is given by

$$r_p = \frac{1}{2\pi} \left(\frac{\Delta K}{2\sigma_{ys}}\right)^2 \qquad\underline{\qquad}\qquad \text{plane stress}$$

therefore $\quad \Delta\delta = r_p \; 2\sigma_{ys}/E$

$$\Delta\delta = \frac{\Delta K^2}{2\pi(2\sigma_{ys})E}$$

Reanalysis of the da/dN versus ΔK results in terms of $\Delta\delta$

produced the following relationship in which crack growth rate

is given by

$$da/dN = A\,(\Delta\delta)^2$$

This is very similar to the relationship found by Dover where

the exponent of $\Delta\delta$ was 3.26.

In the literature discussed so far the main factor which has characterized the crack growth rate has been ΔK. So, for a constant value of ΔK one expects a constant crack growth rate,[37, 40]. However, recent work has cast some doubt on this fact. Von Euw et al[54] using single edge-notch tension specimens and a loading shedding programme to obtain a constant ΔK (using an R value of 0) found that crack growth rates for a/w = 0.25 were about 15% higher that those at a/w = 0.45. Even after considering errors in loading and errors in the compliance function no satisfactory explanation for the behaviour could be given. Independently Khairuzzaman and the author, again using

load shedding procedures, but this time using three point loaded specimens, have observed a retardation in crack growth rate after an initial constant crack growth period. Khairuzzaman[55] using a constant R value obtained at transition to retardation behaviour a value of a/w of about 0.3. By slightly modifying the Paris equation to take into account the ratio of gross stress to yield stress for each load block in the load shedding procedure Khairuzzaman could account for the retardation by using the following equation:

$$da/dN = A\ (\Delta K)^n\ R^1 \quad\quad\quad\text{———— (35)}$$

where $R^1 = \dfrac{\sigma_{max}}{\sigma_{ys}}$ which is an estimate of the increase in plastic zone size when the crack jumps forward, and A and n are experimental constants.

Dowse and Richards[56] also using loading shedding programmes to keep Kmax and ΔK constant found that when they grew a fatigue crack towards the heat affected zone, a decrease in

- 27 -

crack growth rate occurred before the zone was reached. This effect is explained, they say, by taking into account the plastic zone ahead of the crack tip. When the crack grows from the soft parent material towards the harder heat affected zone the point at which the plastic zone impinges on the latter

results in a reduction in crack growth rate. Analysis of the data given in the paper shows that slowing down occurred at about 5 mm from the heat affected zone/parent material interface. However, by calculating the maximum possible plastic zone size for the Kmax values given and assuming plane stress conditions, $2 r_p = 2.22$ mm. Therefore slowing down of the crack growth should have occurred at about 2.22mm from the parent metal/heat affected zone interface for Dowse and Richards' explanation for retardation to hold. This observed retardation in crack growth rate is, however, consistent with observations described previously and is further evidence confirming the effect.

2.4   Micro-mechanisms in Fatigue Crack Propagation

In the theories for crack growth discussed in the previous section crack growth was essentially regarded as growth through an isotropic material. On the macro-scale this is probably a close enough approximation to the real case. On the other hand a closer examination of the mechanisms involved in crack growth shows that micro structure can play an important role. The use of electron fractography techniques has allowed close examination of the fracture surface topography and has given an insight into the micro mechanisms involved in

fatigue crack propagation. In this section some of the main mechanisms involved will be discussed.

Richards and Lindley[40] have categorized fatigue crack propagation in terms of the following mechanisms for steels, generally these mechanisms also apply to other materials:

   i) striation growth

  ii) micro cleavage

 iii) void coalescence

  iv) intergranular fracture

These mechanisms will be considered in turn. Striation growth has been observed in a number of different materials and it has been found that each striation is produced by a single cycle of load[24, 25, 43]. Plumbridge and Ryder[24] point out that the converse of this, that every load cycle produces one striation, is not necessarily valid. This can be observed at very low crack growth rates where a certain number of cycles elapse before the crack front moves forward to produce a striation.
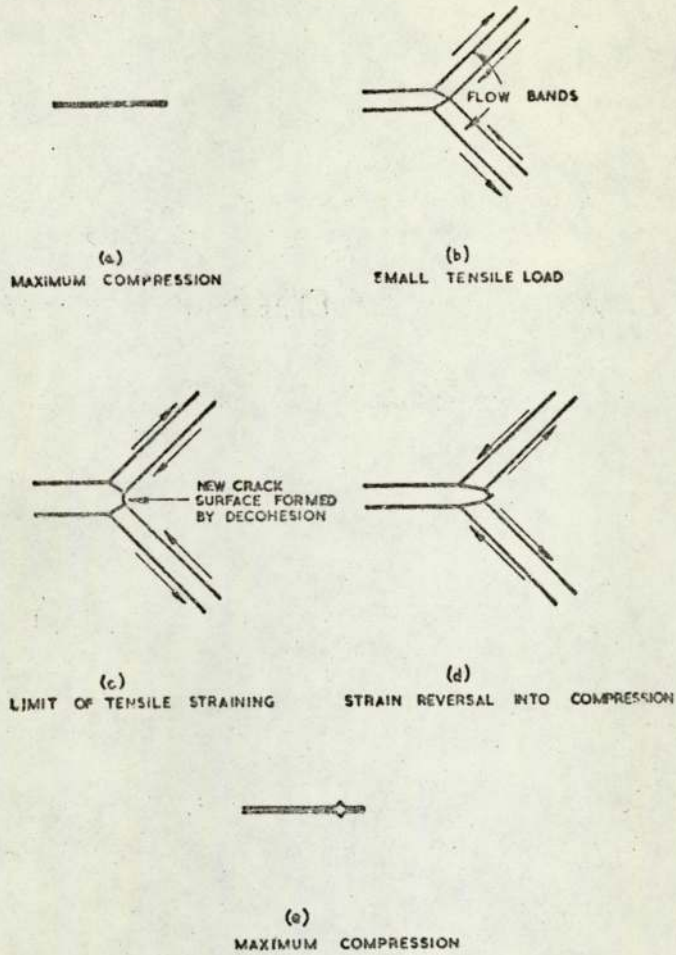
Forsyth et al[57] have distinguished two types of fatigue striation and have termed them type A and type B. Type A are described as ductile striations since they are of a non-crystallographic nature. They have the appearance of ripples and are characterized by a large height to width ratio. Type B are described as 'brittle' striations as these form on certain crystallographic planes. They are usually associated with 'river' markings running parallel to the direction of growth. Brittle striations are characterized by small height to width ratio.

Type A striations are usually found when materials are tested in dry air environments, but not in vacuum[58]. Type B striations occur in corrosive environments[59]. The morphology of fatigue striations differs widely in various materials and depends on the number of slip systems available[24]. The more uniform appearance of striations in f.c.c. metals compared with b.c.c. may be a reflection of this.

Correlations of striation spacing with macro fatigue growth rate have been made and these tend to confirm that each striation is formed by a load cycle for a certain range of ΔK[59,43,60]. Broek[60] has compared macro da/dN with da/dN determined from striation spacing and found that deviations occur at high and low values of ΔK. At high ΔK's void coalescence with ductile tearing and cleavage of inclusions can occur to accelerate crack growth, but striations would still form in the more ductile parts of the matrix. The spacing of these striations would give crack growth rate lower than the macro crack growth rate. Broek[60] and Bates and Clark[43] show that at low ΔK's striation spacings are more than the macro crack growth rate. This occurs because crack growth is not occuring over the whole crack front in every cycle, but discontinuously along it. However, Grosskreutz and Shaw[23] report that at low values of ΔK crack growth can be affected by second phase particles which can effectively hold up crack growth in their vicinity. One would expect that when ΔK is low and the plastic zone size ahead of the crack tip would be small, crack growth would largely be affected by changes in the
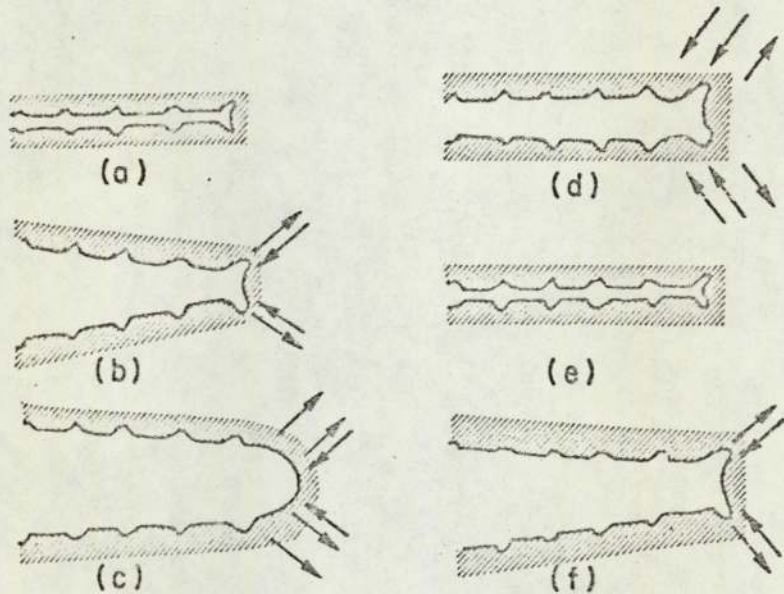
matrix properties. Therefore a statistical distribution of striation spacings would be produced, each contributing to the observed macro crack growth rate.

No precise mechanism of striation formation has yet been established but it is generally accepted that it involves alternate blunting and re-sharpening of the crack tip (see figures 8, 9 and 10). In the mechanism proposed by Tomkins[61] crack growth occurs by a decohesion process (figure 8). During the tensile portion of the load cycle intense plastic flow occurs in two narrow shear bands radiating at $\sim 45^o$ from the crack tip (figure 8b). At maximum load shear decohesion occurs where the strain gradient is a maximum (figure 8c). When the load falls shear flow is reversed and no significant re-cohesion occurs (figure 8d) when the crack closes. The result of the process is an extension of the crack and the production of a striation (figure 8e). A similar process but involving plastic blunting during loading and the formation of 'ears' during unloading is proposed by Laird (see figure 9 a - f). Laird[62] has observed interstriation markings which have the appearance of fine fatigue striations. He suggests that the origin of these markings are slip lines caused by plastic flow during the blunting of the crack tip. McMillan and Pelloux[63] after analysing a large number of electron fractographs of striation replicas propose a simple crack sharpening and blunting mechanism, (figure 10). Pelloux[64] argues that as striations are not observed in vacuum they must be formed as a result of some environmental factor. Therefore the plastic blunting mechanism

(a)
MAXIMUM COMPRESSION

(b)
SMALL TENSILE LOAD

FLOW BANDS

NEW CRACK SURFACE FORMED BY DECOHESION

(c)
LIMIT OF TENSILE STRAINING

(d)
STRAIN REVERSAL INTO COMPRESSION

(e)
MAXIMUM COMPRESSION

The stage II fatigue crack propagation process in a metal.

Fig 8 (after ref 61)

(a)

(d)

(b)

(e)

(c)

(f)

The plastic blunting process of fatigue crack propagation in the stage II mode: (a) zero load, (b) small tensile load, (c) maximum tensile load, (d) small compressive load, (e) maximum compressive load, and (f) small tensile load. The double arrowheads in (c) and (d) signify the greater width of slip bands at the crack in these stages of the process. The stress axis is vertical.

Fig 9 (after ref 62)

suggested by Laird is inoperative in vacuum. Instead a mechanism of crack extension by alternating shear is proposed in which shear is reversible unless an oxide film is formed to prevent slip from occurring. Figure 10 shows this model with no reversed slip due to oxidation of the crack tip. According to Stubbington[65], both ductile (type A) and brittle (type B) exhibit components containing regions of ductile (shear) and quasi-brittle (tensile) fracture. Ductile striations, however, contain equal amounts of shear and tensile components (figure 11, type A), while brittle striations contain a large tensile component, promoted by environmental factors, giving rise to cleavage fracture on the {100} plane (figure 11, type B). This model also explains the differences in height to width ratios between ductile and brittle striations described earlier. The smaller component of shear fracture in type B striation compared with type A results in smaller height to width ratio in the former.

Although cleavage fracture during normal tensile tests in aluminium/ alloys is unknown at room temperature, Stubbington[65] suggests that an ion adsorption mechanism involving dislocation pinning or reduction of energy necessary for crack formation on the cube face was responsible for the formation of brittle striations.

Returning to the case of ductile striation formation, Richards and Lindley[40] found that for a large range of steels striation growth occurred when K_{max} was less than 0.7 - 0.8 of
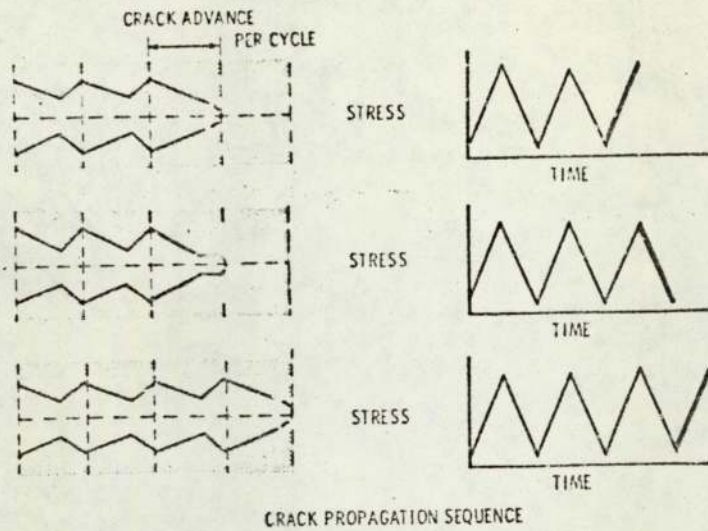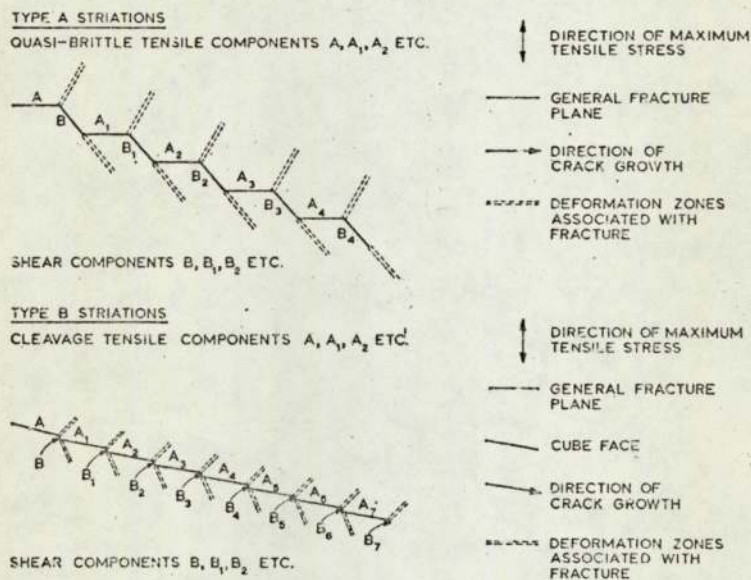
Fig 10 (after ref 63)

Fig 11 (after ref 65)

Kc, higher Kmax and specimen thickness had little effect on
crack growth. This means that within a certain range of
ΔK striation formation is relatively independent of other
loading parameters but mainly dependent on the material. Bates
and Clark[43] analysing crack growth results from titanium,
aluminium and steel tests, where a striation mode of growth
operated, found that the results fell into three bands, figure 12.
However, if a material parameter was taken into account the
results could be unified in terms of striation spacing against
ΔK/E, (where E = Young's modulus) they fall into a single
scatter band - figure 13. The general equation derived from
these results is very similar to one proposed by Donahue et al[46],
discussed in a previous section (equation 28) which was based
on COD and the Laird plastic mode of crack extension. This
is assuming that striation spacing measurements are equivalent
to macro crack growth rate. This assumption seems to be correct
in the case of Bates' and Clark's results for most values of ΔK
although discrepancies occur at high values of ΔK, the reason
for this has been discussed previously. The general agreement
between these two approaches means that probably the mechanisms
involved in the formation of striations and the development of
a crack tip opening displacement must be similar.

The equation given by Bates and Clark (figure 13) is
similar in form to the Paris equation, - if similar metals are
compared Young's modulus can be neglected. If striation
formation is the primary crack growth mechanism, then values
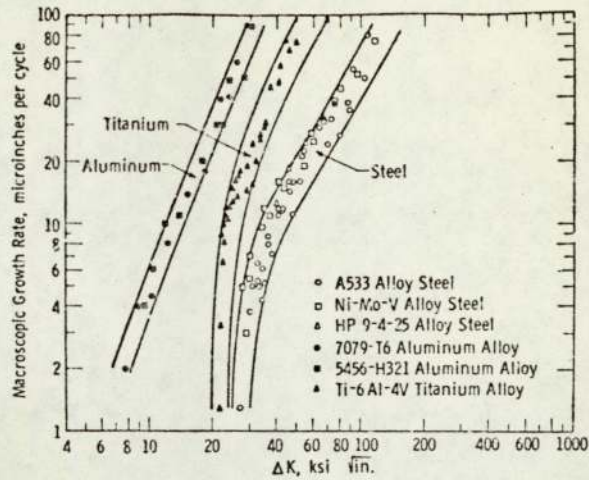
Relationships of macroscopic growth rate to ΔK for three alloy steels, one titanium alloy, and two aluminum alloys tested at 75 F.

Fig 12 (after ref 43)
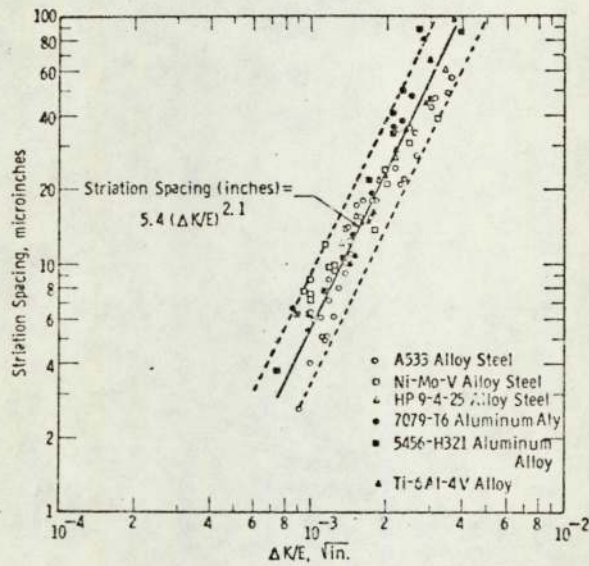
Relationship of striation spacing to $(\Delta K/E)$ for three alloy steels, one titanium alloy and two aluminum alloys tested at 75 F.

Fig 13 (after ref 43)

of pre-exponent (A) and exponent (n) in Paris' equation will
be similar. Richards and Lindley[40] suggest that the reason
for wide variations in A and n are the result of deviation
in the growth mechanism from striation formation. Three other
mechanisms will now be discussed.

Although cleavage fracture does not normally occur in f.c.c.
materials at room temperature a number of workers have observed
fatigue fracture surfaces which can only be described as
'cleavage like' in aluminium alloys[66,25]. This type of
fracture was observed to occur in laboratory air or in corrosive
media. In steels Richards and Lindley[40] have observed micro-
cleavage on the $\{100\}$ of favourably orientated grains of 3%
silicon iron. In other steels the amount of micro-cleavage
depended on microstructure[38]; in a spherodized structure no
microcleavage was observed while in pearlitic steels the amount
of microcleavage increased with lamellar spacing. Increasing
amounts of microcleavage were found to accelerate crack growth
rate compared with the striation mode of crack growth observed
in spherodized steels of similar composition. Another factor
apart from structure which affected the susceptibility of
microcleavage was the influence of K_{max}. For constant values
of ΔK but with K_{max} increasing, microcleavage and hence growth
rate increased. Cleavage of brittle inclusion particles in
other materials has been observed and this also causes acceler-
ation of crack growth [60, 66, 43, 67]. Pelloux[67] proposed
that the influence of second phase particles on crack growth

- 34 -

rate depends on the ratio of the fatigue plastic zone size,

r_p, to the interparticle spacing, s. He suggested that when

i) $r_p < 10s$, crack growth rate depends on the matrix properties;

ii) $r_p \approx s$, crack growth is a result of propagation through

the matrix and second phase particles;

iii) $10r_p \geq s$, crack growth is mainly a result of crack

extension through and around second phase particles. Broek[60]

also shows that at low ΔK fracture occurs around second phase

particles, but at high ΔK voids form due to loss of coherency

of the second phase particles with the matrix. However,

Grosskrentz and Shaw[23] show that at low values of ΔK

second phase particles effectively hold up propagation and act

as crack arresters, which is the opposite of the relationship

proposed by Pelloux.

Recently El Soudani and Pelloux[70] have observed that

voids form around inclusions particles at high ΔK's in a

high strength aluminium alloy. This occurred when the cyclic

plastic zone size was equal to the void spacing which resulted

in a fracture mode transition leading to increased crack

growth rates. Therefore in Pelloux's propositions above the

differences between ii) and iii) become marginal.

As discussed above second phase particles can cause void

formation and mechanism of void coalescence has been proposed

by Forsyth and Ryder[68]. In this mechanism the high hydrostatic

stresses ahead of the crack tip cause voids to form probably at

some discontinuity in the matrix, eg a brittle particle. These

voids eventually link up by thinning of unfractured bridges under biaxial stresses and extend the crack. It would therefore be expected that plane stress situations would

be more favourable to void coalescence than plane strain, although void coalescence has been observed to occur under plane strain conditions, [69, 70]. Griffith et al[69] have shown that in a ferritic weld metal crack growth rate was independent of Kmax at low ΔK values. At higher values of ΔK, Kmax increases crack growth rate by promoting void coalescence. This mechanism was itself a result of a change over from plane strain to plane stress conditions. Crooker et al[71] observed that in a nickel-cobalt steel the amount of void coalescence occurred gradually as ΔK increased, even though the specimens were always under plane strain conditions. El Soudani and Pelloux[70] found that

in a high strength aluminium alloy the fracture mode transition (plane strain to plane stress) was associated with a sharp increase in the amount of void fracture occurring at inclusion sites within the fatigue cyclic plastic zone. They also noted that the extent of void coalescence could be reduced by decreasing the volume fraction of inclusions in the matrix, i.e. a cleaner alloy. This also resulted in a somewhat lower crack growth but only at high ΔK values. Clark[72] attributed the transition in the change in slope of the da/dN ΔK curve

(region III, figure 6) to 'static subcritical growth' super-imposed on the fatigue behaviour which was manifest by dimpling on the fracture surface.

Intergranular fracture has been observed to occur in quenched and tempered high strength steels where the fatigue paths follow the prior austeniste grain boundaries[73]. These grain boundaries are weakened by certain impurity elements, such as bismuth. Corrosive environments also tend to encourage intergranular fracture, but this will be considered in a later section.

The influence of grain size on fatigue crack growth rate would be expected to be some function of the ratio of the grain size to the cyclic plastic zone size. When the plastic zone size was the same order or less than the grain size, grain orientation or grain properties would affect crack growth rate. At cyclic plastic zone sizes greater than the grain size crack growth rate would be controlled by the macro matrix properties. However, Hoeppner[74] found that crack growth was not appreciably affected by grain sizes ranging from 0.06 to 7 mm. in copper. More recently Robinson and Beevers[75] found that at low ΔK in a α-titanium alloy the grain structure was evident on the fracture surface, the fracture path being influenced by the grain orientation. This they termed 'grain orientation control' and it occurs when the reversed plastic zone size is less than the grain size. A small grain size lead to a reduction in crack growth as compared with large grain size material.

2.5.1 The Effect of Corrosion Environment on Fatigue

In the previous sections fatigue has been considered in inert or relatively inert environments, however corrosive environments can greatly affect the fatigue characteristics of a material. For example it has been known for a long while that the endurance limit shown by steels in air environments can be lost completely when a salt water environment is used. In the real design situation, structures come into contact with various corrosive environments, however mild, which will in some way modify the fatigue characteristics of the structure. These factors are very important and should at least be recognised so that their effects can be taken into account during design.

Laboratory air environments ~~have previously been regarded as inert but~~ studied by Bradshaw and Wheeler [58] have shown that various components in air, especially the humidity level, can affect fatigue crack growth. They examined the influence of the partial pressure of water vapour and oxygen on the fatigue crack growth rate of DTD 5070 A and DTD 683 aluminium alloys. Below a certain critical partial pressure crack growth rates were similar or less than the vacuum reference environment, but above this pressure, crack growth rates were accelerated. The effect of gases with the water vapour was to modify the critical pressure, for example nitrogen increased the critical pressure. The effect of frequency of cycling was found to be an important parameter, when fatiguing was reduced by two orders of magnitude (100 to 1 Hz) the critical water vapour pressure increased by one hundred. This behaviour indicated that a contamination mechanism was occurring at the crack tip. A model proposed by

Achter[76] was used to explain the observed behaviour. This model proposes that crack growth rate is altered if the surface up to a distance of one lattice spacing behind the crack tip is covered with an adsorbed oxide or hydroxide monolayer. Since critical pressures of oxygen and of water vapour increased with crack growth rate, Bradshaw and Wheeler concluded that Achter's model was valid. The following relationship was found to give the critical pressure:

critical pressure $(Nm^{-2}) = 4 \times 10^4$ (Hz x da/dN (mm/cycle)).

Hartman[77] performed similar experiments on an aluminium alloy, (2024 – T3) and found that humid argon gave similar crack growth rates as humid oxygen. At high ΔK crack growth rates in dry argon were similar to humid argon, showing a reduction in environmental effect. Wei[78] also points out that the reduced environmental sensitivity observed by Hartman at high ΔK was likely to be the result of a change in fracture mode, i.e. from plane strain to plane stress. This mode of fracture occurs in sheet materials when the plastic zone size becomes large enough, with respect to the sheet thickness, for the crack to rotate from a 90° to a 45° fracture surface. This leads to a reduction in crack growth rate. The reduction of environmental sensitivity due to fracture has also been observed by Walker et al[80] in titanium alloys, Feeney et al[66] and Bradshaw and Wheeler[58] in aluminium alloys. Wei and Landes[81] confirm Wei's[79] contention above by showing no reduced environmental sensitivity at high ΔK when crack growth rates in dry argon and distilled

water were compared for thick sheets of 7075-T651 aluminium.

Liquid Environments.

Generally simple environments such as water and aqueous halide solutions have been used to investigate corrosion fatigue. Wei[78] examined the influence of distilled water on the fatigue crack growth rate in 7075-T651 aluminium and found a nearly ten times increase in growth compared with dry argon. By examining growth rates over a temperature range from 25° to $90^{\circ}C$ he found that crack growth rate was a thermally activated process which depended on ΔK. The apparent activation energies in distilled water ranged from about 0.9 Kcal/mole at $\Delta K = 9$ Ksi $\sqrt{in}$ to 3.6 Kcal/mole at $\Delta K = 6$Ksi $\sqrt{in}$. Wei concluded that the rate controlling process for crack growth was the mechanical process of new crack surface creation. Environmental transport to the crack tip was not considered important as the effect of water accelerating crack growth was nearly the same over a wide range of crack growth rates. Wei suggests that the acceleration of crack growth due to the distilled water results from "pressure mechanism for hydrogen embrittlement", a theory originally put forward by Broom and Nicholson[81]. In this mechanism, hydrogen is produced by water reacting on the clean metal surface at the crack tip and this increases the crack tip stress intensity by diffusing to internal voids ahead of the tip. In a later paper, McEvily and Wei[83] describe this mechanism slightly differently, accelerated crack growth being due to a pressure mechanism of hydrogen embrittlement requiring the synergistic action of fatigue and water-metal surface reaction.

Exactly how the hydrogen pressure mechanism works is not described.

Gerberich et al[84] using a similar approach to Wei[78] measured corrosion fatigue activation energies in a metastable austenitic steel. The values obtained compared with the activation energy for the diffusion of hydrogen through steel. Similar values were also obtained by Van der Sluys[85] in a different steel but in this case crack extension was produced under stress corrosion conditions. These results suggest, because of the activation energies involved, that some hydrogen embrittlement process is occurring to accelerate crack growth.

Hartman[77] has suggested that the fatigue corrosion mechanism is due to changes in the elastic properties of oxide at the crack tip due to water adsorption. This results in an increased back stress on the dislocations near the crack tip compared with a dry oxide layer. Wei[79] points out that this is improbable as the oxide layer would not be thick enough to affect appreciably the back stress on the dislocations to account for a ten times increase in crack growth rate observed in distilled water. Also frequency effects could not be accounted for by this mechanism. Further reference to this type of mechanism will be made at a later stage in the discussion when more complex aqueous environments will be considered.

Feeney et al[66], examining the influence of different environments in various aluminium alloys found that a transition occurred in the da/dN - ΔK curve which was not associated with the transition from 90° to 45° fracture. Although the transition appeared to show a reduction with more aggressive environments

(i.e. $3\frac{1}{2}$% NaCl solution compared with wet air), it was in fact related to the ability of the matrix to accommodate plastic strains. The transition was prominent with the softer alloy, i.e. 2024-T3, becoming less prominent with the harder 7075-T6 and 7178-T6 alloys. Because of the observed transition a single value of n in the Paris equation could not be used. Below the transition very high values of n were observed. Marked susceptibility to environmentally enhanced fatigue crack growth in $3\frac{1}{2}$% NaCl solution was observed in 2024-T3 and 7075-T6 while in 7178-T6 faster growth occurred in distilled water. The latter observation was probably due to the fact that $3\frac{1}{2}$% NaCl in 7170-T6 caused intergranular fracture resulting in crack blunting and hence a decrease in crack growth rate compared with the transgranular mode observed in distilled water.

Fatigue influenced environmental crack growth

Fatigue pre-cracked specimens, similar to those used for fracture toughness testing have been used to assess stress corrosion variables. Brown[86] has noted that under static loading conditions there exists a critical stress intensity factor below which further crack growth does not occur for a specific material/environment combination. This stress intensity in mode I opening is termed K_{1scc}[87]. Times required to determine K_{1scc} depend on the material and environment used; for titanium alloys in salt water typical exposure times are of the order of 10 hours, while in aluminium alloys typical times are more than 500 hours. This is not necessarily so for stress corrosion tests in the short transverse direction. Stress

corrosion cracks *in aluminium alloys* almost always follow intergranular paths,
while corrosion fatigue cracks can propagate in either a trans-
granular or intergranular fashion. The type of fracture occurring
is controlled to some extent by the direction in which the
crack grows; in wrought materials, especially aluminium alloys,
the short transverse direction is most susceptible to inter-
granular cracking. In other directions stress corrosion crack
growth rates tend to be reduced.

Johnson and Paris[88] point out that if environmental
fatigue crack growth occurs above K_{Iscc} failure will occur in
relatively short times as stress corrosion cracking can outpace
fatigue crack growth. They describe this method of crack growth
as 'fatigue-influenced environmental crack growth'. Below
K_{Iscc} the situation is described as 'environment-accelerated
fatigue crack growth'.

Wei and Landes[89] have proposed a superposition model for
fatigue-influenced environmental crack growth in which the
corrosion fatigue crack growth rate can be predicted from the
fatigue crack growth in an inert environment and the contribution
from stress corrosion cracking. This model is given by the
following equation:

$$\left[da/dN \right] c = \left[da/dN \right] R + \int r \, da/dt \times \left[K(t) \right] dt$$

where $\left[da/dN \right] c$ = fatigue crack growth rate in a corrosive
environment

$\left[da/dN \right] R$ = fatigue crack growth in an inert reference
environment

$\int r \, da/dt \times \left[K(t) \right] dt$ = integrated crack growth rate from
stress corrosion tests

$$K(t) = K_{min} + \Delta K/2 \, (1 - \cos\omega t)$$

$$\omega t = 2\pi f t$$

$$f = \text{frequency}$$

$$t = \text{time}$$

The graphical computational procedure is illustrated in figure 14. Using the above procedure Wei and Landes were able to predict corrosion fatigue crack growth rates in a number of different materials. Gallagher[90] was able to substantiate the Wei-Landes hypothesis on 4340 steel in $3\frac{1}{2}\%$ NaCl where ΔK was above K_{Iscc}.

Gerberich et al[84] have proposed a similar model to the above but have refined it so that the integrated stress corrosion crack growth rate is found by utilising the mean value theorem to assess the average stress intensity in the fatigue cycle. This method overcomes the graphical methods used by Wei and Landes. Paris et al[91] using a model similar to the Wei-Landes hypothesis found that they could not account for corrosion fatigue at low frequencies (0.1 Hz). For D6a steel the model tended to overestimate the crack growth rates. They suggested that this was because at low frequencies the specimen does not encounter an environmental component for the total duration of time at elevated K levels above some environmental threshold. Instead it approaches a condition more closely allied to that of sustained load behaviour where a propagation-arrest type behaviour can occur. This would result in a decrease in growth rate and hence the overestimation of crack growth rate produced by the model.
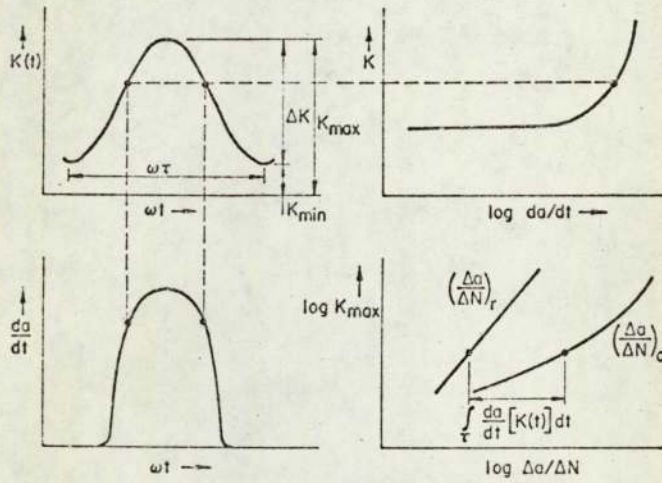
Schematic diagram illustrating the suggested method of analysis. (a) stress intensity spectrum in fatigue (top left); (b) rate of crack growth under sustained load in an aggressive environment (top right); (c) environmental contribution to crack growth in fatigue (bottom left); and (d) integrated effects on environment and K_{max} on fatigue crack growth rate (bottom right).

Fig. 14 (after ref 89)

Crooker and Lange[92] were unable to relate corrosion fatigue crack growth behaviour to stress corrosion crack growth in a number of steels when ΔK was above K_{Iscc}. They attributed this lack of correspondence to the fact that very long times are required under stress corrosion conditions for cracks to propagate. Low frequencies of cycling used (approx. 0.1 Hz) did not provide sufficient time for stress corrosion cracking to exert a strong influence. These results show that the Wei-Landes hypothesis can only be applied where stress corrosion crack growth rates are of a similar order of magnitude as fatigue crack growth rates. Corrosion fatigue above K_{Iscc} does not necessarily mean that stress corrosion cracking will exert an influence to accelerate crack growth rates. These factors are illustrated again by considering Barsom's work.

Barsom[93] performed corrosion fatigue crack propagation tests in 3% sodium chloride solution on a 12 Ni - 5Cr - 3Mo steel at different cycling frequencies. A frequency dependancy on crack growth was found; the lower the frequency the faster the crack growth rate. At high frequencies (10 Hz) environmental effects were low and the crack growth rate approached that obtained in air. Although these tests were nominally carried out below K_{Iscc}, reanalysis of Barson's data show that his tests probably covered a range of stress intensities above and below K_{Iscc}. The K_{Iscc} obtained for the steel was 66 MNm$^{-3/2}$ and the fatigue tests were performed over a range of ΔK from 17.6 to 60.5 MNm$^{-3/2}$ with an R value of 0.4. Although ΔK was below

K_{Iscc}, K max was not. When Kmax = K_{Iscc}, $\Delta K = 39.5$ MNm$^{-3/2}$, therefore any part of the waveform above this ΔK will experience stress corrosion (c.f. Wei–Landes hypothesis[89]). Barsom's data, even at 0.1 does not show any crack growth acceleration above $\Delta K = 39.5$MNm$^{-3/2}$, therefore the influence from stress corrosion must be very small.

Environment accelerated fatigue crack growth

The above analysis of Barsom's work shows that in some cases fatigue above K_{Iscc} can be treated as environment accelerated fatigue crack growth. Speidel et al[97] have tried to rationalise the effects observed during corrosion fatigue and have defined three regions in the crack growth rate – ΔK curve, figure 15. In region 1, crack growth rate is highly dependent on ΔK, but there exists a corrosion fatigue limit ΔK_{lcf}, analagous to ΔK_{th}, below which crack growth does not occur. For a number of aluminium, magnesium, titanium and steel alloys this threshold value is given by the following equation and is independent of various aqueous halide environments:

$$\Delta K_{Icf} = (2.7 \pm 0.3)10^{-5}E \quad \text{(units MNm}^{-3/2}\text{)}$$

This shows that the primary variable on the corrosion fatigue limit is Young's Modulus (E). It should be noted that in figure 15 Spiedel et al show that corrosive and inert environments approach the same threshold values of low ΔK's, but no evidence for this is given. It would be interesting to see how the values of ΔK_{lcf} compare with ΔK_{th}. McEvily and Wei[83]

show that there is in fact a reduction in apparent threshold ΔK in corrosive media compared with inert environments.

Region II (see figure 15) was defined as the region of true corrosion fatigue which is independent of stress corrosion, i.e. environment accelerated fatigue crack growth. This region can be described by Paris's equation. Specific additions of ionic species in aqueous environments caused acceleration of corrosion fatigue. A similarity between fatigue corrosion and stress corrosion was shown in that ionic additions which caused stress corrosion also caused acceleration of crack growth under corrosion fatigue conditions; ionic additions which do not cause acceleration of stress corrosion also do not show acceleration of corrosion fatigue. These ionic species are shown in Table I. As would be expected, the Wei-Landes summation hypothesis cannot be used in region II.

Region II (figure 15) is defined as "stress corrosion under cyclic loading", i.e. fatigue influenced environmental crack growth. Material-environment combinations conducive to stress corrosion and where Kmax is above K_{Iscc} show behaviour described by region IIIa. In this case crack growth is the summation of components of fatigue and stress corrosion, therefore the Wei-Landes hypothesis can be used. Region IIIb is shown by material-environment combinations where stress corrosion cracking rates are very much slower than fatigue crack growth rates.

Garrett[98] reporting unpublished work by Ford showed that in an aluminium 7% magnesium alloy that the environmentally controlled fatigue crack propagation rate was governed by the stress intensity controlled oxide rupture rate, the dissolution

- 47 -
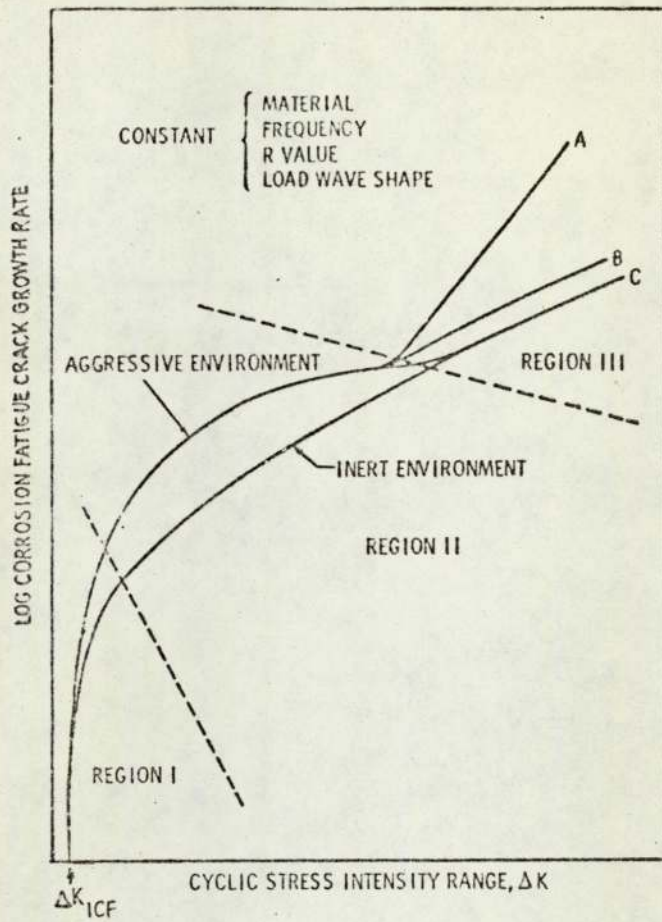
Schematic representation of the influence of stress intensity on the growth rate of corrosion fatigue cracks.

Fig 15 (after ref 97)

TABLE 1 — Effect of Various Additions to Aqueous Environments
on Acceleration of Subcritical Crack Growth in High Strength Light Metals

Alloys	Stress Corrosion		"True" Corrosion Fatigue (Region II)	
	Additions Which *Can* Accelerate Crack Growth	Additions Which *Do Not* Accelerate Crack Growth	Additions Which *Can* Accelerate Crack Growth	Additions Which *Do Not* Accelerate Crack Growth
Aluminum base (7079-T651)	Cl^-, Br^-, I^-	$SO_4^=$	Cl^-, Br^-, I^-	$SO_4^=$
Titanium base (Ti-6Al-4V)	Cl^-, Br^-, I^-	$SO_4^=$	Cl^-, Br^-, I^-	$SO_4^=$
Magnesium base (ZK60A-T5)	Cl^-, Br^-, I^- $SO_4^=$		Cl^-, Br^-, I^- $SO_4^=$	

(after ref 97)

rate of the metal or partially passivated surface and the passivation rate. Here we have a mechanism in which the environment directly affects the crack tip surface by film formation but the amount of crack acceleration that occurs depends on the fatigue crack growth rate. At low ΔK the rate of passivation is greater than the oxide rupture rate so that environmental crack growth is governed by the metal dissolution of the partially passivated surface. Oxide rupture rates increase with increases in ΔK but the rate of passivation cannot keep up with oxide rupture rate, so crack growth rates increase. An upper limit to which the environmental effects can occur is set by the limiting value of solution renewal rate to the crack tip. At this stage the mechanical component of fatigue is predominant. The mechanism is illustrated in figure 16. The shape of the curve is very similar to the one given by Spiedel in the previous figure.

Barsom[93] proposed that two opposing mechanisms occur during environmental fatigue crack growth: the driving force being provided by fatigue, hydrogen embrittlement and stress corrosion cracking and the resisting force being oxide film formation and crack blunting. By performing tests once more in 3% sodium chloride solution, but this time adjusting the pH of the solution (by addition of sodium hydroxide) to 13.5, crack growth rates obtained were frequency independent and similar to growth rate in air. This showed that sufficient hydroxyl ions were present to passivate the metal surface to provide the resisting mechanism to accelerated crack growth.
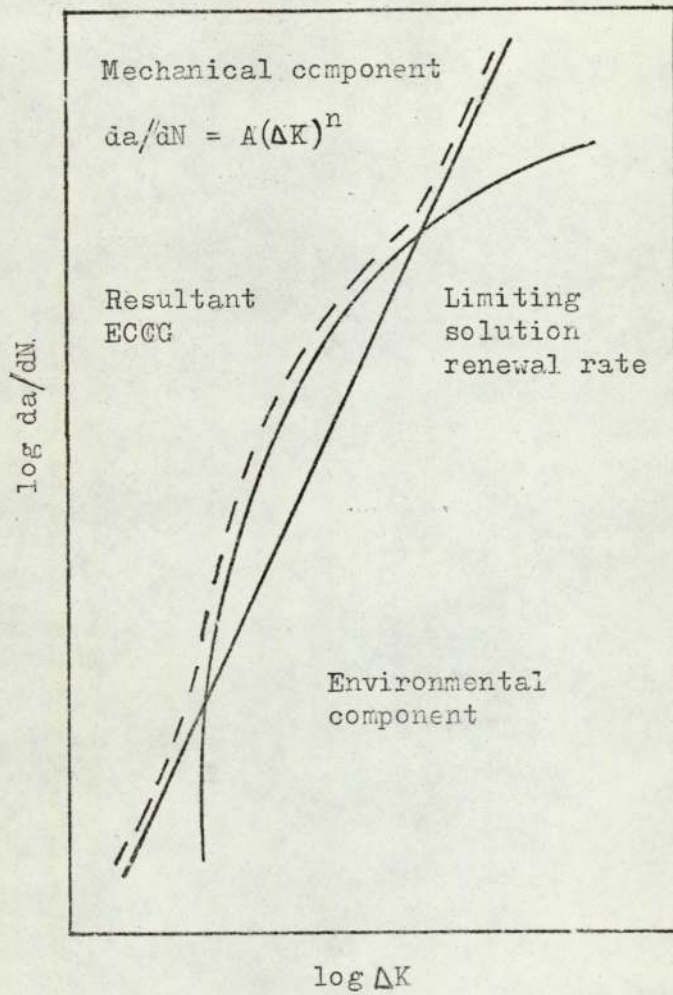
Fig 16

Graph illustrating Ford's model of
environmental corrosion crack growth
(ECCG) – (From ref 98)

The use of corrosion inhibitors has been made by Stoltz and Pelloux[96] who were able to reduce corrosion fatigue crack growth rates in a 7075-T6 aluminium alloy by a factor of 10, resulting in the same crack growth rate as obtained in air. A 1.7 molar concentration of sodium nitrate was added to the 0.2 molar concentration of the sodium chloride solution environment to achieve this. It was proposed that the passivation mechanism occurring was the preferential displacement of Cl^- ions at the crack tip by NO_3^- ions.

Effect of polarization on corrosion fatigue

Barsom[94] has measured the pH of the corrosive solution at the crack tip using a freezing technique. While the pH of the bulk solution remained at pH7, the pH at the crack tip was 3, even when anodic or cathodic polarization was applied to the specimen. Both anodic and cathodic polarization, however, increased crack growth rate. Cathodic protection did have a beneficial influence but only at short crack lengths. At longer crack lengths fracture resulted from a hydrogen embrittlement mechanism which accelerated crack growth. Cathodic protection can therefore be used to advantage when smooth specimens are used or where specimens have very short cracks. This has been shown to be the case by Petit et al[95] who used cathodic protection satisfactorily to increase fatigue lives of type 135 pipe steel in sea water.

Stoltz and Pelloux[96] examined the influence of various applied potentials on the corrosion fatigue crack growth of 7075-T6 in $3\frac{1}{2}$% NaCl. Although there was some scatter in the

results, cathodic protection was beneficial only at low ΔK, this effect being more pronounced in overaged material compared with the peak aged condition. Barsom's[94] results in steels under cathodic polarization showed that hydrogen embrittlement had occurred, while Stoltz and Pelloux's material was not sensitive to this form of environmental attack. The results of both workers showed that anodic polarization caused dissolution at the crack tip and accelerated crack growth. Stoltz and Pelloux observed that at small cathodic potential (just less than open circuit potentials) some reduction in crack growth rate was observed - this was attributed to crack branching. Speidel et al[97] performed similar tests to the above but in different aqueous halide solutions. By using cathodic polarization they were able to slow crack growth rates down to those observed in distilled water. Once more anodic polarization resulted in an increase in crack growth rates and caused pitting of the fracture surfaces.

Brittle cleavage-type striations, with cleavage facets close to $\{100\}$ planes have been observed in corrosion fatigue of aluminium alloys[63]. Stoltz and Pelloux[96], using a polarity reversal technique have shown that in 7075-T6 aluminium in salt water, anodic potentials enhanced the crystallographic dependancy of striation formation by cleavage (i.e. brittle striations) while cathodic polarization, above a certain threshold potential, caused a change in fracture plane orientation resulting in ductile striation formation.

2.6   The Effect of Stress Environment on Fatigue

Generally the effect of frequency on fatigue crack growth
rate, of tests performed in air, tends to be small. Where
frequency does show an effect, it is due to one of two
factors:

   i)   environmental corrosion fatigue due to humidity in the
        air

           rheological effects at the crack tip and the   the latter
  ii) { intrinsic frequency effect of the material; ~~this~~ would

   be shown by materials which are strain rate sensitive.
Which of these two factors are operating on a material can be
determined by performing the tests in vacuum or an inert
environment and comparing the results with those obtained in air.

When an environment accelerates fatigue crack growth it
does so, because the high stress region of the crack tip
provides a highly active site for chemical processes to occur.
The amount of damage produced in this region is dependent both
on time available for attack and the stress conditions at the
crack tip. This means that frequency of cycling and waveform
shape will affect the amount of acceleration of crack growth
rate produced by a specific corrosive environment. A limiting
factor on the corrosive effect would be the solution renewal
rate to the crack tip; again this would be affected by frequency
and wave shape.

Bradshaw and Wheeler[58] have shown that DTD 683 alloy
(which has a similar composition and strength to 7075-T6)
exhibits an intrinsic frequency effect, crack growth rates being
faster at low frequencies. They attributed this effect to over-

ageing of the material ahead of the crack leading to faster
crack growth rates. Hartman, reported by Wei[79] showed that
2024-T3 alloy also exhibited an intrinsic frequency effect,
although Feeney et al[66] testing a similar alloy did not find
it. This result is probably attributed to the fact that
Hartman's 'dry' environment contained 10-20 ppm of water vapour
while Feeney et al contained less than 2 ppm, therefore corrosion
fatigue could be occurring in the former.

As has been described elsewhere, Bradshaw and Wheeler
showed that the critical pressure of water vapour for accelerated
crack growth increased as frequency of cycling increased. However
at high water vapour pressures (approximately 15 torr) crack
growth rates were relatively independent of frequency. It should
be noted that in laboratory air frequency effects were apparent.

Krupp et al[99] show results contrary to these observations
when 7075-T6 aluminium was tested in a moist environment in
which the relative humidity was 10%. It was found that low
cycling frequencies resulted in faster crack growth rates than
high frequencies. Wei and Landes[81] show a similar effect in
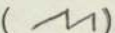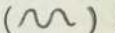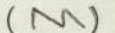the same alloy when a distilled water environment was used.
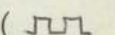
Barsom[93] has investigated the influence of frequency on
corrosion fatigue behaviour of a ⊠12 Ni-5Cr-3Mo steel tested
in 3% sodium chloride, with the tests being conducted essentially
below K_{Iscc}. He produced the following relationship to account
for frequency:

$$da/dN = D_o (t) (\Delta K)^2$$

Where $D_o(t)$ is constant for any given frequency and t is a
function of time. Because $K^2 = EG$ the above equation becomes

$$da/dN = D(t) \Delta G$$

By plotting the time dependent function, $D(t)$, against frequency
a curve is obtained which shows that at high frequencies $D(t)$

tends to the $D(t)$ value obtained for tests performed in air.
So there is a limiting frequency above which environment ceases
to influence fatigue behaviour. One can speculate that this
limiting frequency is related to the inability of the environ-
ment to renew itself at the crack tip.

Barsom[100] has also investigated the influence of waveform ᴀₙ steel.
He found that corrosion fatigue crack growth occurred only
during periods of slowly increasing tensile stress. Thus
corrosion fatigue crack growth rates under positive sawtooth,
(⋀⋀), triangular (⋀⋀) and sine waves (⋀⋀) at the same
frequency (0.1 Hz) were equal. Whereas corrosion fatigue crack
growth rates under negative sawtooth (⋀⋀) and square waves

(⊓⊔) at 0.1 H_z are approximately equal to crack growth rates
at 10 Hz under sinusoidal loading. The negative sawtooth,
square (at 0.1 H_z) and sine waves (at 10 H_z) gave similar crack
growth rates to those obtained in air which were independent
of frequency and waveform. Therefore only slowly increasing
tensile loading produces a corrosive effect while very fast
increases in loading do not provide sufficient time for corrosive
attack to occur.

Hudak and Wei[101] performed tests similar to those done
by Barsom but on 7075-T651 alloy using distilled water environ-
ments. However they were not able to find any difference in

crack growth between the positive and negative sawtooth wave-
forms. Bradshaw et al[102] were also unable to find any
significant difference in crack growth rates in DTD 5070 tested
in air and using rectangular, pulsed and sine waves at 1 Hz,
even though this alloy shows a frequency effect in air.

Selines and Pelloux[103] however were able to confirm
Barson's general conclusions using 7075-T6 alloy in $3\frac{1}{2}\%$
sodium chloride solution. By using positive and negative
sawtooth, square and sine waves at 0.1 Hz and 10 Hz they were
able to show that the corrosion fatigue effect was primarily
due to the load rise time i.e. the opening time of the crack
at specific values of ΔK, the time spent at peak load having

a negligible effect on crack growth.

The following functional relationship was found to describe
the observed behaviour:

$$(da/dN)\ corrosion = A\ (\Delta K)^{2.2}\ (\Delta t)^{0.1}$$

where Δt is the rise time in seconds, and A a constant.
Selines and Pelloux suggest that this time dependancy function
may be a result of oxide film formation which will hinder crack
tip blunting. The oxide limits the uniform escape of dislocations
around the crack tip, thus fracture will occur by cleavage rather
than by shear. This results in higher crack growth rates.
Cleavage-like features were observed in the fracture surfaces
of specimens tested in salt water. Some of the observations
therefore tend to support Selines and Pelloux's hypothesis,
however a more convincing support for the hypothesis would be
obtained if it could be shown that there is a greater amount of
cleavage-type fracture produced by positive sawtooth waves; these
factors are not discussed in their paper.

The above mechanism, which is similar to one proposed by

Stubbington[65] to explain the formation of brittle striation

described previously, is at variance with observations made by

Wei[79]. He argued that the image force on the dislocations

resulting from the oxide film was not great enough to account

for the large changes in crack growth rate observed. These

arguments were specifically aimed at explaining the effect of

water only; therefore, it is probable that they may not be

applicable to more complex environments such as salt solutions.

3. OBJECTIVES OF EXPERIMENTAL WORK

The aims of the experimental work presented are to establish the relationships between fatigue crack growth rate and a design parameter, which will normally be the stress intensity range obtained in simple environments for a weldable aluminium alloy. In order to determine the major environmental parameters (mechanical and chemical) which influence crack propagation rate, the effect of mechanical loading variables such as frequency, waveform shape and stress ratio in a number of corrosive environments are investigated. It is expected that the study of these variables will cover some of the important loading characteristics encountered during the service life of a structure. A further aim is to rationalize the behaviour of the mechanical and environmental variables so that some understanding of the underlying mechanisms controlling fatigue crack growth rate can be gained.

A number of investigators[58,77, 78, 79] have found that water vapour in the atmosphere can cause acceleration of fatigue crack propagation over that obtained in a dry environment. The size of this acceleration is dependent on the frequency of fatigue cycling. However evidence of intrinsic material sensitivity to cycling frequency in inert environments, has been reported to occur in some precipitation hardening aluminium alloys[58]. The phenomenon was attributed to changes in the mechanical properties, affecting fatigue crack growth rate, ahead of the crack tip caused by overageing or resolution of hardening precipitates. Therefore to investigate the influence of frequency and waveform on the fatigue behaviour of Hiduminium 48

and also to produce a base line for comparison with the corrosion fatigue results at different frequencies, this parameter was studied. Both the longitudinal and transverse plate directions were tested to investigate whether frequency effects were influenced by variations in material morphology, since mechanical properties are to some extent influenced by direction.

For the study of more aggressive environments simple liquids were used, which were de-ionized water and $3\frac{1}{2}\%$ sodium chloride solution. These environments represent two media likely to be encountered by structures during service. For instance the salt water would be representative of marine environments and the de-ionized water of rain conditions on land. Whilst these environments might not normally be regarded as particularly aggressive for aluminium structures, in the presence of a sharp defect the combination of high localized stresses and even mildly corrosive liquids can make the situation critical as regards crack extension. Defects in structures can arise from manufacturing faults or bad design in which high localized stresses can cause premature crack initiation. Fatigue cracks can also initiate from areas of high stress concentration such as the toes of welds. The initiation of such cracks may not be detrimental to the life or safety of the structures in themselves, but the growth of these defects or, more precisely, their rate of growth, is an important factor to be considered. The importance of the influence of 'mild' environmental conditions has been shown by Feeney et al.[66] who found that in some high strength aluminium

alloys using distilled water could result in faster crack growth rates than using sodium chloride solutions.

Since the influence of corrosion on crack extension may be regarded as a time dependent phenomenon, variation in the fatigue loading process such as frequency of cycling and waveform shape would be expected to be important. Wei and Landes[81] have shown that if part of the fatigue cycle is above K_{1scc} then the corrosion fatigue crack growth rate is the summation of the dry environment fatigue component and the stress corrosion crack growth rate. Therefore the summation hypothesis may be used to determine the influence of frequency and waveform or even the effect of stress ratio. However the Wei-Landes hypothesis can only be applied to situations where the stress corrosion crack growth rate and the fatigue crack growth rate (dry) are of similar magnitude. In cases where the hypothesis is invalid or when Kmax is below K_{Iscc} Barsom[100] has shown that for some steels the effects of corrosion are dependent on some function of the rate of rise of load in the fatigue cycle. Bearing in mind these findings stress corrosion tests were carried out to determine the mode of corrosion fatigue crack propagation, i.e. whether it was predominantly influenced by stress corrosion crack extension or not. Once the corrosion fatigue mode was known the most suitable mechanical parameters describing the mechanism of crack growth could be determined.

Since the material investigated was a high strength weldable aluminium alloy it was considered important that the effect of welding on the parent material properties should be studied. The important region for study would then be the heat

- 58 -

affected zone (HAZ), which arises from the heat treatment received by the parent material during welding causing a change in mechanical properties.

The design of a welded structure is controlled by the weakest link in that structure. Generally three areas of possible material weakness can be identified, and these are:

   i) the parent material

  ii) the HAZ

 iii) the weld metal

In terms of fatigue either of the above areas can be influenced by the presence of stress concentrations which will modify the crack initiation and initial growth characteristics of the material. Therefore to critically evaluate a welded structure subject to fatigue loading, the crack growth characteristics of defects located in each of these regions needs to be known. However in the present work attention will be restricted to the parent and HAZ material.

More specifically, the aims of investigating the HAZ were to:

   i) determine the relationship between da/dN and ΔK at different stress ratios and compare these results with the parent material.

  ii) determine the response to corrosion fatigue with respect to frequency.

Once these relationships are known it would be possible to determine the fatigue sensitive region in a welded fabrication. A designer can therefore identify the critical area of the

- 59 -

structure and calculate either a safe life or an inspection

schedule so that the particular component can be replaced

or repaired before cracks reach a critical size for fracture.

4. EXPERIMENTAL METHODS AND MATERIALS

4.1 Material

The aluminium-zinc-magnesium alloy used was HIDUMINIUM 48 which is an alloy developed by High Duty Alloys. This was supplied by Star-Wrought Products, Briton Ferry, Glams., in the form of 15mm. thick rolled plate in the fully age

hardened condition. The plate had undergone solution treatment at $480^{\circ}C$ which was followed by a controlled quench. The plate was then cold stretched to remove any distrotion and residual quenching stresses. Finally an ageing treatment at $120^{\circ}C$ for 24 hours was given to obtain full strength. The composition of the as received plate was then checked spect-roscopically and this is compared with the manufacturer's specification in Table 4.1.

To check the mechanical properties of the material Hounsfield No. 12 tensile test pieces were cut from the plate in two directions, these were parallel and at right angles to the rolling direction. These specimens are designated following code numbers 31 and 21 respectively (Table 4.2). Hardness surveys were made to check for possible variations of prop-erties in the three primary directions in the plate (Table 4.3). To assess the toughness of the plate fracture toughness tests were made. Further, the toughness of the material in two directions, as in the tensile tests, was measured. The frac-ture toughness tests were carried out on 12.5mm. thick 3-point load specimens according to recommended methods[104]. A fatigue crack was first initiated from the machined notch and

Table 4.1

Chemical Analysis - Hiduminium 48

Composition - wt. %

	Zn	Mg	Cu	Ni	Mn	Fe	Si	Ti	Cr	Zr	Al
Manufacturer	4.59	2.45	0.17	0.02	0.24	0.24	0.18	0.03	0.15	0.12	bal
Analysis	4.85	2.50	0.13	0.02	0.23	0.25	0.16	0.02	0.17	0.13	bal

Table 4.2

Mechanical Properties - Hounsfield No 12 specimens

Room temperature tests

Orientation	0.2% proof stress σ_{ys} MN/m^2	Ultimate tensile stress MN/m^2	Elongation %	Reduction of area %
21000XX type 1	499	536	12	25
2	498	537	14	28
3	499	536	11	20
4	499	536	11	20
31000XX type 1	480	506	14	28
2	483	506	13	26
3	480	506	13	29
4	480	506	13	26

then grown at a low stress intensity range, $\simeq 10 \text{MN}/\text{m}^{3/2}$ until until a/w was equal to 0.5. Fracture testing was carried out at room temperature at a slow loading rate, $\simeq 0.2$mm./minute crosshead deflection, in an Instron tensile test machine. The position of the specimen with respect to the plate and their dimensions are given in Figure 4.1, while the results obtained are given in Table 4.4. The Kc values determined are valid K_{1c} results, i.e. they are predominantly the plane strain values, as the specimen thickness is greater than that given by the inequality:

$$B \geq 2.5 \left[\frac{K_{1c}}{\sigma_{ys}} \right]^2$$

where 'B' $\simeq$ 9mm. and the actual specimen thickness is 12.5 mm.

Welded material

In order to study the HAZ properties of 15mm. thick Hiduminium 48 plate, the plate was welded using a mechanized MIG process. A double V edge preparation was machined onto the plate transverse to the primary plate rolling direction. The fatigue crack propagation direction was the same as that used previously in the 21 orientation tests on the parent material, i.e. crack growth at right angles to the rolling direction. The consumable used was NG61 (Al-6Mg) wire. Parent material filler wire would have been preferable becuase it would give a higher strength weld metal, but unfortunately this was not available. However, NG61 filler is used industrially to weld Hiduminium 48 and the HAZ produced would essentially be independent of the composition of the filler wire, therefore the use of this consumable would still result in valid data being produced.

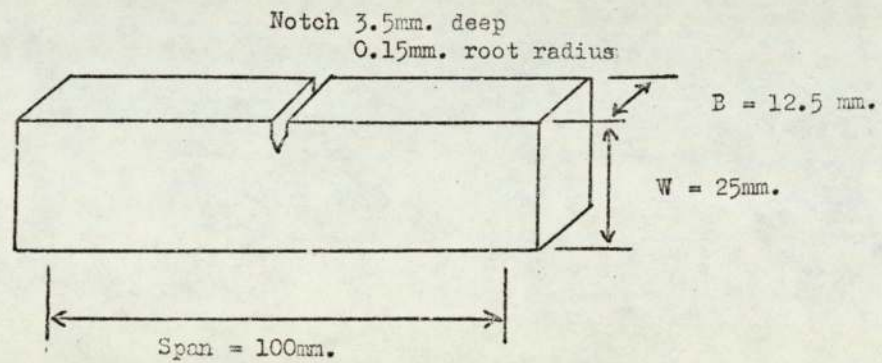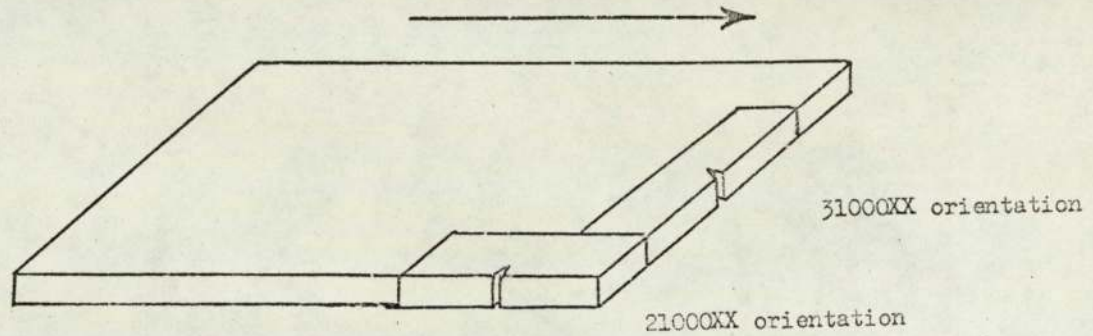Orientation of fatigue
specimens taken from
plate

31000XX orientation

21000XX orientation

Notch 3.5mm. deep
0.15mm. root radius

B = 12.5 mm.

W = 25mm.

Span = 100mm.

Fig. 4.1 Dimensions of fracture toughness
and fatigue specimens

Table 4.3

Vickers Pyramid Hardness - 10Kg. Load

Surface	Hv (mean)	Std. deviation
Rolled	164	2.5
Longitudinal transverse	168	2.5
Short transverse	163	1.9

Table 4.4

Fatigue Toughness Results

Orientation	Specimen No.	K_{Ic} MN/m$^{3/2}$
Notch parallel to rolling direction	31000X1	29
	31000X2	26
	31000X3	29
	31000X4	31
Notch at right angles to rolling direction	21000X1	31
	21000X2	30
	21000X3	24

Hiduminium 48 gains its strength mainly through the
precipitation of an η-phase ($MgZn_2$) during ageing. As a
result of the weld thermal cycle reversion can occur in the
HAZ. Reversion occurs when the temperature rises above that
of the GP zone solvus and results in the re/solution of
coherent GP zones formed during age hardening below the GP
zone solvus. Any precipitates which have begun to lose their
coherency do not revert. The reversion process leads to a
drop in hardness of the HAZ, but after ageing GP zones
will again form, resulting in some re-hardening.

The welds were made at the Alcan Research Laboratories,
Banbury. Details of the edge preparation and welding procedure
are given in Table 4.5.

Hardness survey

After welding the plates were allowed to age naturally
before tensile and fatigue tests were carried out. To note
the change in hardness resulting from ageing, hardness trans-
verses were made in the thickness of the plate across the weld
soon after welding. The indentations were made at a distance
one quarter of the plate thickness from one edge of the plate.
After natural ageing (about three months) a further transverse
was made and this is shown in Figure 4.2 together with scatter
bars of 11 different transverses made at different positions
along the weld run.

Welding had resulted in softening of the parent material
and this soft HAZ extends for approximately 30mm. either side
of the weld centre line. The transverse made soon after
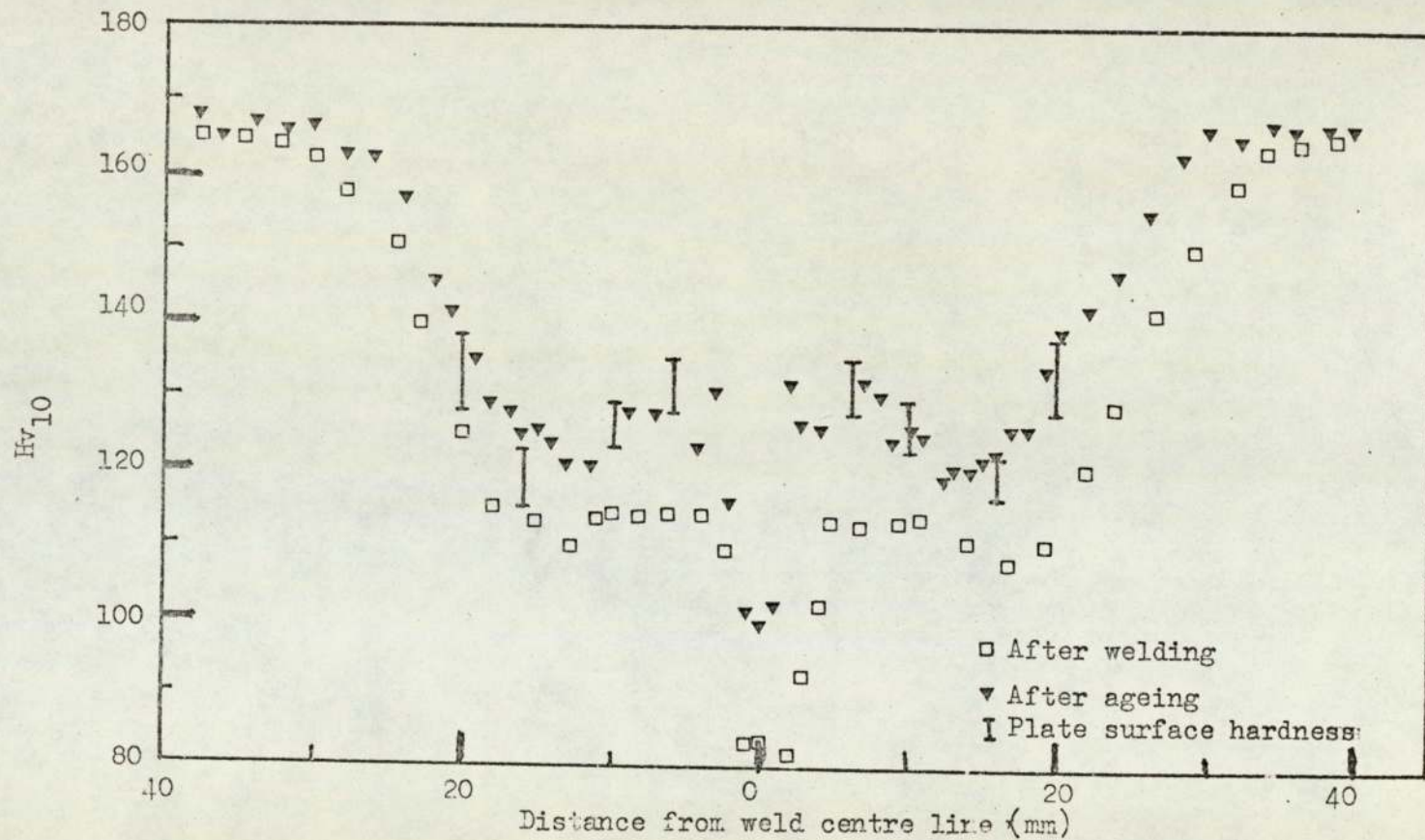welding shows that for 15mm. either side of the weld centre

Fig. 4.2 Hardness traverse across weld
(through the plate thickness at right angles to weld)

Table 4.5

Details of welding procedure

Welding current	390 – 400 amps.
Arc voltage	27
Transverse speed	660 mm/minute
Filler wire	NG 61 – 1.6mm. diameter
Shielding gas	Argon
Gas flow	1400 litres/hour
Gas nozzle size	16mm.
Torch angle	18°
Plate restrained during welding	
Edge preparation	Double V, with an included angle of 90°

line there is a region of constant hardness (in the HAZ). After ageing hardness occurs in bands, 10mm. from the weld centre line. A band between 10 and 15mm. from the centre line remains stable with virtually no hardening occurring. Variations in HAZ hardness through the plate thickness parallel to weld are small compared with the previous transverses and fall with the scatter bars in Figure 4.2. Therefore the HAZ has a relatively planar front at distances of 7 and 14mm. from the weld centre line, even though the edge preparation was a double V. This is further confirmed by the appearance of the heat affected zone revealed, after etching with Tuckers macro etch, Figures 4.3 and 4.4.

Tensile properties of the HAZ

As a result of the large width of the HAZ it was considered possible that tensile properties within the HAZ could be measured. Hounsfield No. 10 tensile test pieces were taken with their longitudinal direction prallel to the weld run so that the whole of the relevant HAZ would be within the test piece. Hardness transverses had shown that the position of the hardness peak and trough were located at distances of 7 and 14mm. from the weld centre line.

The results of the tensile tests are given in Table 4.6 and these show that the procedure was successful in detecting differences in properties within the HAZ. Although the hardness in the HAZ at 7mm. from the weld was about 7% higher than the 14mm. HAZ, the equivalent increase in yield strength (0.2% proof stress) was about 14%.
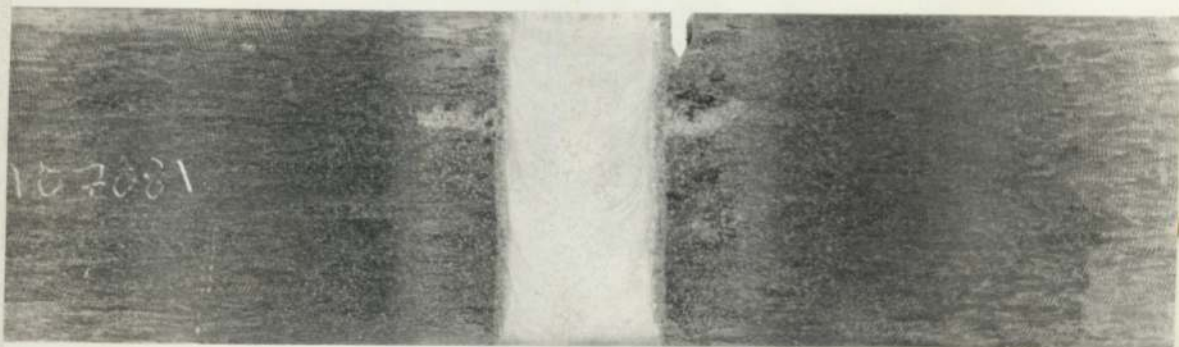
Figure 4.3   Etched surface of welded fatigue
specimens showing the extent of the HAZ and
location of the notch (21070XX series).

Figure 4.4   Thickness section of fatigue specimen
showing weld head profile.

Fracture toughness

Standard 3 point bend fracture toughness specimens
25 x 12.5mm. in section were machined from the plate with
the notch located in the HAZ at 7 and 14mm. from the weld
centre line. Fracture testing was carried out according to
recommended procedure[104]. The load crack opening displace-
ment trace showed that yielding occurred before fracture,
therefore K_{1c} could not be measured. K_q calculated from the
5% offset load was similar to the K_{1c} for the parent material
but the tensile and hardness results indicated that the HAZ
was tougher than this (Table 4.7). Stress intensity,
calculated on the basis of maximum load attained (Kmax)
resulted in only a small increase in toughness. A further
estimate of the toughness was made by calculating the equivalent
energy fracture stress intensity factor (K*) from the load/COD
curve. (A description of method is given in Appendix 1). In
this way the equivalent elastic fracture load P* is determined
and K* can be calculated in the normal way, i.e.

$$K* = \frac{P* \; Y}{B \; W^{\frac{1}{2}}}$$

Successful use of the equivalent energy approach for calcul-
ating fracture stress intensity factors has been reported by
Merkle.[119] K* was calculated from load displacement data on
25mm. thick steel specimens and compared with valid K_{1c} values
obtained from the same material but 300mm. thick.

The values of K^{*} obtained from the HAZ are about $50MN/m^{3/2}$,
however K* is higher for the harder region, at 7mm. from the

weld centre line, than for the softer 14mm. region (Table 4.7).
The previous mechanical tests suggest that the 14mm. region

should be tougher. Comparing the HAZ regions in terms of the
relative toughness, defined as K_{1c}/σ_{ys} (or $K*/\sigma_{ys}$), the
higher toughness of the 14mm. region becomes apparent since
for this region $K*/\sigma_{ys} = 0.364$ and for the 7mm. region
$K*/\sigma_{ys} = 0.358$.

4.2 Test Methods

Specimen details

Various specimen geometries are available for fatigue
crack propagation work. Commonly used types include compact
tension (CTS), centre cracked tension and single edge notch
bend specimens. It was decided that the latter was the most
convenient specimen design for the fatigue work. The specimen
dimensions used were the same as those recommended for fracture
toughness testing, which were described in Section 4.1. Bending
was achieved by 3 point loading.

On the plain plate material specimens were taken from both
the 31 and 21 plate orientations (Figure 4.1) i.e. with a
through plate thickness crack running parallel and at right
angles to the primary rolling direction respectively.

Similar rectangular specimens were taken from the welded
plate material. The excess metal from weld plus the surface
of the 15mm. thick plate was milled off to give a specimen
thickness of 12.5mm. The plates were welded together so that

fatigue specimens could be taken from the heat affected zone
transverse to the weld but with the notch at right angles to the
rolling direction, i.e. the 21 orientation. Since the hardness
traverse and tensile tests had indicated that the HAZ consisted

- 66 -

Table 4.6

Tensile Properties of the HAZ

Specimen	Yield Strength σ_{ys} MN/m^2	Tensile Strength σ_{uts} MN/m^2	Elongation %	Reduction of Area %
20700XX	160	233	16	22
	163	237	15	20
21140XX	146	210	16	25
	140	209	15	28
21000XX	499	536	12	23

Table 4.7

Fracture Toughness of the HAZ

Specimen	KQ	K max	K*
	$MN/m^{3/2}$		
21140XX	29) 33 } 31 29)	39	52
20700XX	26) 27 } 27 28)	40	58
21000XX	30	30	30

of two distinct regions, one soft and the other relatively hard, specimens were notched so as to sample both these regions. Although the weld edge preparation was a double V hardness testing had shown that the HAZ was substantially plannar through the plate thickness (Figure 4.2). Therefore the fatigue crack will sample a uniform HAZ region provided that the crack grows straight.

For identification purposes the HAZ specimens were numbered as follows:

i)   21070XX, notch 7mm. from the weld centre line, 'hard' region

ii) 21140XX, notch 14mm. from the weld centre line, 'soft' region.

Fatigue machine

Two types of fatigue machine were available: a Servo Consultants Electrohydraulic machine of 50KN maximum capacity and a 20 KN Amsler Vibrophore. The electrohydraulic machine allows various waveforms and frequencies to be selected and also allows constant load amplitude tests, independent of changes in compliance due to crack extension in the fatigue specimen to be made. The useable frequency range of this machine extends from 0.1 Hz to 100 Hz, and sine, sawtooth and square waves could be selected. The vibrophore, on the other hand, produces a fixed frequency, depending on the specimen compliance and fixed waveform. Both these machines were used in the experimental work, however the vibrophore was used in the high frequency cycling tests, i.e. > 100Hz. In order to obtain a large range of ΔK the fatigue loads were calculated on the basis that K_{1c} was attained when a/W was about 0.6 which is the limit of the compliance function. Also, preliminary tests

had shown that a useful range of crack growth could be obtained,
for low stress ratios, when a mean load of 1.7 KN and an
amplitude of 1.3 KN was used.

Crack length measurement

There are two methods in general use for measuring crack
length. These are the visual and electrical potential drop
methods. In the visual method, the progression of the fatigue
crack on the surface of the specimen is monitored using a
travelling vernier microscope. This method suffers from the
problem that it is difficult to automate and only measures the
surface crack length, giving no idea of the actual behaviour of
the crack front. The potential drop method, however, can
easily be automated to give a graphical output of crack length
versus number of cycles. Both these methods were used.

In the visual method adopted, fine lines were scribed at
0.5mm. intervals onto the specimen surface and the progress of
the crack was monitored using a x20 magnification microscope
(Figure 4.8). When the fatigue crack crossed a scribe line
the number of fatigue cycles elapsed were noted. As mentioned
above this method does not take into account bowing of the
crack front through the thickness of the specimen, and therefore
leads to an underestimate of crack length. However, it was
found that bowing tended to be prominent only at short crack
lengths. Difference in crack length between the centre and
surface were typically less than 15% at the beginning of
fatiguing. This resulted in an underestimate in ΔK of 8%.
However in terms of the average ΔK along the crack front the

maximum error in ΔK resulting from bowing is $\sim 4\%$. Other factors which lead to errors in calculating ΔK derive from poor specimen/anvil alignment. This results in an irregular crack front in which one side of the front leads the other. If at the end of each fatigue experiment the final crack lengths at each edge of the specimen differed by more than 7% (which gives a 16% error in ΔK) the test was considered invalid.

A graph showing the effect that errors in crack length measurement have on ΔK is shown in figure 4.5. The main reason for the rapid increase in ΔK errors with a/W is the increasing steepness of the compliance function with a/W.

Some of the disadvantages in measuring crack length visually can be overcome by using the potential drop method since (i) it can be automated and (ii) it tends to give an average value of crack length. The potential drop method used was that developed by Khairuzzaman[55], which was based on the work by Gilbey and Pearson[117]. The method depends on changes in a voltage drop across a crack, when a current is passed through a specimen, due to increases in the resistance of the ligament under a crack increasing in length. These voltage changes are small, therefore high current densities are required to produce a measurable potential drop. A series of calibration curves relating voltage drop against crack length has been produced by Jack and Yeldham[107]. The calibration curve used, shown in figure 4.6, requires that the potential leads are placed on the notch surface, i.e. $x = 0$. With reference

to the graph,

    Va = potential drop across the notch

    Vo = potential across unit length of the material

    W = specimen width

    a = crack length

    y = lead spacing

A convenient lead spacing was one in which $y = \pm 0.1$ W either side of the notch centre line. An estimation of the current required to give useful values of potential drop is obtained by considering Figure 4.6. The slope of the curve above $a/W = 0.2$ is approximately linear, then for an accuracy of 0.15mm. in length, i.e. 0.006W for the specimen used, the change in Va/VoW is 1.03×10^{-2}. Therefore the accuracy to which ΔVa must be measured is given by:

    ΔVa $= 1.03 \times 10^{-2}$ VoW

Vo is obtained from the specimen geometry, current and relativity of the material

    $Vo = \dfrac{Ap}{BW}$

where   A = current

    p = resistivity of the material $\simeq 3 \times 10^{-8}\Omega$m

    B = specimen thickness, 12.5mm.

therefore ΔVa $= 1.03 \times 10^{-2} \dfrac{A\,p}{B}$

If the voltmeter used has an accuracy of 1μV i.e. ΔVa $= 1\mu$V then the current required is about 40 amps. This was supplied from a Farnell constant current unit. The potential drop was measured with a Rikadenki D.C. microvoltmeter which had an accuracy of 1μV on the 100μV scale. To maintain this accuracy

when the voltage exceeded 100 μV a backing-off voltage supplied
from a potentiometer was used. In order to obtain a permanent
record of the voltage reading from the voltmeter the output
from the meter was recorded on a Kent chart recorder. From
knowledge of the cycling frequency of the fatigue test the
time axis was converted to the number of cycles elapsed. A
schematic diagram of the potential drop apparatus is given
in Figure 4.7.

The current leads were attached to the specimen via
copper contact plates bolted to the ends of the specimen. This
procedure enabled contact resistance to be reduced. To
measure Va, leads of nichrome wire were capacitance discharge
welded 0.1W either side of the notch centre line. The factor
VoW was also measured on the specimen surface but away from the
notch using a lead spacing equivalent to the specimen width.
Leads from the specimen to the voltmeter were screened to
prevent pick-up of extraneous electrical signals. It was
found unnecessary to insulate the specimen from the loading
anvils on the fatigue machine as problems resulting from multi-
current paths were not encountered. This probably results
from the high constant resistance between the aluminium and
steel anvils coupled with the low voltage ($\simeq$ 4v) from the
constant current supply.

During operation of the apparatus the monitored voltage
remained stable, the total interference being no more than
$\pm$ 0.2 μV. However, to achieve this the laboratory temperature

- 71 -
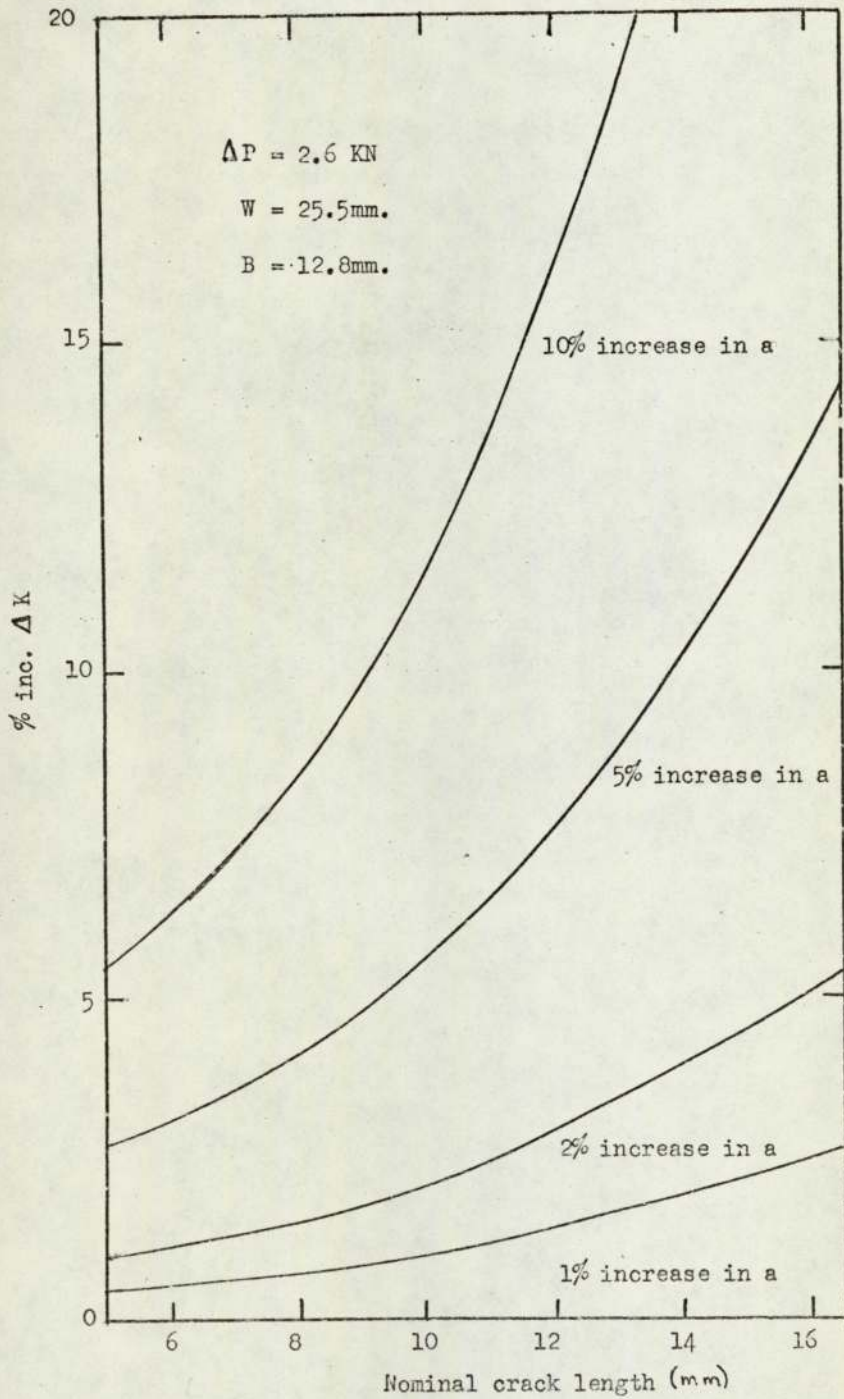
Fig. 4.5 Diagram showing the change in ΔK resulting from errors in crack length
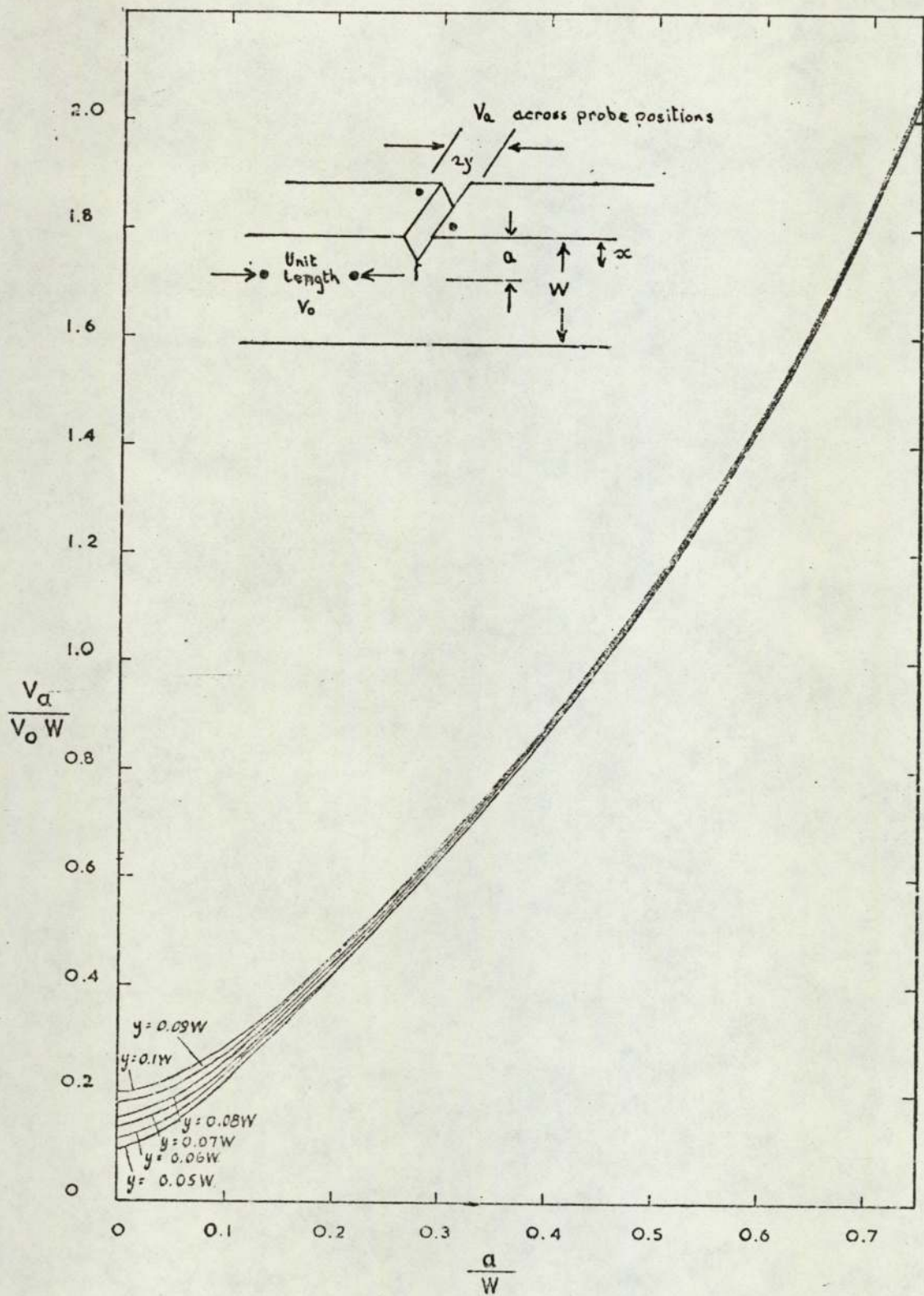
FIG. 4·6 GRAPH OF $\frac{V_a}{V_o W}$ VERSUS $\frac{a}{W}$ FOR POTENTIAL MEASURING
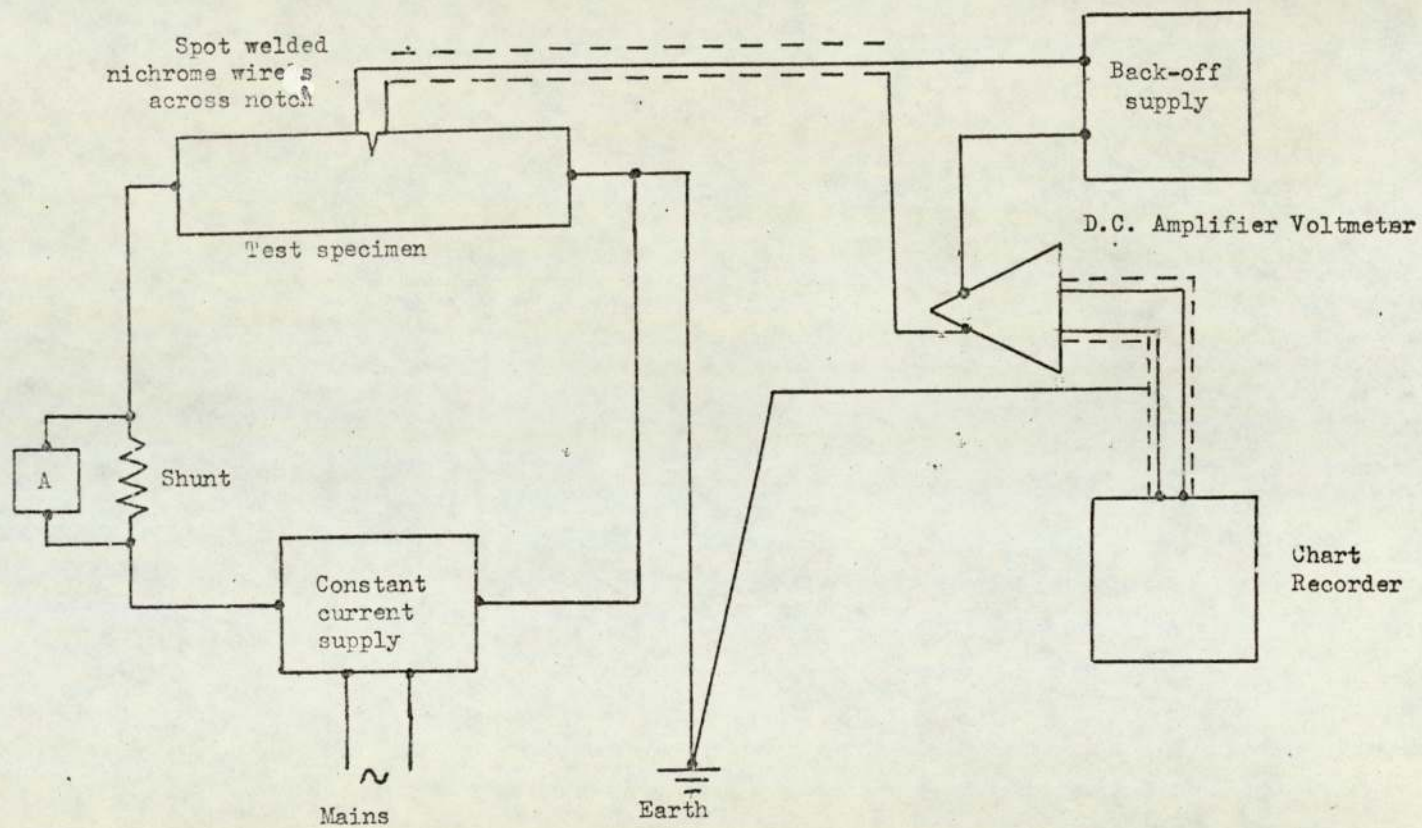
POINTS AT $x = 0$, $y = \pm$ VALUES SHOWN.

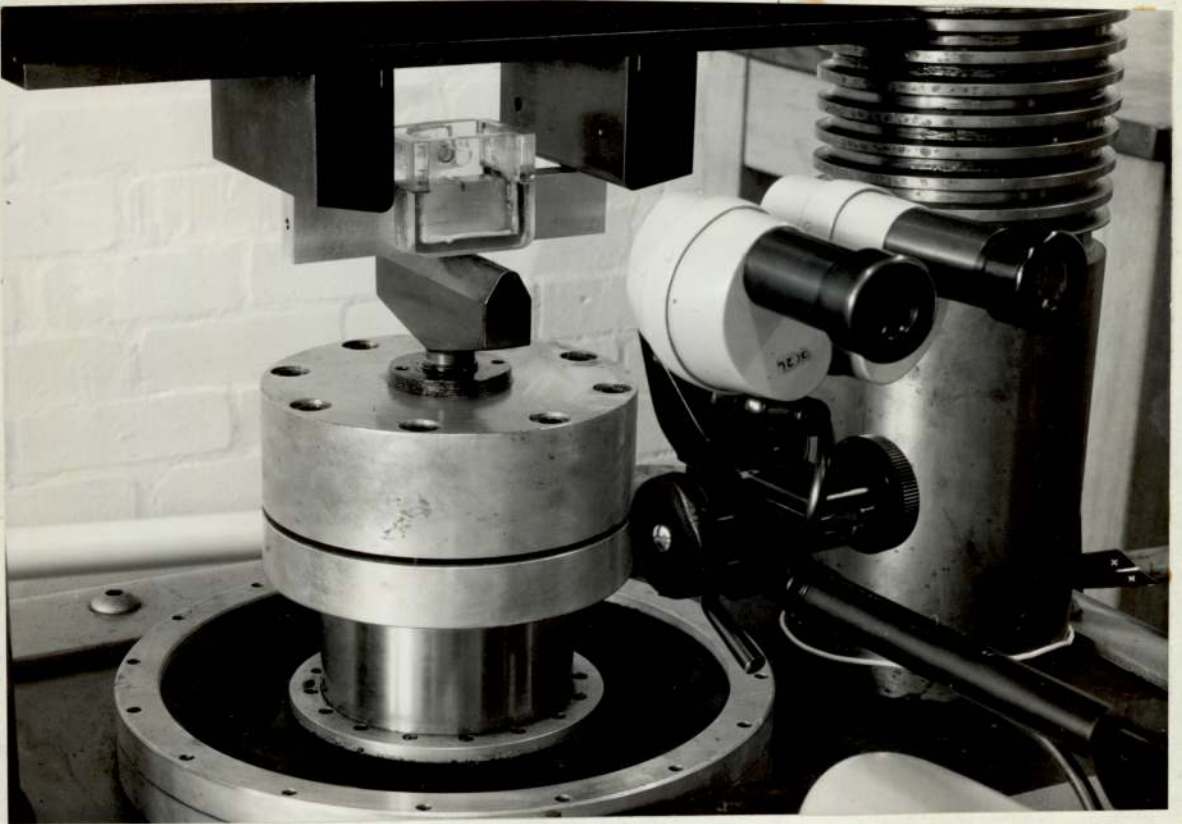Fig. 4.7 Schematic potential drop circuit

Figure 4.8 Photograph showing visual method of monitoring crack length together with the method of holding the environment.

had to be stable. Variations in temperature due to draughts or the close proximity of electric lights caused changes in voltage. Changes in laboratory temperature of less than 5°C were found not to affect voltage. Figure 4.9 shows the arrangement of the potential drop equipment, while Figure 4.10 shows details of the connections and specimen loading.

In order to convert the voltage readings into crack lengths, the calibration given in Figure 4.6 was used. The equation of the curve at $x = 0$ and $y = 0.1W$ is described by the following polynomial:

$$a/W = C_o + C_1X + C_2X^2 + C_3X^3 + C_4X^4 + C_5X^5$$

where $X = Va/VoW$

$C_o = -0.10178$ $C_1 = 0.82574$

$C_2 = -0.46218$ $C_3 = 0.26608$

$C_4 = -0.09541$ $C_5 = 0.01351$

A check on the accuracy of the method was made by visually measuring the surface crack length by the method described previously. The results obtained by these two methods are compared in Figure 4.11. The correlation between the two methods is good considering that the points represent results from a number of different specimens. Errors occur at low crack lengths where the potential drop method overestimates crack length. This arises from the fact that the potential drop method gives the average crack length of a bowed crack front while the visual method only gives the surface length. Since bowing was more pronounced at short crack lengths differences in crack length measured by the two methods are understandable.

Figure 4.9   Fatigue machine and potential
drop equipment .

Figure 4.10   Photograph showing current and
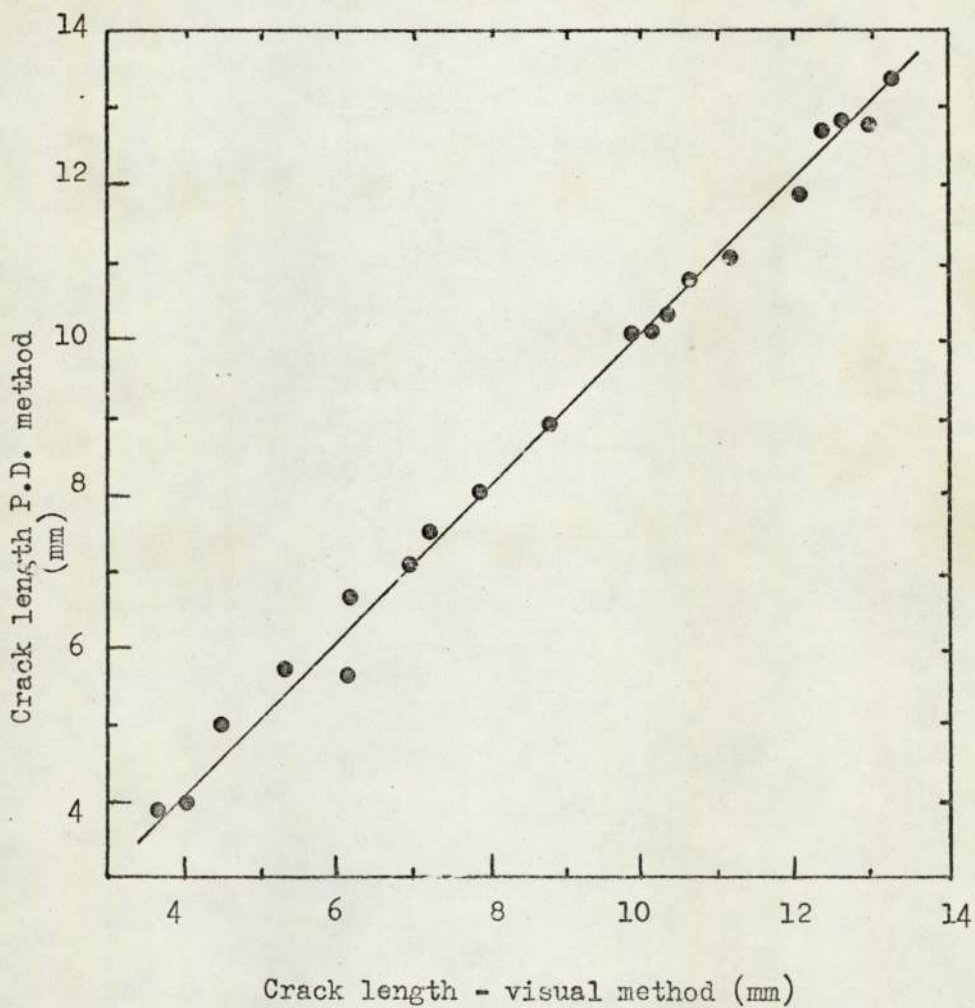potential measuring leads on fatigue specimen
loaded in bend rig.

Fig. 4.11

Comparison of crack lengths obtained by
the potential drop and visual methods

The maximum error in crack length as measured by the potential drop method was 0.25mm. and this compares with the theoretical accuracy resulting from the current and specimen size used of 0.15mm. Reference to the ΔK error diagram in Figure 4.5 shows that this results in an error of ΔK of about 3%.

The potential drop method for measuring crack length was attempted in the HAZ tests; however, it proved to be unsuccessful when the calibration curve, Figure 4.6, was used. This resulted from differences in electrical conductivity between the weld metal, HAZ and parent material. In view of these difficulties, the visual method of monitoring crack length was adopted.

Measurement of crack growth rate

Two methods of measuring fatigue crack growth rate are possible. The first method involves the differentiation of a crack length versus cycles curve while the second involves the ratio of finite differences in crack lengths to number of cycles, i.e.

$$da/dN = \left[\frac{a_{n+1} - a_n}{N_{n+1} - N_n} \right]$$

$$\text{at} \quad a = (a_{n+1} + a_n)/2$$

The first method can be solved either by graphical methods or by the differentiation of the equation describing the a versus N relationship. Graphical methods tend to be laborious and can be inaccurate at low and high crack growth rates. Use of a simple computer programme to fit polynomials to the data was attempted. However, the method proved to be inaccurate

since the use of a high degree polynomial results in inflexions in the resulting a versus N curve while low degree polynomials result in poor fitting to the data points. Similar difficulties resulting from polynomial curve fitting procedures have been reported by Davies and Fedderson[108]. Recently McCartney and Cooper[109] have applied spline fitting techniques to obtain functions relating the crack length/cycles data. This method is said to overcome the problems of polynomial fitting. However since this method came to the attention of the author only after the experimental work had been completed it was not used.

The method of finite differences is relatively simple to use but it tends to give higher scatter in da/dN than graphical methods. However the problem of scatter can be reduced provided that the intervals between the crack length measurements are sufficiently large. This was the method of measuring crack growth rate finally adopted. The crack length interval $(a_{n+1} - a_n)$ used was 0.5mm. which resulted in an acceptably low level of scatter in crack growth rate.

To facilitate the handling of the data produced from the fatigue tests a simple computer programme was devised so that the input of cycles and potential drop resulted in the output of crack growth rate and ΔK.

Loading procedure

In order to determine the relationship between stress intensity range (ΔK) and crack growth rate two loading methods can be used. A constant load amplitude maintained

independent of crack length results in a continuous rise in
ΔK. Alternatively a load shedding procedure can be used to
maintain a constant ΔK irrespective of crack length. If ΔK
is the major parameter controlling crack growth rate then both
methods of loading should result in the same fatigue behaviour.

To determine the influence of the type of loading on fatigue
crack growth constant load amplitude and load shedding tests
were carried out. Two load shedding procedures were chosen
using (i) constant mean and maximum loads but reducing
amplitude, and (ii) constant minimum load with reducing
amplitude.

A fatigue crack was initiated from the machined notch of
a single edge notch specimen loaded under three point bending,
using a load of 2.5 ± 2.1 KN. After growing the crack from
$a/W = 0.15$ to $a/W = 0.2$, loading profiles illustrated in
Figure 4.12 were used. For profiles (a) (constant mean load)
and profile (b) (constant minimum load) the load amplitude
(ΔP) was shed in steps of 0.1KN since this was the smallest

load reduction that could be made on the fatigue machine. For
a specified ΔK, the crack length increase allowed before each
load reduction was calculated as follows.

The stress intensity at any crack length, between $a/W = 0.2$
and $a/W = 0.6$, is calculated using the following:
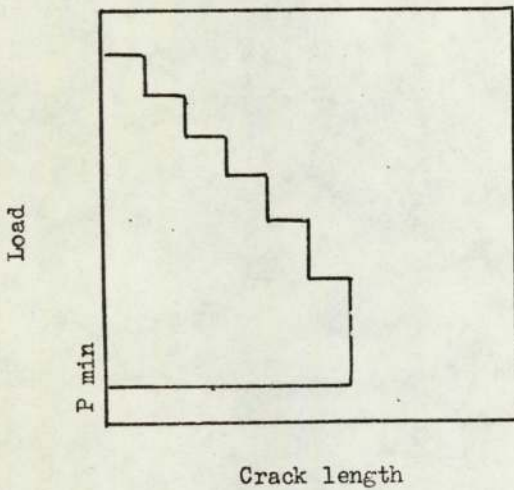
$$K = \frac{Y\,P}{B\,W^{\frac{1}{2}}}$$

or for fatigue

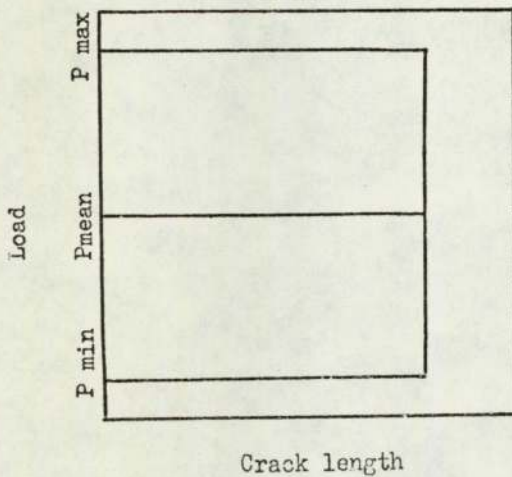$$\Delta K = \frac{Y\Delta P}{B\,W^{\frac{1}{2}}}$$

Fig. 4.12 Loading Profile
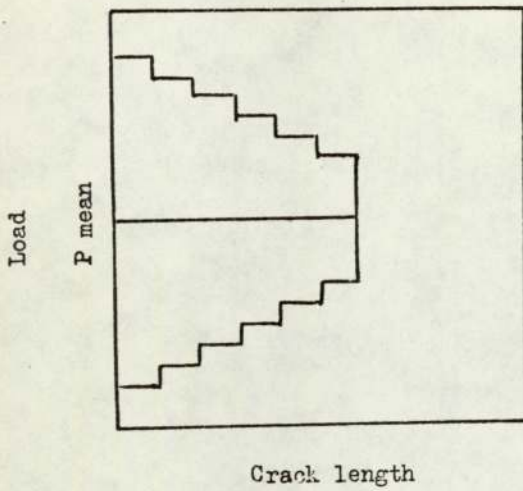
Load profile (a)
(Constant ΔK -
constant mean load)

Load profile (b)
(Constant ΔK -
constant minimum load)

Load profile (c)
(Increasing ΔK -
constant load
amplitude)

where $\Delta K = Kmax - Kmin$

$\Delta P = Pmax - Pmin$

and   Y is the compliance or K calibration function which

is a polynomial in a/W.

Therefore the increase in crack length for a specified load

reduction in order to keep ΔK constant is obtained from Y;

$$\frac{\Delta K \text{ constant } BW^{\frac{1}{2}}}{\Delta P} = f \ (a/W)$$

For profile (a) Y and hence crack length 'a' was calculated

from reductions in ΔP of 0.1KN.

(b) Y calculated from reduction in Pmax of

0.1 KN but keeping Pmin constant.

The tests were carried out at four different values of ΔK,

and these were nominally 6, 8, 10, and 15 $MN/m^{3/2}$. Crack length

was measured using the potential drop method, and a fatigue

cycling frequency of 50Hz was used. Load reductions were made

at predetermined cracks, beginning as a/W = 0.2, smoothly

without stopping the fatigue machine. The number of fatigue

cycles at each load reduction were noted together with crack

length. From this data crack growth rate was calculated. At

least 15 load reductions were made so that a reasonably accurate

crack growth rate could be determined.

Three constant load amplitude tests (profile c) were

carried out using a load amplitude of 2.6KN (i.e. 1.5 $\pm$ 1.3KN)

at a stress ratio of 0.07. However two further tests were

carried out using the same amplitude but a stress ratio of

0.48, i.e. 3.7 $\pm$ 1.3 KN. Crack growth rates were calculated

using the method of finite differences.

Other tests on the parent material and HAZ regions were
carried out under constant load amplitude conditions using the
following loads after crack initiation, i.e. ΔP = 2.6KN;
1.7 $\pm$ 1.3KN, for a stress ratio of 0.13 and ΔP = 2.6KN;
3.7 $\pm$ 1.3KN, for a stress ratio of 0.48. These load amplituded
gave a useful range of ΔK of about 5 to 30 $MN/m^{3/2}$ when the
crack grew from a/W = 0.2 to a/W = 0.6.

Frequency and waveform variation

Three main fatigue frequencies were used, the lower bound
being 10Hz whilst the upper $\sim$ 120Hz. Subsidiary tests in air
where stress ratio effects were being invesitgated were carried
out at 50Hz. However since the fatigue tests in the HAZ regions

produced extremely low crack growth rates the lower bound
cycling frequency, in air, was raised to 50Hz, so that
inordinately long testing times would be avoided. Whilst the
two lower bound frequency tests were carried out on the Servo
Consultants Electrohydraulic Fatigue machine the upper bound
was done on an Amsler Vibrophore. In this type of machine
the frequency of cycling depends on the mass and stiffness of
the specimen, the stiffer the specimen the higher the resonance
frequency. Increases in crack length reduce specimen compliance
and therefore the frequency of cycling falls. For the specimen
type used the frequency fell from about 135Hz at the beginning
of the test (a/W = 0.2) to about 115Hz at the end of the test
(a/W = 0.6). This 15% change in frequency was no thought to
be significant since the lower bound frequency was a factor of
twelve below the average upper bound.

In all the above cases the cycling waveform used was sinusoidal. The influence of waveform variations ~~were~~ was investigated on the parent material (in the 31 orientation) at a constant frequency of 10Hz, using sine, square and triangular wave shapes. These waveforms were produced on the Electro Hydraulic fatigue machine. However, due to inertia effects and the design of the valves, the production of pure waveforms is not possible. The simplest waveform that this type of machine can produce is a sawtooth wave since the rate of flow of fluid in and out of the piston is constant. Reproduction of a sine wave is more difficult because the rate of flow of fluid is continuously changing. The 'squareness' of a square wave depends on how fast fluid can be supplied and removed from the piston. However, at relatively low cycling frequencies reasonable waveform shapes can be produced. Figure 4.13 shows the type of waveform obtained. These line drawings are accurately copied from Polaroid photographs taken off the cathode ray oscilloscope connected to the load cell of the fatigue machine.

In all the tests on both parent and HAZ material where frequency and waveform were being investigated the loads used were 1.7 ± 1.3 KN with a stress ratio of 0.13. Experiments were carried out first in an air environment to determine any frequency effect on crack growth rate but mainly as base line for comparison with the corrosion fatigue tests.
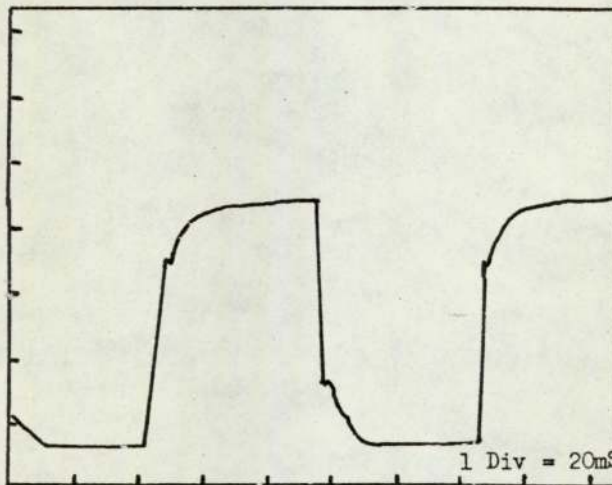
Corrosion fatigue tests

Two environments were used in the corrosion fatigue experiments (i) de-ionized water and (ii) a $3\frac{1}{2}\%$ sodium chloride

Sine wave

1 Div = 20mS

Triangular wave

1 Div = 20mS

Square wave

1 Div = 20mS
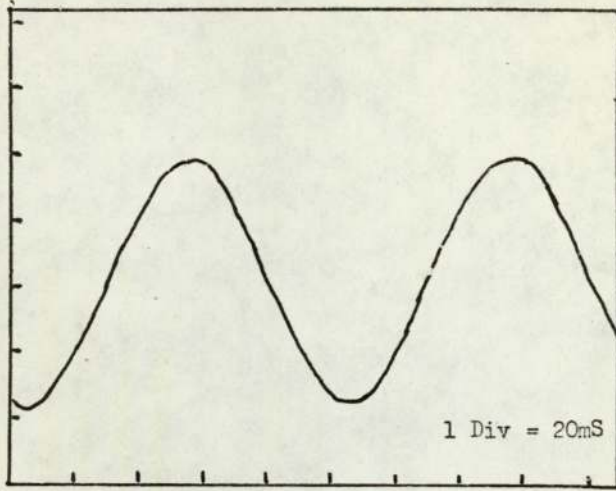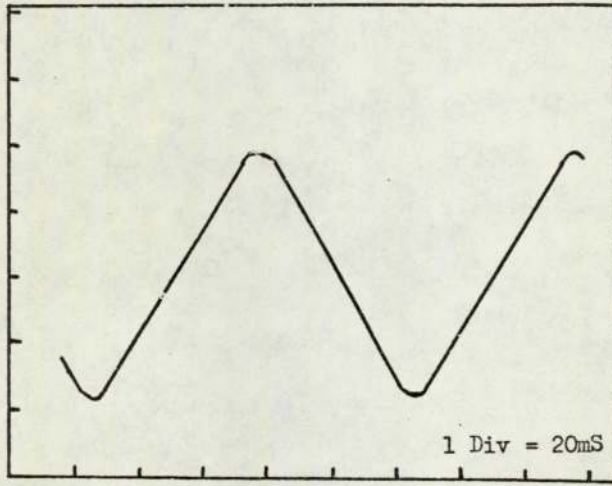
Fig. 4.13 Trace showing waveform profile

solution. The environment was contained in a 20ml. capacity
perspex chamber surrounding the notched area of the specimen
(Figure 4.4). Measurement of the laboratory temperature
showed that it remained fairly stable and was within the range
$23 - 25^{\circ}C$. As a result special temperature control of the
environment was not considered necessary.

The influence of waveform (using the shapes and loading
variables described in the previous section) was first
investigated using the parent material in the 31 orientation
and a de-ionized water environment. This was followed by the
use of the $3\frac{1}{2}\%$ NaCl solution. Further tests to study the
influence of frequency were carried out on the parent material
using $3\frac{1}{2}\%$ NaCl because de-ionized water did not greatly affect
crack growth rate. In these tests sinusoidal waveforms with
frequencies from 1Hz to 120Hz were used. Since it was found
that the actual waveform shape was not a major variable in
the corrosion fatigue experiments (in a $3\frac{1}{2}\%$ NaCl environment)
tests on the HAZ material were carried out using sinusoidal
waveforms at 10Hz and 120Hz.

Further tests to study the effect of stress ratio on
fatigue in a salt water environment were carried out in the
parent (21 orientation) and the HAZ (21070XX and 21140XX)
materials. In these tests a sinusoidal loading of 3.7 ± 1.3KN
(R = 0.48) at a frequency of 10Hz was used.

In the HAZ tests crack length was monitored visually,
however, for the parent material the potential drop method
was used. An obvious criticism of this procedure is that the
applied potential will affect the electro-chemical conditions
in the crack and hence influence crack growth. However, the
voltage potentials involved are small, the maximum voltage

across the fatigue fracture surfaces resulting from the applied current is $200 \mu V$, while the voltages due to electro-chemical interactions are over two orders of magnitude larger than this. Therefore the influence of the potential method on crack growth would be expected to be small. As a check on this hypothesis two corrosion fatigue tests were run under identical conditions in $3\frac{1}{2}\%$ NaCl solution, except that in one test the potential drop method was used to measure crack length while in the other a visual crack monitoring technique was used. The tests were carried out on the 31 orientation specimens using a square wave loading at a frequency of 10Hz and the loads were $1.7 \overset{+}{-} 1.3$KN. Figure 4.14 shows the crack growth ΔK relationship for the two crack length measurement techniques. There is no significant difference in the two techniques, therefore use of the potential drop method does not influence corrosion fatigue behaviour.

Stress corrosion tests

To determine the level of ΔK at which corrosion fatigue would be influenced by stress corrosion, stress corrosion tests were performed in the more aggressive of the two environments selected, i.e. $3\frac{1}{2}\%$ NaCl solution. The test specimens were similar to those used in the fatigue experiments and the machine notch was extended by fatigue at a low value of stress intensity ($\Delta K \approx 10$MN/m$^{3/2}$) in order to maintain a sharp crack tip profile. The specimens were loaded in 3-point bending in a modified creep machine. The area round the notch was surrounded by a perspex chamber containing 20ml. of $3\frac{1}{2}\%$ NaCl solution.
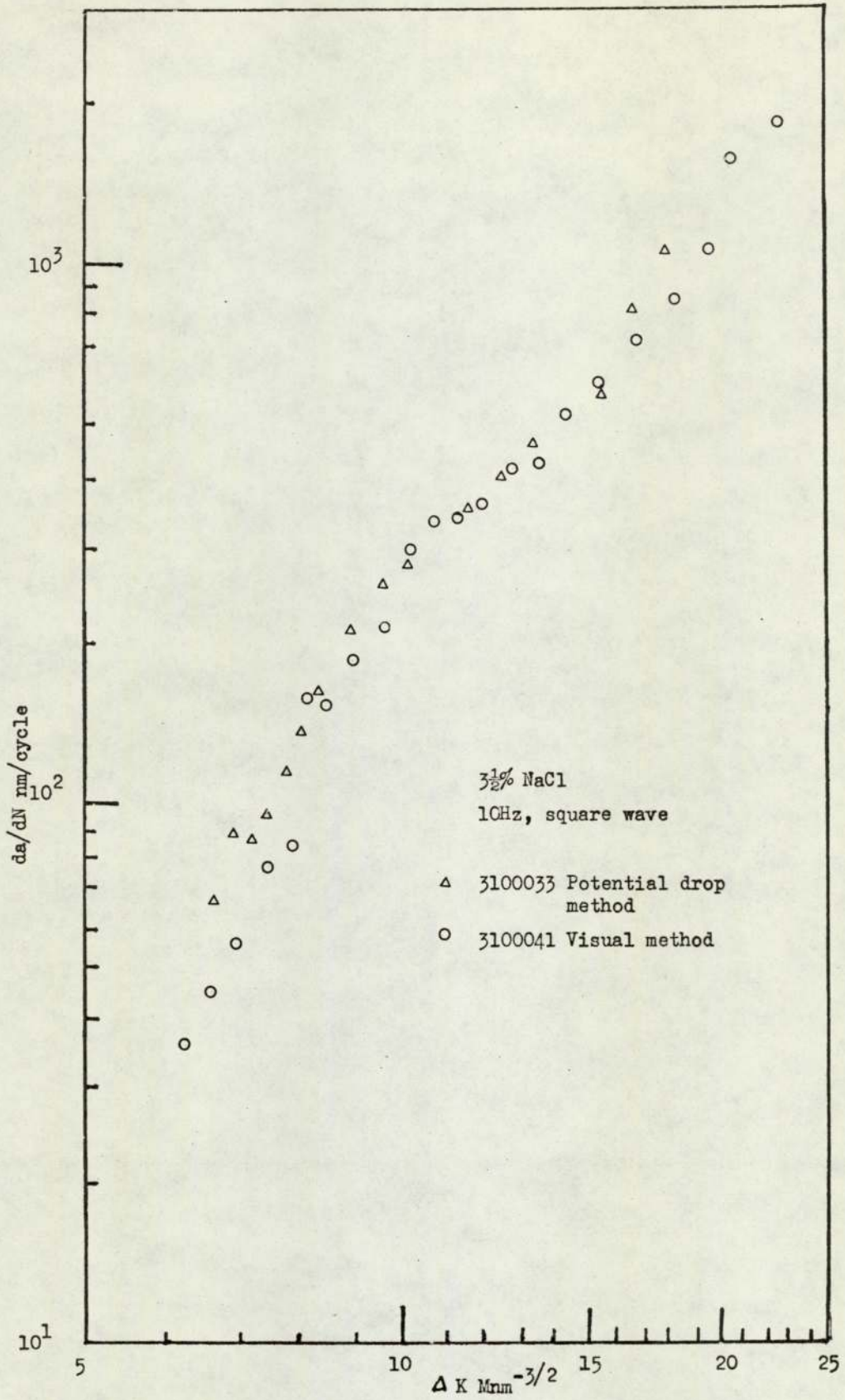
Fig. 4.14 Comparison of Potential Drop and Visual

Methods in measuring crack length in salt water

This solution was changed daily while the test proceeded. A specimen of the 31 orientation, i.e. crack parallel to the rolling direction, was loaded to give a stress intensity of 75% of K_{1c}. Deflection of the specimen resulting from any crack extension was monitored with an electrical resistive displacement transducer placed on the anvils. The deflection was used to calculate crack length by a compliance method and this is described in Appendix 2. From the plot of crack length with time the crack growth rate at a specific stress intensity was determined by graphical differentiation of the curve.

Metallography and Fractography

A metallographic examination of the plate was made to determine the distribution and composition of the inclusions and the type of grain structure present. Three planes in the plate were examined which were:

i)   the rolled surface

ii) the longitudinal transverse surface; the plate thickness parallel to the rolled surface

iii) the short transverse surface; the plate thickness at right angles to the rolled surface.

Planes (ii) and (iii) are equivalent to 31 and 21 orientation fatigue fracture surfaces.

The metallographic specimens were polished using a mixture of γ-alumina and water and etched in Tuckers solution. Inclusion composition analysis was measured using an AEI Microprobe Analyser.

The fatigue fracture surfaces were examined using a Cambridge 1A Stereoscanning Electron Microscope. Normally no

cleaning of the fracture surface was carried out prior to examination except when corrosion fatigue specimens were examined. In these cases surface corrosion product was removed by ultrasonic cleaning in 'Inhibisol'.

The fracture surfaces were mounted in the microscope at an angle of 45° to the electron beam. This results in an apparent foreshortening of dimensions in the vertical direction by a factor of $1/\sqrt{2}$.

5. EXPERIMENTAL RESULTS

5.1 Load Profile and Stress Ratio Effects

The test results for the two load shedding profiles
(a) and (b) (Figure 4.12) constant mean load and constant
minimum load programmes to obtain constant ΔK are given in
Table 5.1. These results show that for a constant ΔK crack
growth rate was not constant but depended on crack length. A
diagram of the crack length versus number of cycles curve
(Figure 5.1) illustrates the typical trend observed. Initially
the crack growth rate was low but this was followed by the
expected constant growth period. Finally at about a/W = 0.4
the crack growth slowed down. This phenomenon was characteristic
of both profiles.

The results of constant load amplitude tests (load pro-
file (c)) (Figure 4.12) using two values for stress ratio
(R = 0.071 and 0.48) are shown in Figure 5.2. Both curves show
a characteristic change in slope from Region 1 to Region 2
growth. The transition occurs at about $\Delta K = 8MN/m^{3/2}$ when
R = 0.48 and at about $12 - 13$ $MN/m^{3/2}$ when R = 0.071. The
influence of high stress ratios in increasing the crack growth
rate is clearly marked at ΔK below about $12MN/m^{3/2}$. However
at higher ΔK's crack growth rates for both curves merge and

become independent of stress ratio.

The crack growth rate versus ΔK data obtained for two
stress ratios 0.13 and 0.48 for each of the HAZ tests, 21140XX
and 21070XX are given in Figures 5.3 and 5.4. Since the
fracture toughness test showed that valid K_{1c} could not be
measured directly the validity of applying fracture mechanics
analyses to the fatigue data may be questioned. The reversed

Table 5.1 Programme loading, constant ΔK results.

Specimen	ΔK MNm$^{-3/2}$	Crack growth rate - nm/cycle			a/w	Transition			Load ratio R.	
		initial	constant	final	initial	first	second	final		
Load profile a										
310002	5.9	3.3	6.13	–	0.200	0.236	--	0.366	0.071	0.275
310005	7.9	27.7	48.4	20.8	0.207	0.240	0.457	0.540	0.056	0.490
310003	9.8	56.6	140.0	93.3	0.202	0.236	0.453	0.538	0.044	0.470
310004	14.8	83.5	173.7	–	0.200	0.228	--	0.398	0.030	0.280
Load profile b										
310008	5.9	--	3.2	--	0.200	--	--	0.323	0.071	0.118
310008	6.9	--	4.35	--	0.343	—	--	0.465	0.087	0.100
310006	7.9	1.79	9.9	7.55	0.208	0.260	0.394	0.430	0.056	0.095
310007	9.8	--	79.2	45.8	0.200	--	0.398	0.551	0.044	0.111
310009	14.8	--	142.5	--	0.315	--	--	0.532	0.038	0.071
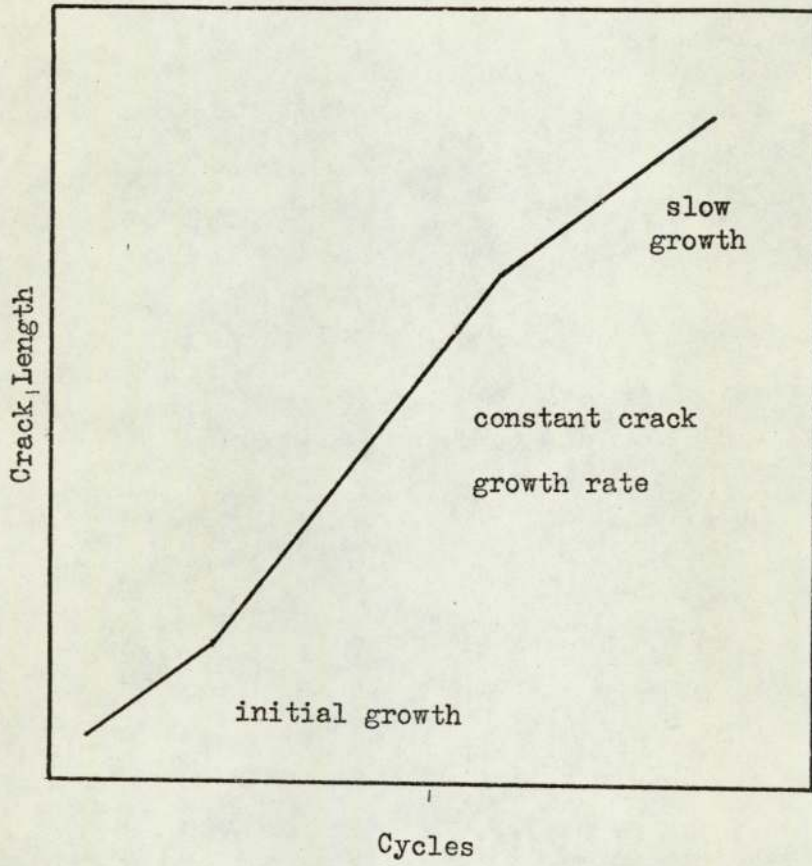
Fig. 5.1 Crack length versus cycles curve
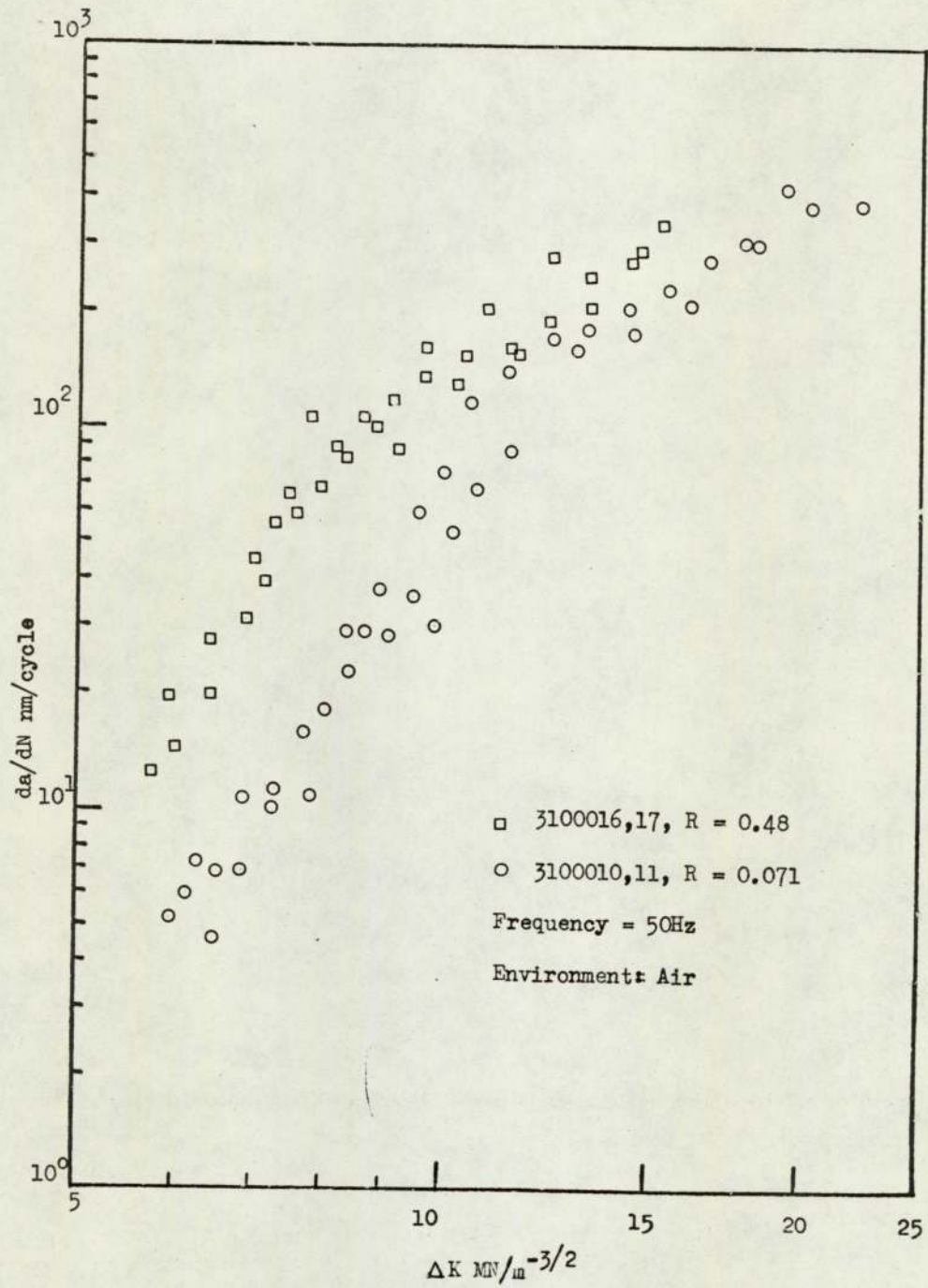obtained under constant ΔK conditions

Fig. 5.2 Influence of stress ratio (R) on crack growth rate (constant load amplitude tests)
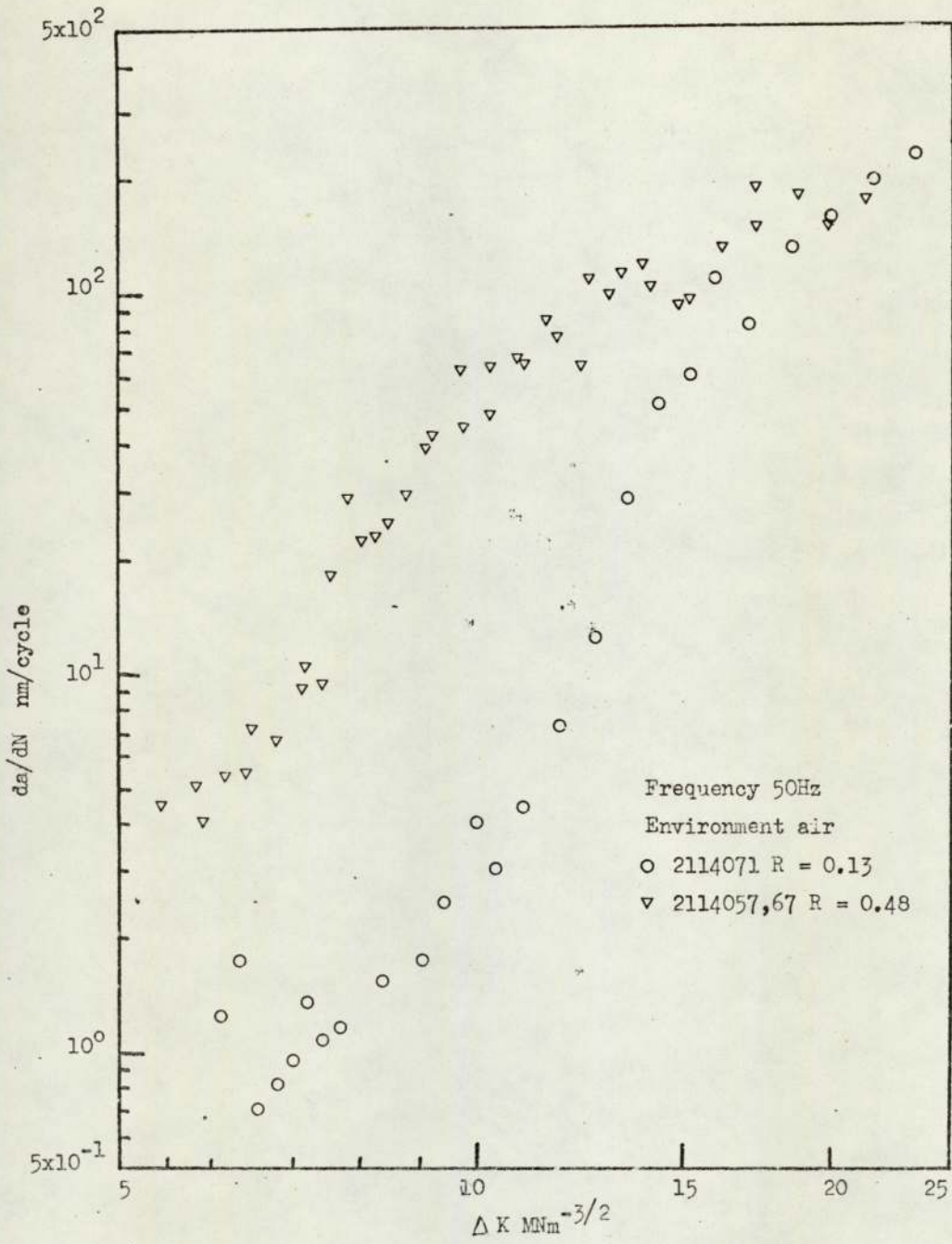
Fig. 5.3 Crack Propagation rate in soft HAZ
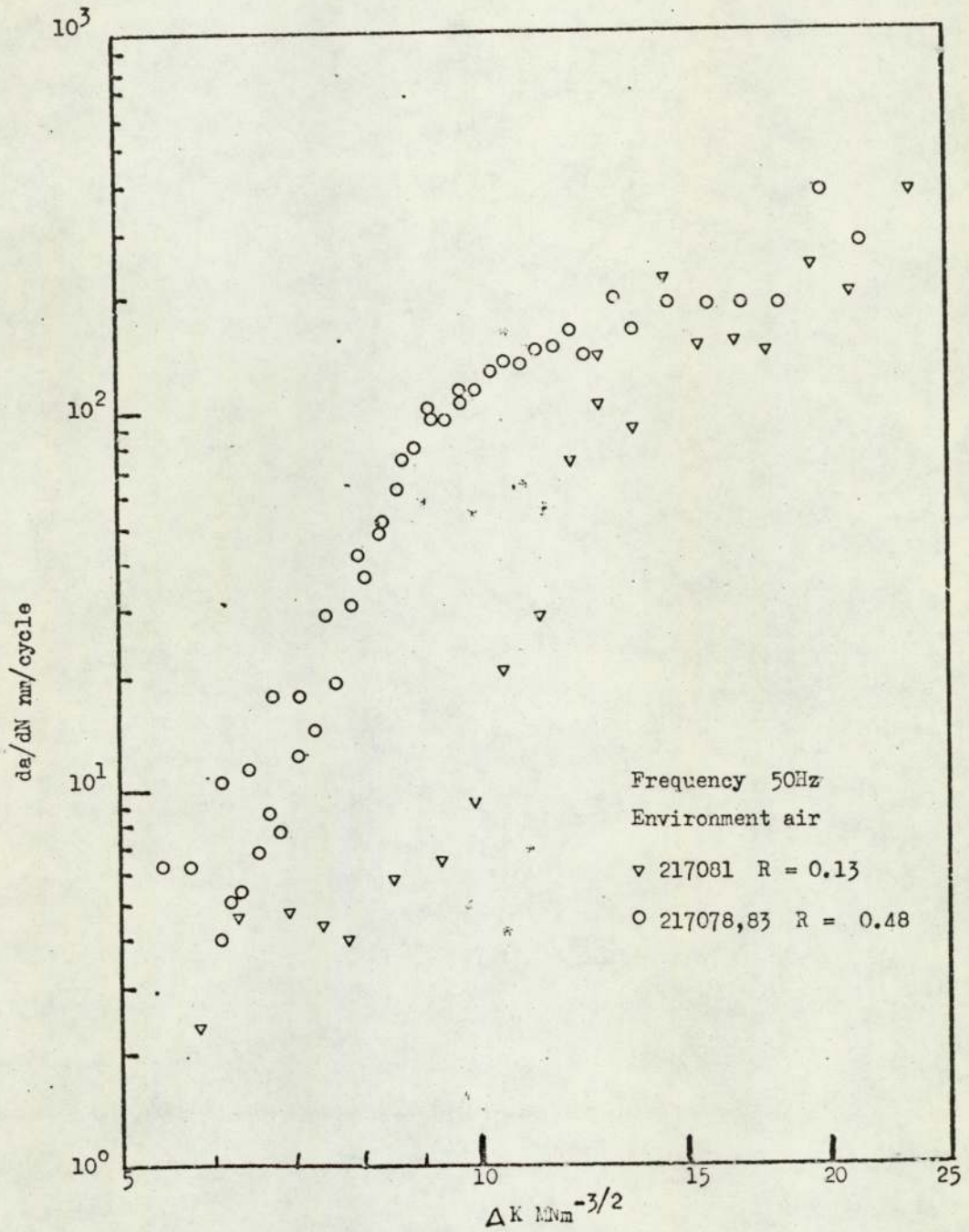14mm. from weld centre at two stress ratios

Fig. 5.4 Crack propagation rate in hardened HAZ,

7mm. from weld centre line, at two stress ratios .

plastic zone size under plane strain conditions is given by:

$$r_p = \frac{1}{6\pi}\left[\frac{\Delta K}{2\sigma_{ys}}\right]^2$$

At a ΔK of 20 MN/m$^{3/2}$ the value of r_p in the HAZ is about
0.2mm. which is less than 1/50 of the specimen thickness. There-
fore linear elastic analyses for fatigue are applicable since
plastic zone is small in comparison with specimen thickness.

Generally the pattern of crack growth in the HAZ is
similar to the parent material in that the stress ratio effect
is prominent at low to medium ΔK's while above a certain
transition ΔK the effect on crack growth rate diminishes.
However the most significant difference between the parent
material and the HAZ is in crack growth rate. For instance at
a stress ratio of 0.13, the 21140XX position (soft HAZ) resulted
in a crack growth rate about an order of magnitude lower than
the parent material. A further factor evidenced by the low
stress ratio tests in the HAZ is the inflection in the crack
growth rate − ΔK curve at low values of ΔK. This leads to
a reduced or constant crack growth rate period even with an
increasing ΔK. The use of a substantially higher ΔK or
higher stress ratio eliminates the effect.

Influence of corrosive environments

The influence of stress ratio on the corrosion fatigue
behaviour, in $3\frac{1}{2}\%$ NaCl solution, in the parent material and the
two HAZ regions are shown in Figures 5.5, 5.6 and 5.7. This
time the stress ratios used were the same for the parent and
HAZ, i.e. 0.13 and 0.48. However frequency of cycling was
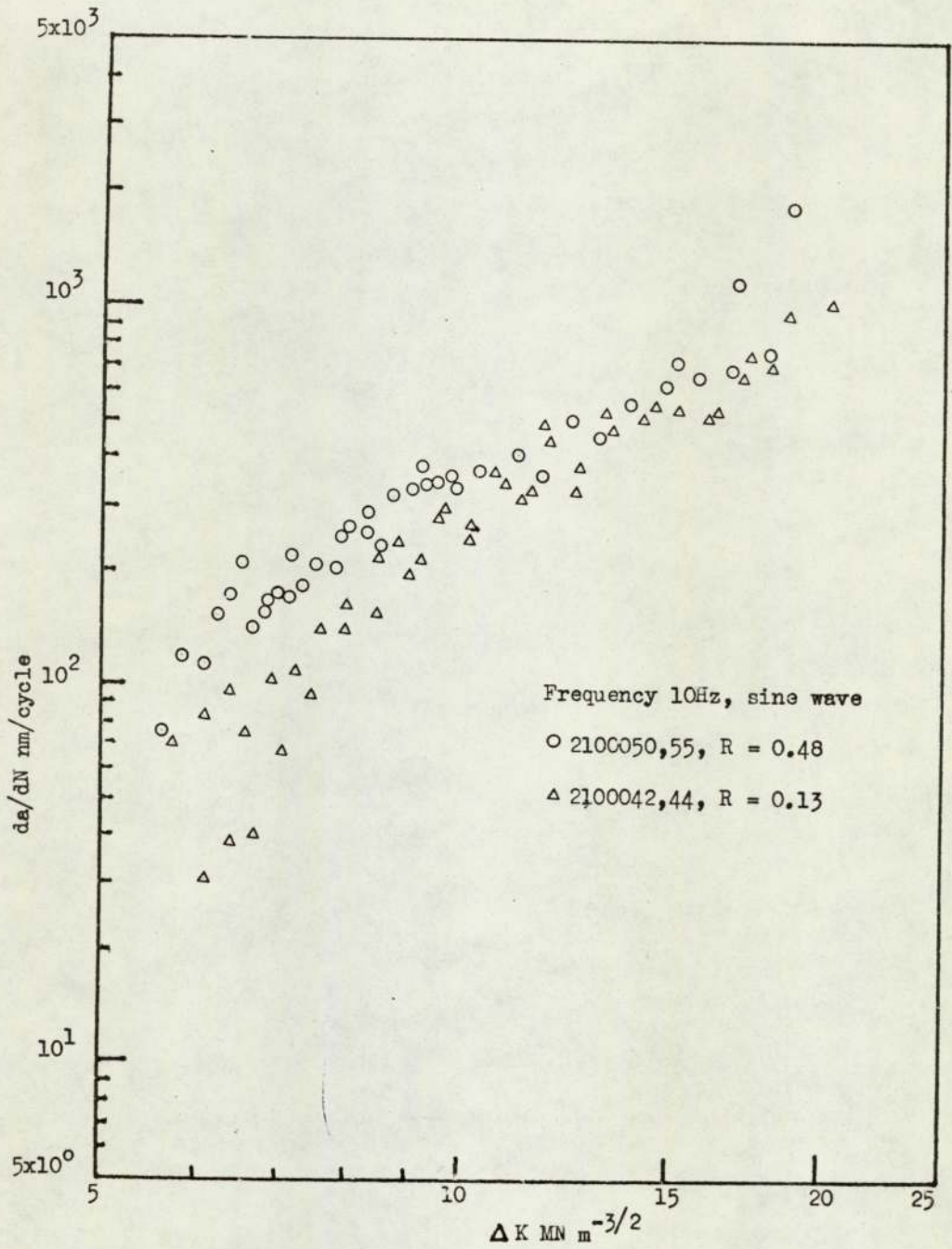10Hz compared with the 50Hz used in the air environment tests.

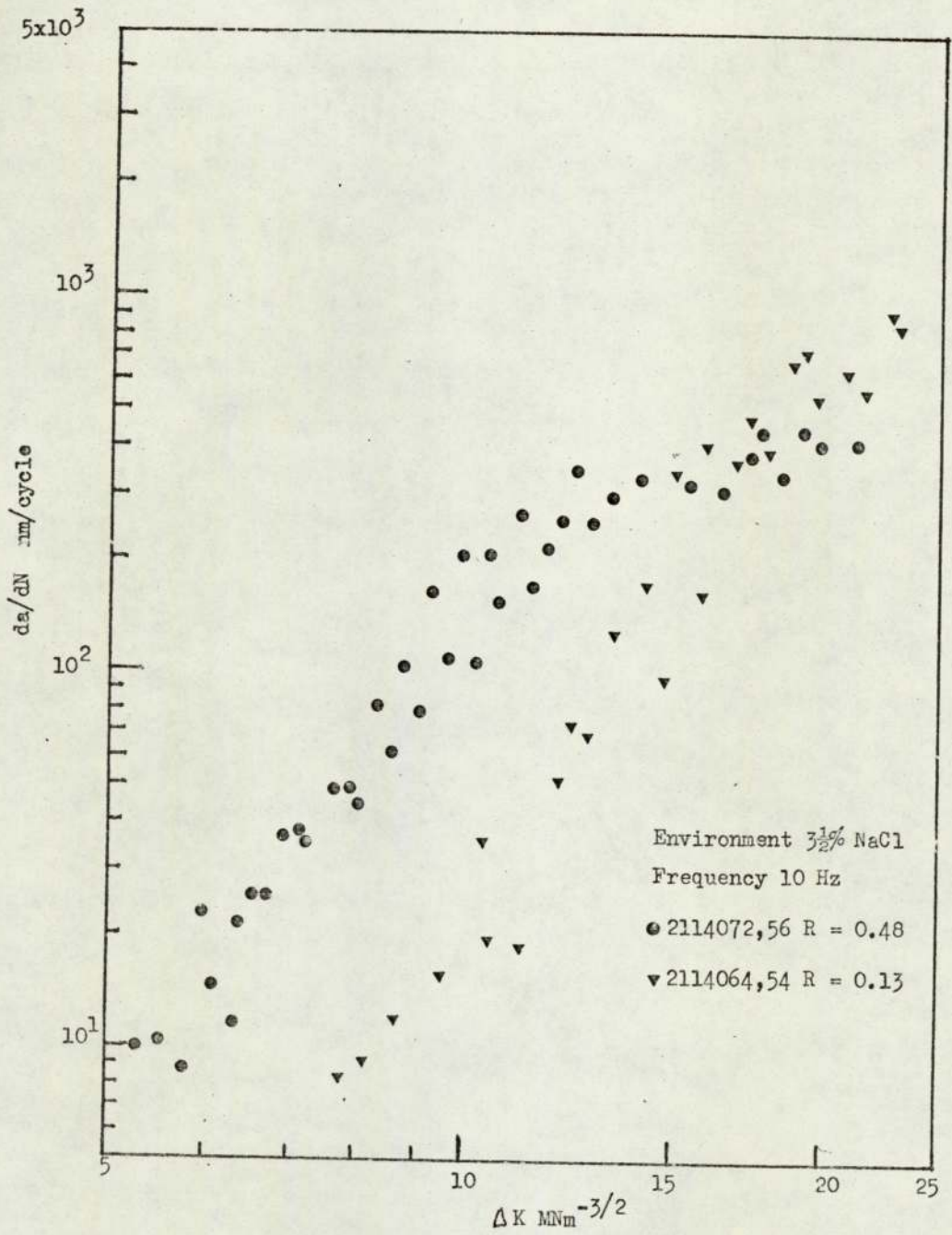Fig. 5.5 Influence of stress ratio (R) on crack propagation in $3\frac{1}{2}\%$ NaCl

Fig. 5.6 Influence of salt water on the crack
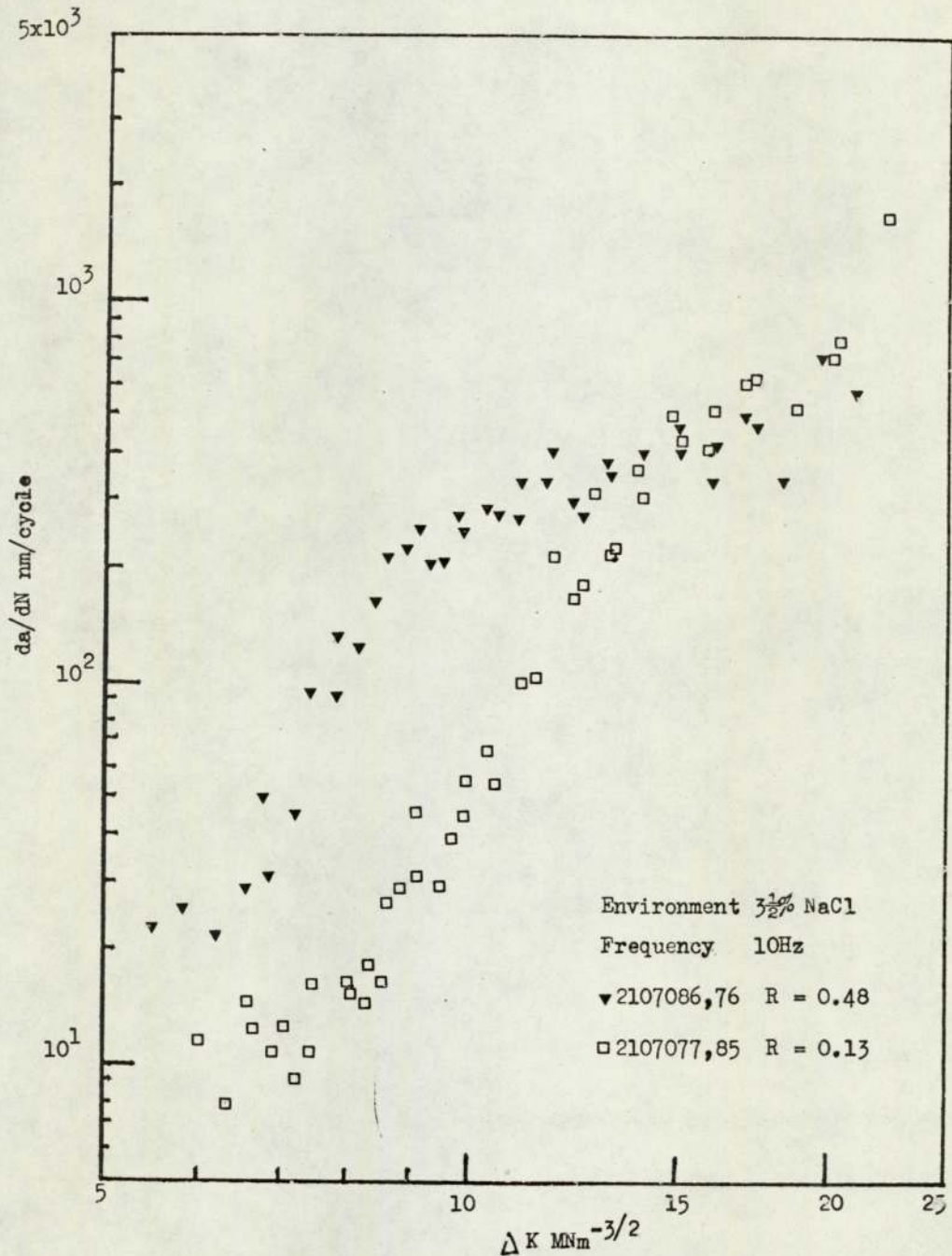propagation in the soft HAZ at two stress ratios

Fig. 5.7 Influence of salt water on the crack
propagation in the hard HAZ at two stress ratios

In the parent material an increase in stress ratio of a factor of four times has resulted in a small increase in crack growth rate; only at ΔK's below $10MN/m^{3/2}$ is there a discernible effect. Below this value of ΔK the use of a high stress ratio results in an approximately times two increase in crack growth rate. This difference compares with a times $8 - 10$ increase in crack growth rate with high stress ratios observed in an air environment. Therefore the environmental influence is not particularly sensitive to mean or maximum stress intensity, except at low ΔK's, but is mainly dependent on the range of stress intensity factor, i.e. ΔK.

In the HAZ, as in the parent material, the maximum environmental influence occurs below $\Delta K = 11MN/m^{3/2}$. Crack growth rates in the 21140XX material are increased by about one order of magnitude whilst the harder HAZ, i.e. the 21070XX material is only increased by a factor of five. Even so the crack growth rate in the softer HAZ is slower than in the hard HAZ, but compared with the parent material both HAZ regions are an order of magnitude slower. Again as in the parent material, the influence of stress ratio is only apparent at low ΔK's; at high ΔK's the data for the two stress ratios merge together. This is evidence of the diminishing influence of mean stress, or mean stress intensity.

Stress corrosion tests

The stress corrosion crack growth rates obtained from fatigue pre-cracked specimens in the 31 plate orientation are shown in Figure 5.8. The tests were carried out in $3\frac{1}{2}\%$ NaCl
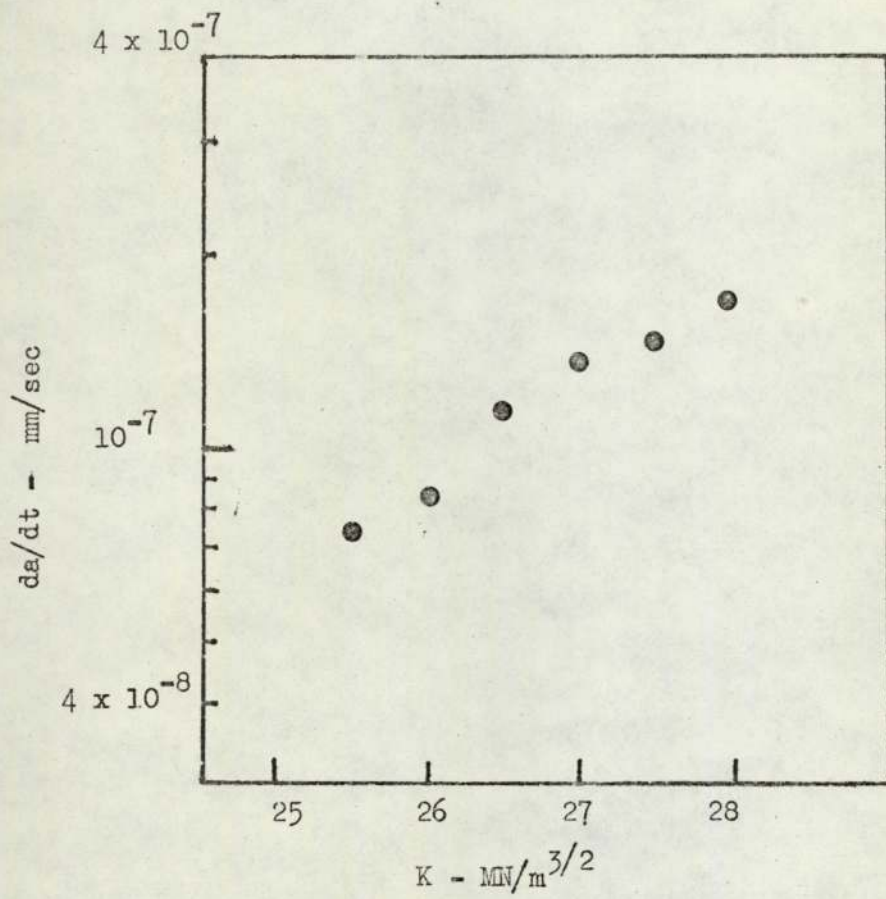
- 85 -

Fig. 5.8 Stress corrosion crack growth
rate in $3\frac{1}{2}\%$ NaCl (31000XX orientation)

solution and the results obtained over a test period of about 100 hours. Testing was stopped before complete fracture of the specimen occurred.

5.2 Frequency and Waveform Variation

The influence of frequency on crack growth rate, in air, for two specimen orientations, 31 and 21 (with fatigue cracks growing parallel and at right angles to the plate rolling direction) are shown in Figures 5.9 and 5.10. For both orientations over a cycling range from 10 to 120Hz only a small frequency effect is apparent. However the lower frequency tests result in faster crack growth rate.

Comparison of the crack growth data for the two specimen orientations shows that the direction of crack growth does not influence the crack growth rate.

The use of triangular, square and sine waveforms (shown in 4.9) at a constant cycling frequency of 10Hz and their effect on crack growth rate are shown in Figure 5.11. The influence of the different wave shapes cannot be differentiated and it is concluded that they all fall in the same scatter band.

In the HAZ the influence of frequency is less apparent than in the parent material (Figures 5.12 and 5.13). However the lowest cycling frequency is now 50Hz instead of 10Hz. This reduction in the difference between high and low frequency from a factor of 12 to $2\frac{1}{2}$ would therefore make resolution of any frequency effect difficult. The influence of waveform shape on the HAZ fatigue characteristics was not examined since the material showed no frequency effect and also because the parent material was not influenced by wave shape.
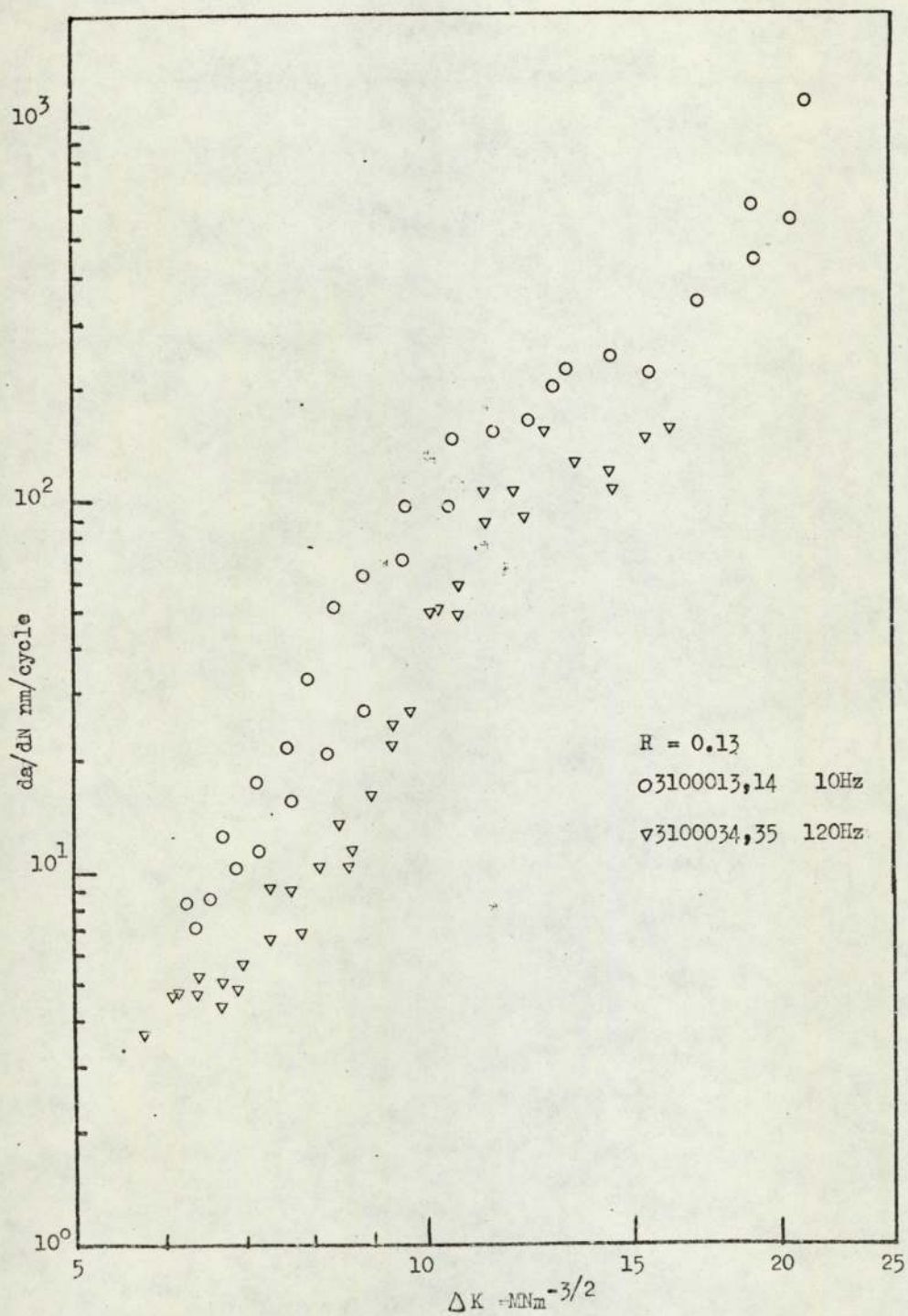
Fig. 5.9 Influence of cycling frequency (sine wave)
on crack growth in air with crack parallel to
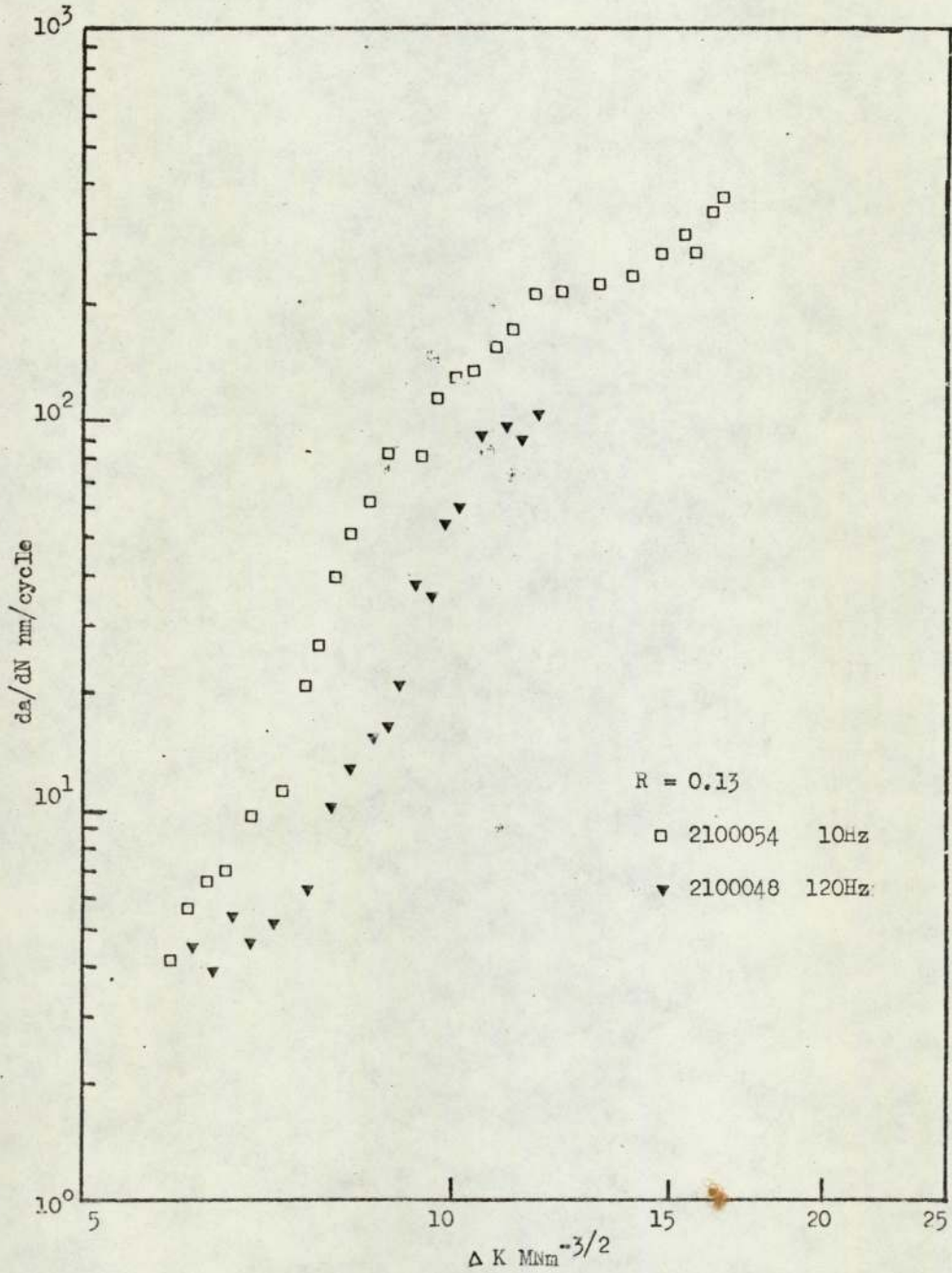primary rolling direction

Fig. 5.10 Influence of cycling frequency on crack growth
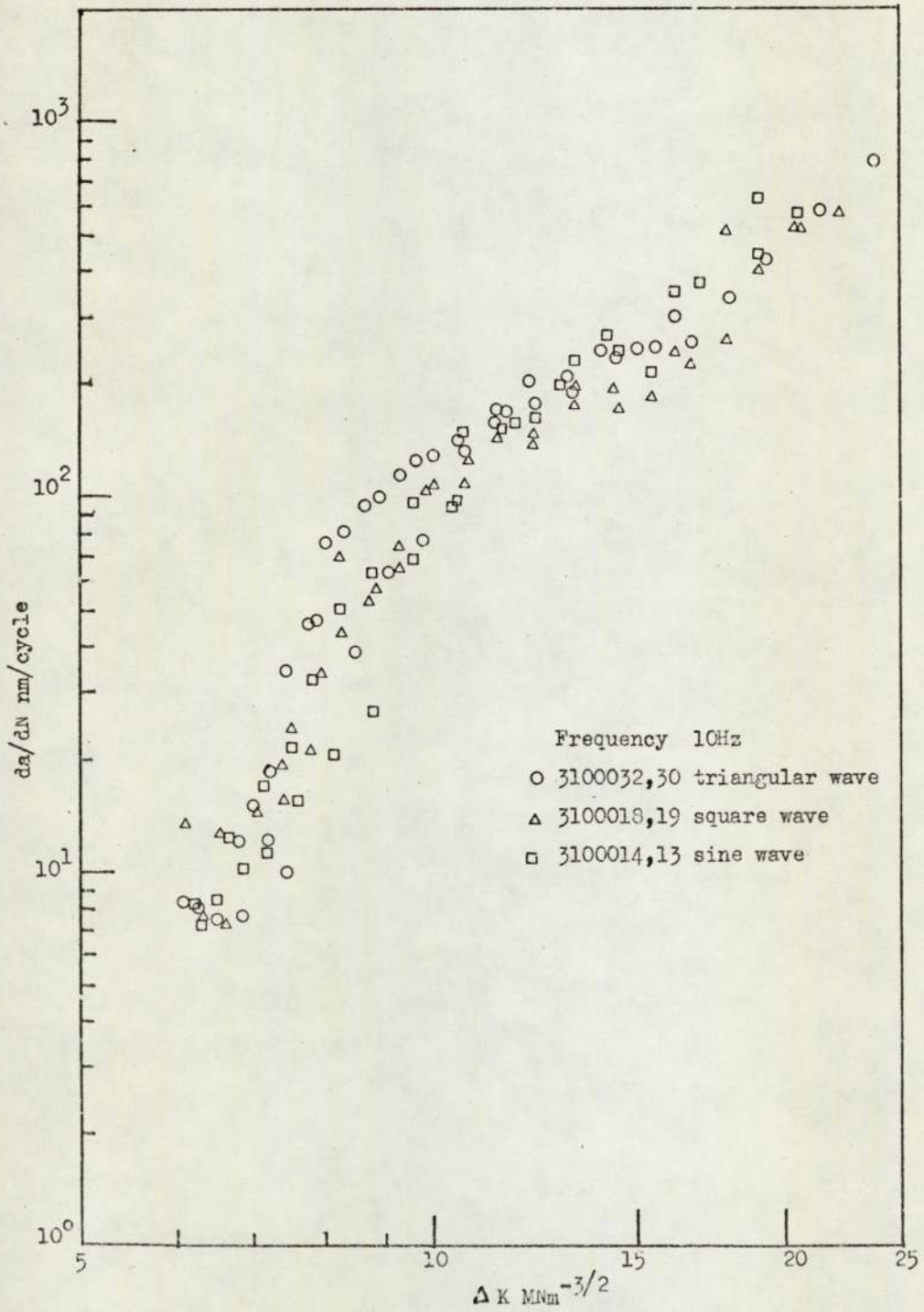in air with crack at right angles to primary rolling
direction

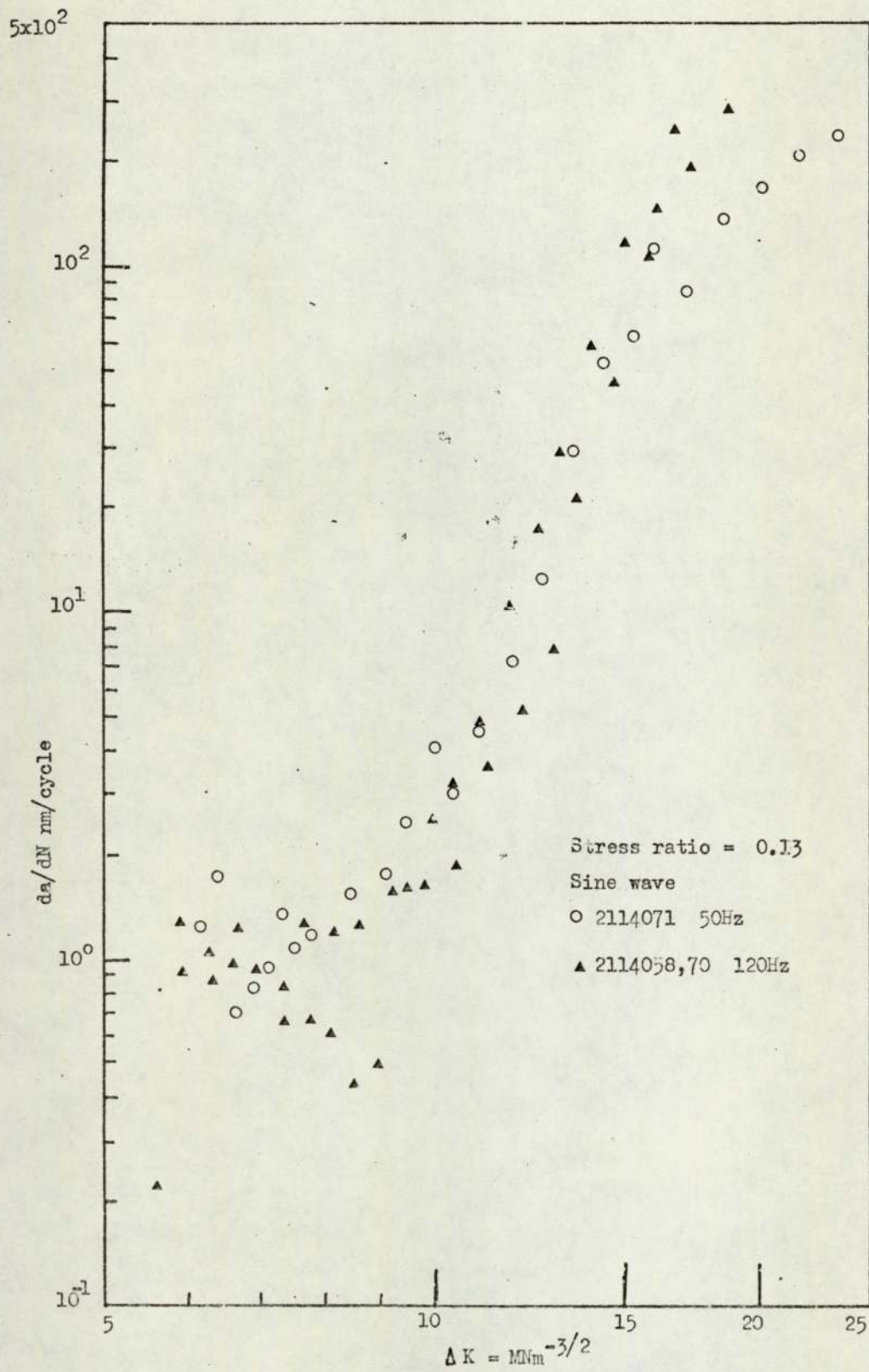Fig. 5.11 Influence of waveform on crack propagation in air.

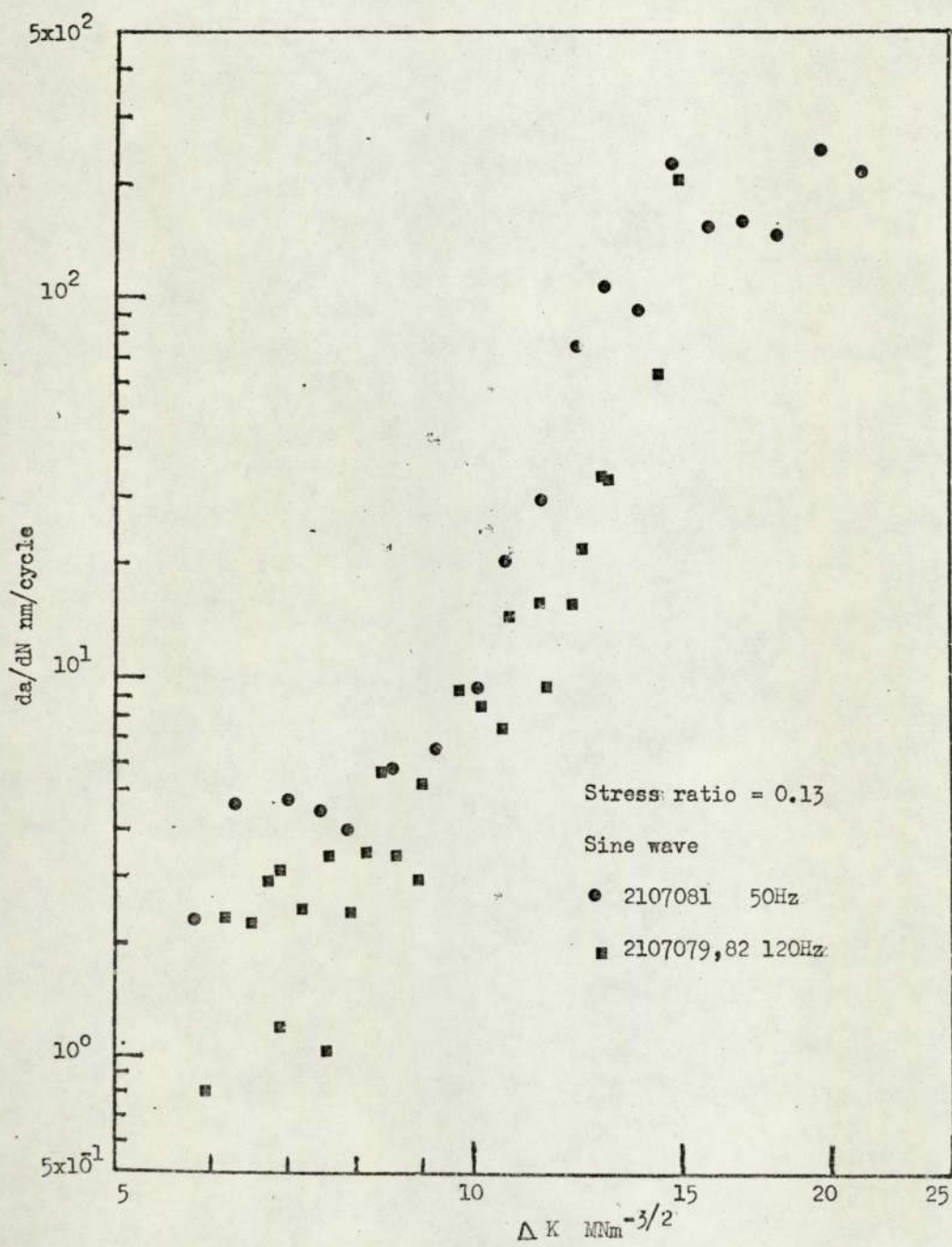Fig. 5.12 Influence of frequency of cycling on crack growth in soft nAZ (air)

Fig. 5.13 Influence of frequency of cycling on
crack growth in hard HAZ (air)

Corrosive environments

The influence of square, triangular and sine waves at a
frequency of 10Hz in the parent material under de-ionized water
and $3\frac{1}{2}\%$ NaCl solution are shown in Figures 5.14, 5.15 and
5.16. For comparison the scatter bands obtained from tests in
air using similar wave shapes, Figure 5.11, are also shown.
These tests indicate that in de-ionized water environmental
influences are not apparent for all the waveforms below
$\Delta K = 10MN/m^{3/2}$. At higher ΔK's environmental influences are

greater but there is no influence of waveform. The data from
the tests in $3\frac{1}{2}\%$ NaCl solution show no threshold value of ΔK,
below which environmental effects are not apparent. However
crack growth rates are increased by a factor of five times
over the values obtained in air. The influence of salt water
solution apart from increasing crack growth rate also reduces
the inflexion in the crack growth curve to eliminate Region 1
growth.

Comparison of the influences of waveform on the salt water
corrosion fatigue behaviour shows that crack growth is
dependent on waveform; slightly faster growth occurs under the
triangular wave than the square wave loading.

The effect of varying frequency from 1Hz to 120Hz under
sine wave loading is given in Figure 5.17. An increase in
crack growth rate with decrease in frequency is apparent.
However the effect is relatively small since the two orders of
magnitude decrease in frequency has resulted in only a 3 - 4
times increase in crack growth rate. Comparison of Figure 5.17
with Figure 5.16 shows that the data for a frequency of 10Hz
falls midway between the 1Hz and 120Hz results.

In the soft HAZ region (21140XX specimens, Figure 5.18) there is no significant influence of frequency on corrosion fatigue. Therefore the environmental component of fatigue crack growth is independent of frequency within the range of 10Hz to 120Hz. The harder HAZ (21070XX specimens, Figure 5.19) does exhibit a higher degree of environmental sensitivity especially in the mid-range values of ΔK.

Comparison of these corrosion fatigue results with the data obtained in air (Figures 5.12 and 5.13) show that at high ΔK's the fatigue crack growths in air and salt water at 120Hz are similar. A further important observation is that constant crack growth rate at low ΔK, characteristic of the air environment tests, is absent in the salt water environment.

5.3 Metallography

The inclusion distribution in the three planes as revealed after polishing are shown in Figures 5.20, 5.21 and 5.22. Comparison of the rolled surface with the other planes shows that the inclusions are roughly plate like. The inclusions are flat and large in the rolled plane while on the other planes they are thin and elongated.

Analysis of the inclusions using an AEI Microprobe Analyser showed that they were mainly of two types, some being rich in iron, manganese and chromium, while others were rich in silicon but also contained some magnesium. Comparison of the X-ray images for iron and silicon with the optical image of the same area showed that the silicon rich inclusions were darker in colour than the iron rich inclusions. Accurate analysis of the inclusions examined with the Microprobe Analyser

was not possible since the inclusions were small in comparison with the diameter of the electron beam. This resulted in interference signals from the matrix surrounding the inclusion. A 'Kevex' Energy Dispersive X-ray analyser attached to a stereoscanning electron microscope was also used to check the composition of the inclusion. This confirmed the qualitative results obtained on the Micro Probe Analyser, except that some magnesium rich particles were detected.

Examination of the etched specimen (Figures 5.23, 5.24 and 5.25) shows that the structure is in a partially recrystallized condition. Recrystallization and some incipient grain growth has occurred in the vicinity of the inclusions. Where the grains are visible they show they are mainly two dimensional in that they have length and breadth with respect to the rolling surface, but little thickness. The structure can be imagined as consisting of layers of 'pancake' type grains stacked on top of each other through the thickness of the plate.
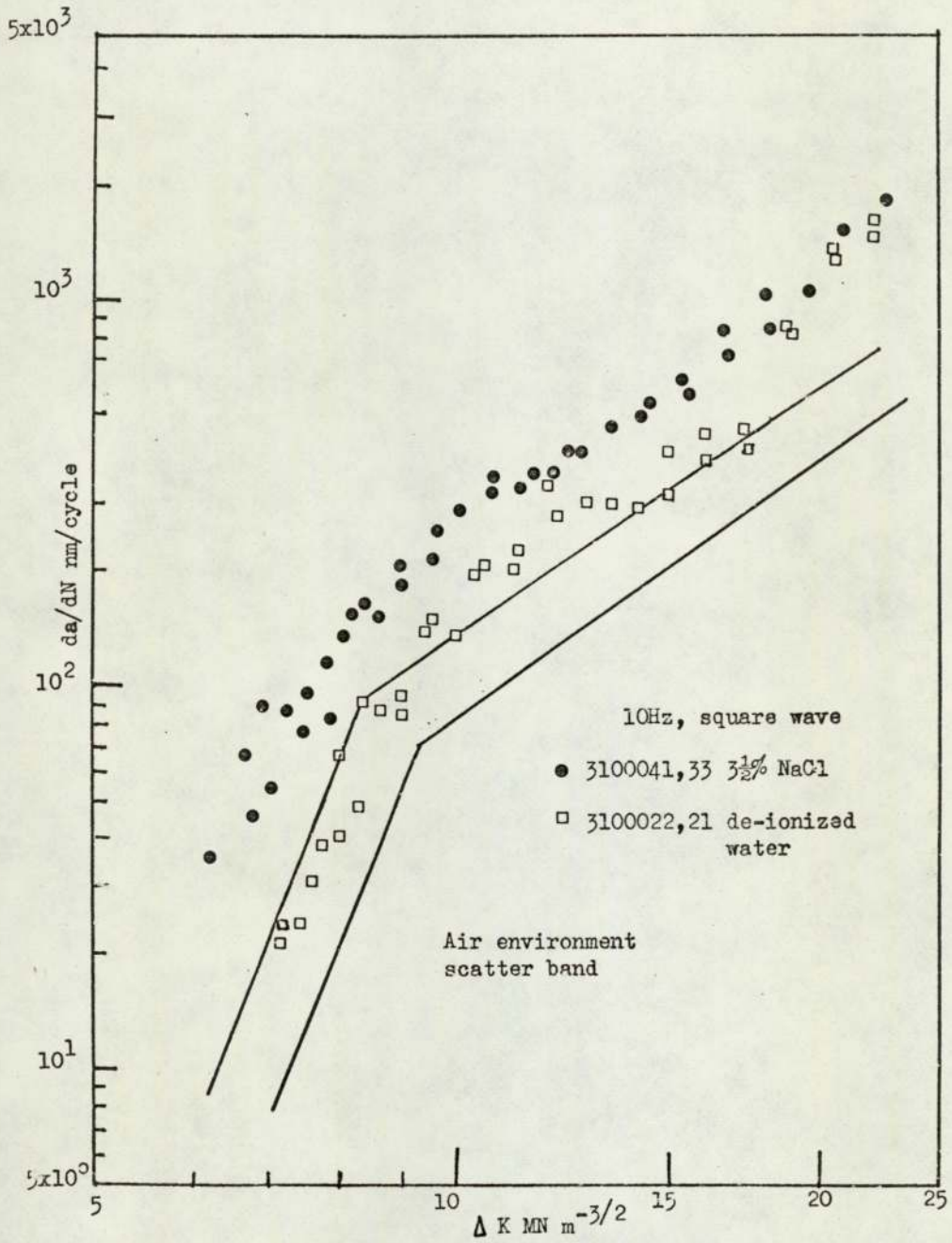
Fig.5.14 Effect of environment on crack

propagation using square wave loading

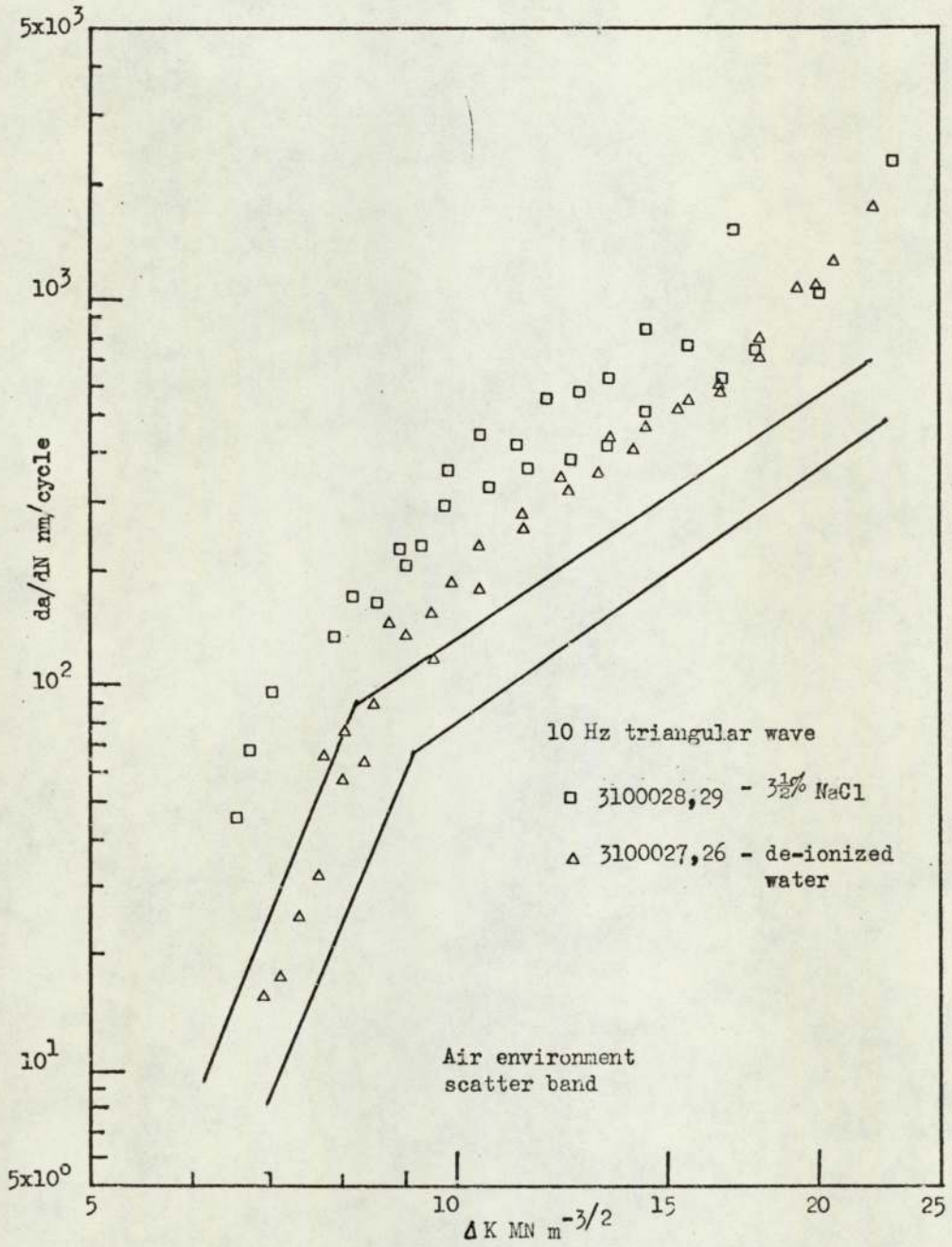Fig. 5.15 Effect of environment on crack
propagation using triangular wave loading
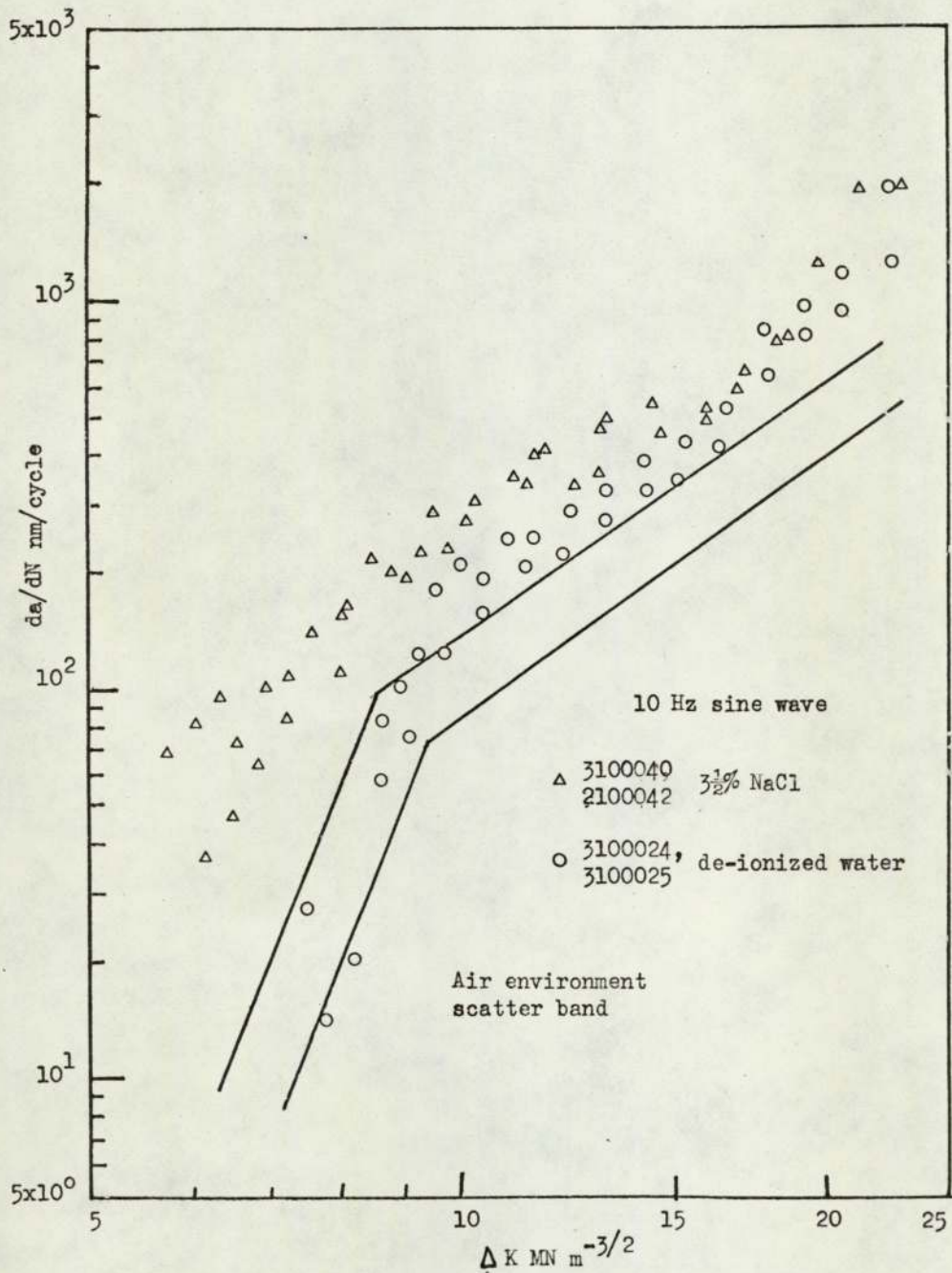
Fig. 5.16 Effect of environment on crack

propagation using sine wave loading
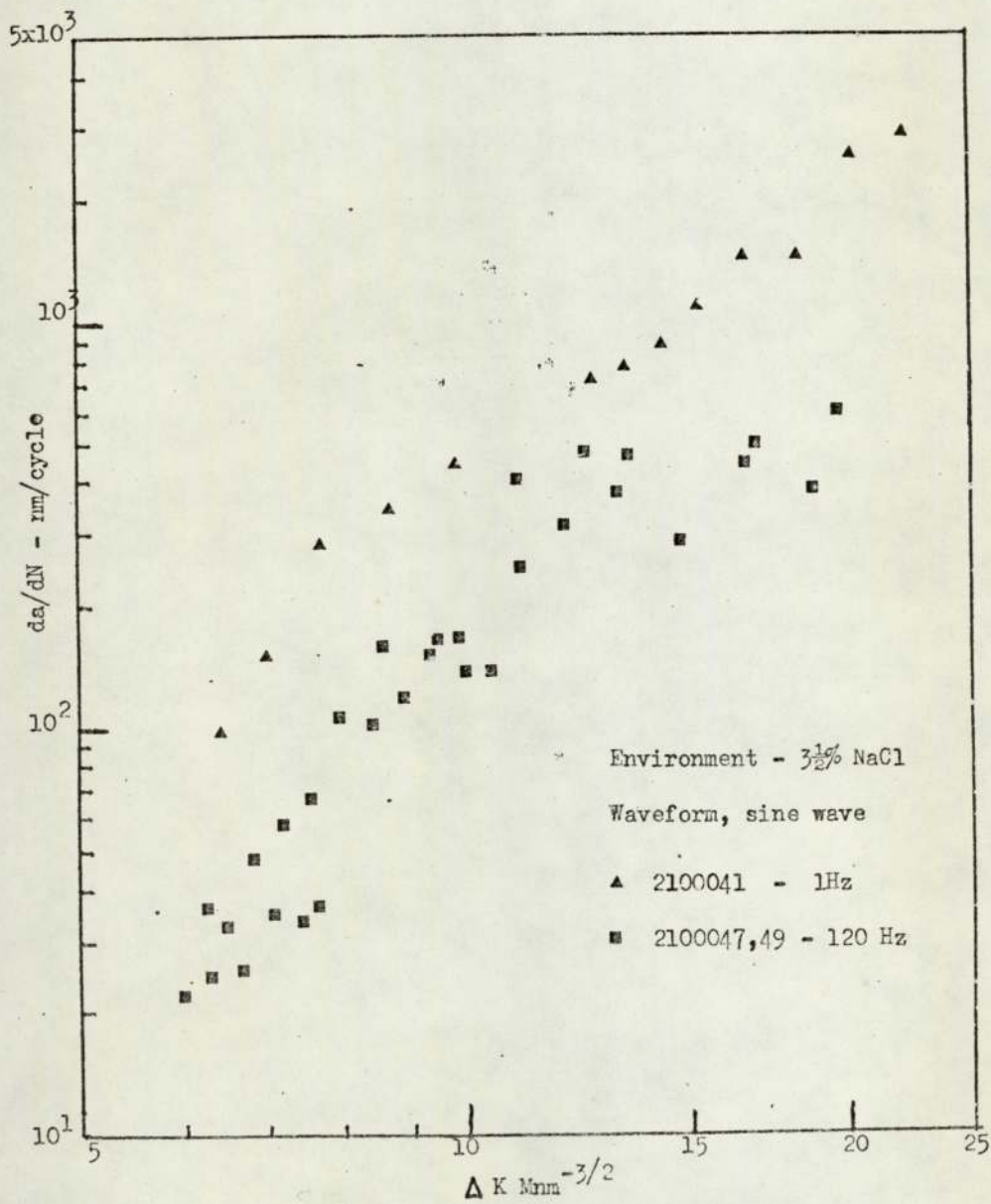
Fig. 5.17 Influence of frequency on crack growth
rate in salt water
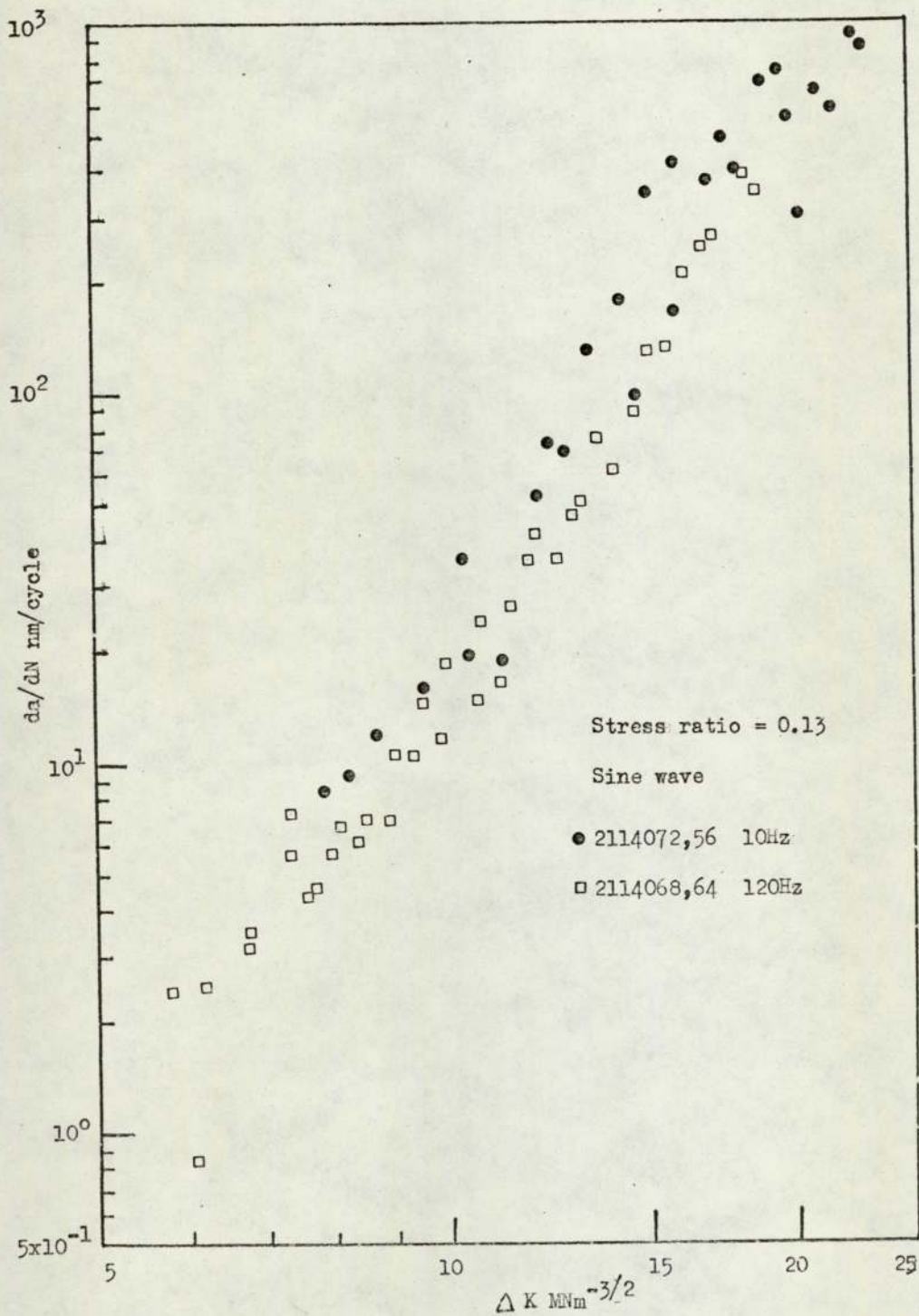
Fig. 5.18 Influence of frequency of cycling in soft

HAZ ($3\frac{1}{2}\%$ NaCl)
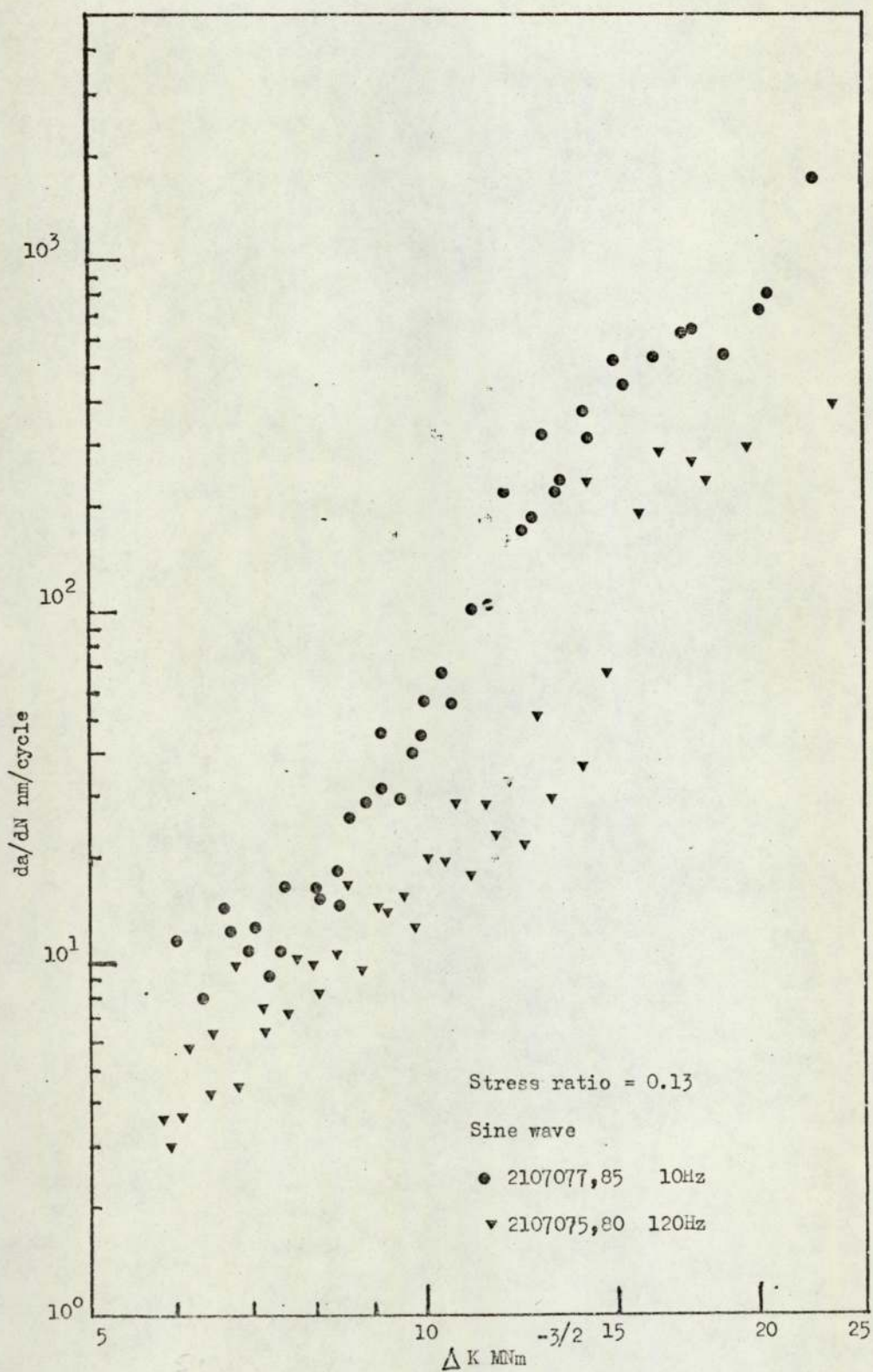
Fig. 5.19 Influence of frequency on cycling in crack growth
in hard HAZ ($3\frac{1}{2}\%$ NaCl)

Figure 5.20   X 350

Polished surface showing inclusion orientation
Longitudinal — rolled surface.
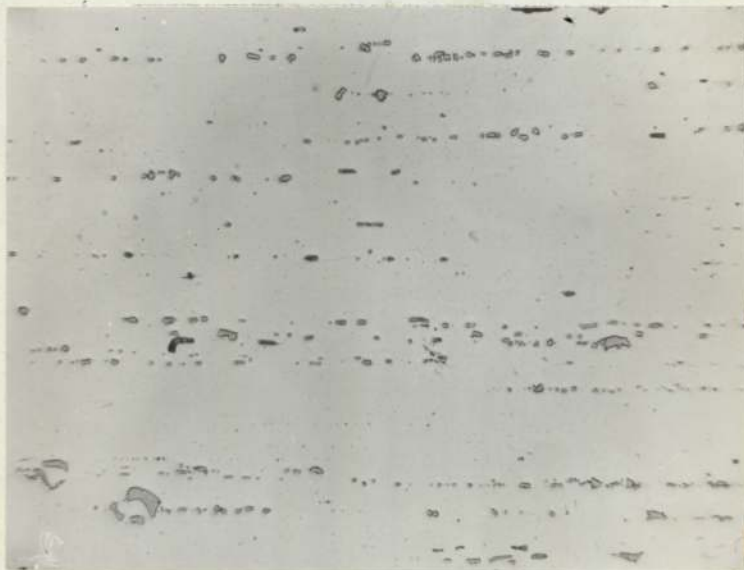
Figure 5.21   X 350

Longitudinal transverse section
(equivalent 31 orientation fracture plane).

Figure 5.22   X 350

Short transverse section,
21000XX fracture plane.

Figure 5.23   X 200

Etched rolled surface.

Figure 5.24   X 200

Longitudinal transverse etched surface.

Figure 5.25   X 200

Short transverse etched surface.

6. DISCUSSION OF RESULTS

Load shedding and stress ratio effects

The influence of load shedding programmes (Figure 4.8) to obtain crack growth data at constant values of ΔK show basically that constant crack growth rate, independent of crack length, as postulated by Paris only occurred over a limited range of crack lengths (Table 4.1). The initial slow growth period can be attributed to achievement of s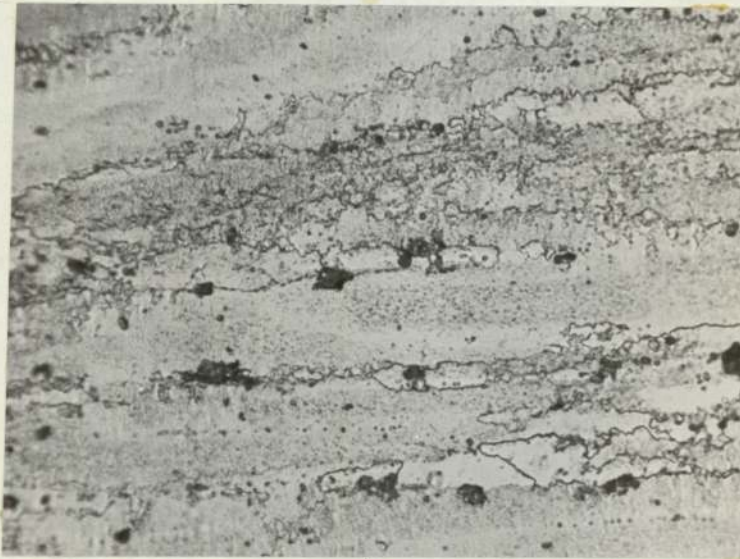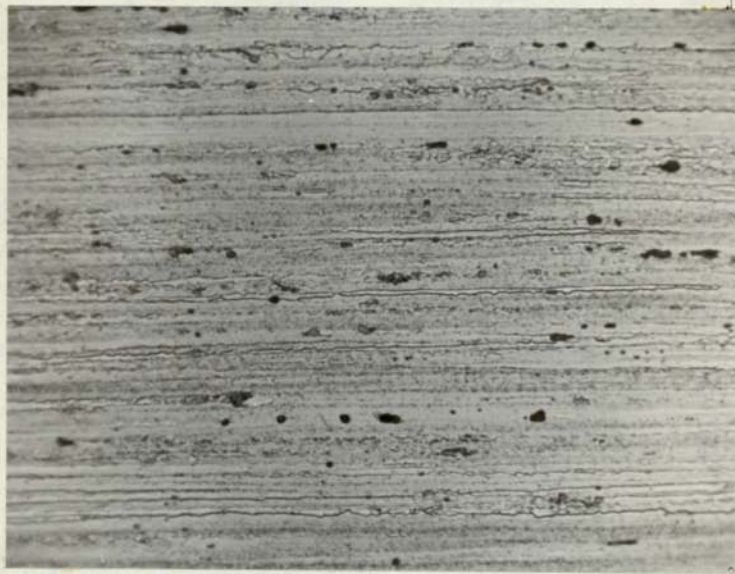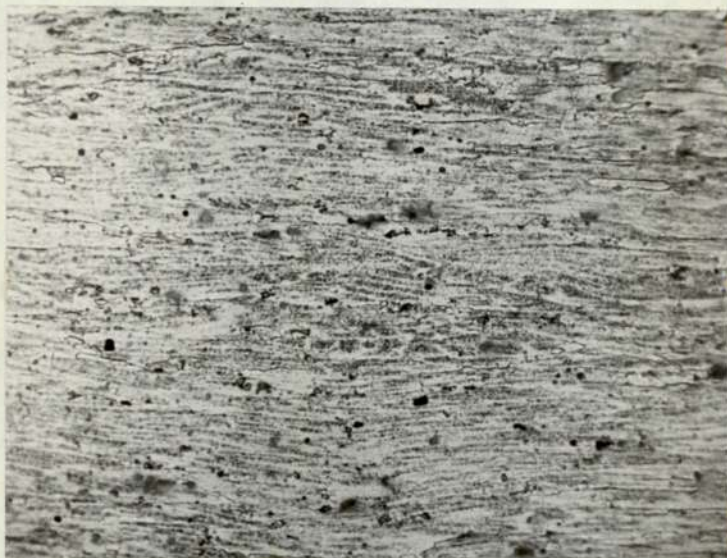table conditions after the initiation of the fatigue crack. However the slowing down behaviour at $a/W > 0.4$ is less easily explained. It should be noted that the stress ratio (R) in all cases increased with increasing crack length. Therefore the decrease in crack growth rate cannot be described in terms of a decrease in R, since an increase in crack growth rate would be expected. The fall of 25 – 50% in crack growth rate cannot be explained in terms of errors in the compliance function because the transition to slow growth occurs within the valid range of the function. The influence of the central load anvil modifying the stress distribution at the crack tip is discounted since the crack is remote from loading point. The calibration curve for the potential drop method shows that errors in measuring crack length could be considered as negligible.

As a result of the load shedding procedure ΔK rises above its nominal value prior to each load reduction. This increase in ΔK becomes more apparent as crack length increases since the compliance function changes more rapidly. The ratios of nominal ΔK (ΔKn) to the actual ΔK (ΔKp) prior to the load

reduction were calculated at each stage in the load shedding. The initial and final ratios for the programme are given in Table 5.1. However when $\Delta Kn/\Delta Kp$ falls below 0.95 a transition to slow crack growth occurs, Table 6.1. This 5% increase in ΔK above its nominal value represents a 10% increase in plastic zone size. Therefore when the new plastic zone, due to ΔKn, has to grow inside the old one, due to ΔKp, the crack propagation rate is reduced.

Von Euw[54] observed similar slowing down behaviour in aluminium when using a load shedding programme to achieve constant ΔK in single edge notch tension specimens. However he was unable to offer an explanation for the phenomenon. Similarly Khairuzzaman[56] observed a slowing down effect in En 24 steel tested under 3 point bending. He was able to explain the effect in terms of the ratio of maximum stress to yield stress. The following equation was derived: $da/dN = (\Delta K)^n R'$, where $R' = \sigma_{max}/\sigma_{ys}$. σ_{max} was defined as the maximum load divided by the gross cross sectional area. However the significance of this definition is not clear since in bending stress is given by $\sigma = yM/I$ and for $y = W/2$, $\sigma_{max} = 6Pmax/BW$. Therefore the value of R' is about six times too small.

Figure 6.1 shows the crack growth rates obtained using the two load shedding programmes together with the constant load amplitude results obtained using two R values. The solid points represent the constant growth periods, while the open points represent the average slow crack growth rate. Most of the load shedding results fall outside the constant amplitude scatter bands showing that crack growth is dependent on the type of loading used. The constant mean load programmes (profile (a)) give higher crack growth rates than the constant minimum

- 91 -

Table 6.1

Specimen	$\Delta Kn/\Delta Kp$		
	Initial	Final	Transition
310002	0.963	0.943	–
310004	0.970	0.951	–
310008	0.963	0.952	–
310008	0.953	0.944	–
310009	0.980	0.964	–
310007	0.975	0.940	0.956
310006	0.972	0.948	0.955
310005	0.973	0.929	0.946
310003	0.975	0.943	0.949

Ratio of nominal (ΔKn) to actual value of ΔK
(ΔKp) at the end of each load shedding block

Constant crack growth rate
▲ constant mean load (profile a)
● constant minimum load (profile b)
Slow crack growth
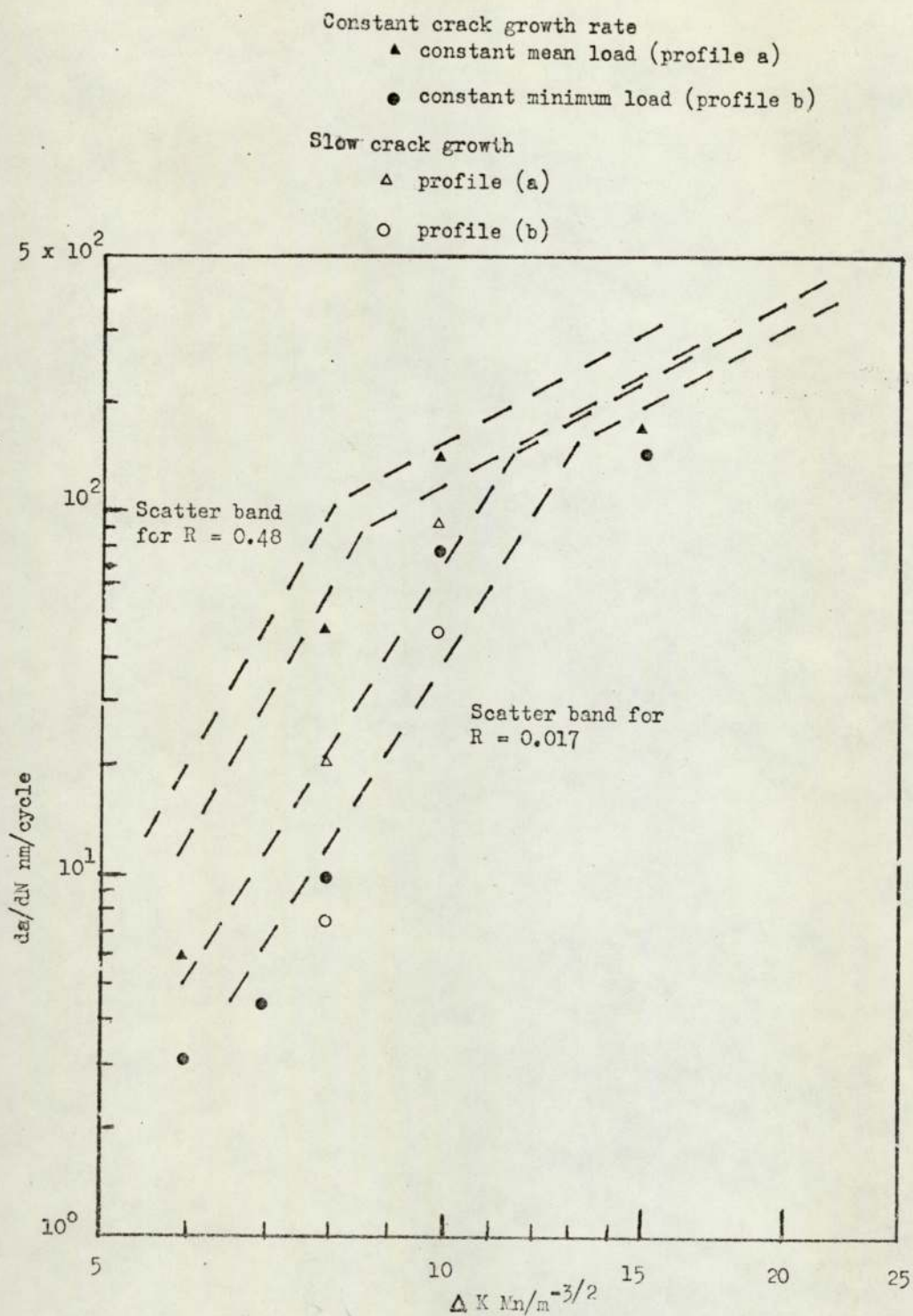△ profile (a)
○ profile (b)

Fig 6.1 Comparison of load shedding, constant ΔK,

with constant load amplitude tests

load amplitude programmes (profile (b)). This is expected as the stress ratios for profile (a) are, on average, higher than those for profile (b). It is apparent from these results that the type of loading programme used influences the crack growth rates obtained. Therefore the ability of Δ K to uniquely characterize crack growth is in doubt. However, it was on the basis of these results that it was decided to continue further tests using constant load amplitude procedures instead of constant Δ K programmes. The reasons for this are outlined below:

1) Uncertainty in the relevance of the slowing down behaviour during load shedding programmes.

2) The majority of the data published has been obtained using constant load amplitude methods, therefore comparison of results would be simpler.

3) Real structure would be subject to constant load amplitude rather than continuously falling amplitude conditions.

4) Since the da/dN curves were not linear, use of load shedding tests would result in a large number of tests being made in order to characterize crack growth rate behaviour of the material.

It has been shown[36] that in aluminium alloys crack growth rate is dependent on mean load and that the higher the mean load for the same load amplitude the higher the crack growth rate. Therefore the higher the R value the higher the crack growth rate. However Figure 5.2 shows that above Δ K = 12MN/m$^{3/2}$ crack growth rate becomes independent of mean load and also independent of maximum load.

Pearson[34] was able to account for the effect of stress ratio in aluminium alloys by using a modified version of Forman's equation[30]. Forman's equation is given by:

$$da/dN = \frac{A \, (\Delta K)^n}{(1 - R) \, Kc - \Delta K}$$

and Pearson's modification is:

$$da/dN = \frac{A \, (\Delta K)^n}{\left[(1 - R) \, Kc' - \Delta K\right]^{\frac{1}{2}}}$$

where Kc' is the limiting value of Kmax obtained during fatigue just before fast fracture.

Both Forman's and Pearson's equations have been applied to the present data (shown in Figure 5.2) and the relationships obtained are shown in Figure 6.2. The value of Kc used was $30MN/m^{3/2}$ and for Kc' a value of $35MN/m^{3/2}$. This latter figure represents the highest value of Kmax observed during fatigue testing. The relationships resulting from these equations is poor. Both equations overcorrect the data for high ΔK's. Therefore consideration of stress ratio and a material property parameter Kc in this does not account for crack growth rate in this alloy.

A further problem not taken into account by the above equations or by Paris's equation is the pronounced change in slope exhibited by this alloy. Liu and Iino[106] have observed three regions in the crack growth rate versus ΔK curve. Hiduminium 48 shows similar behaviour, especially at low stress ratios in that region 1 exhibits a steeper gradient in region 1, at low ΔK's, than in region 2, at medium ΔK's. Region 3 is
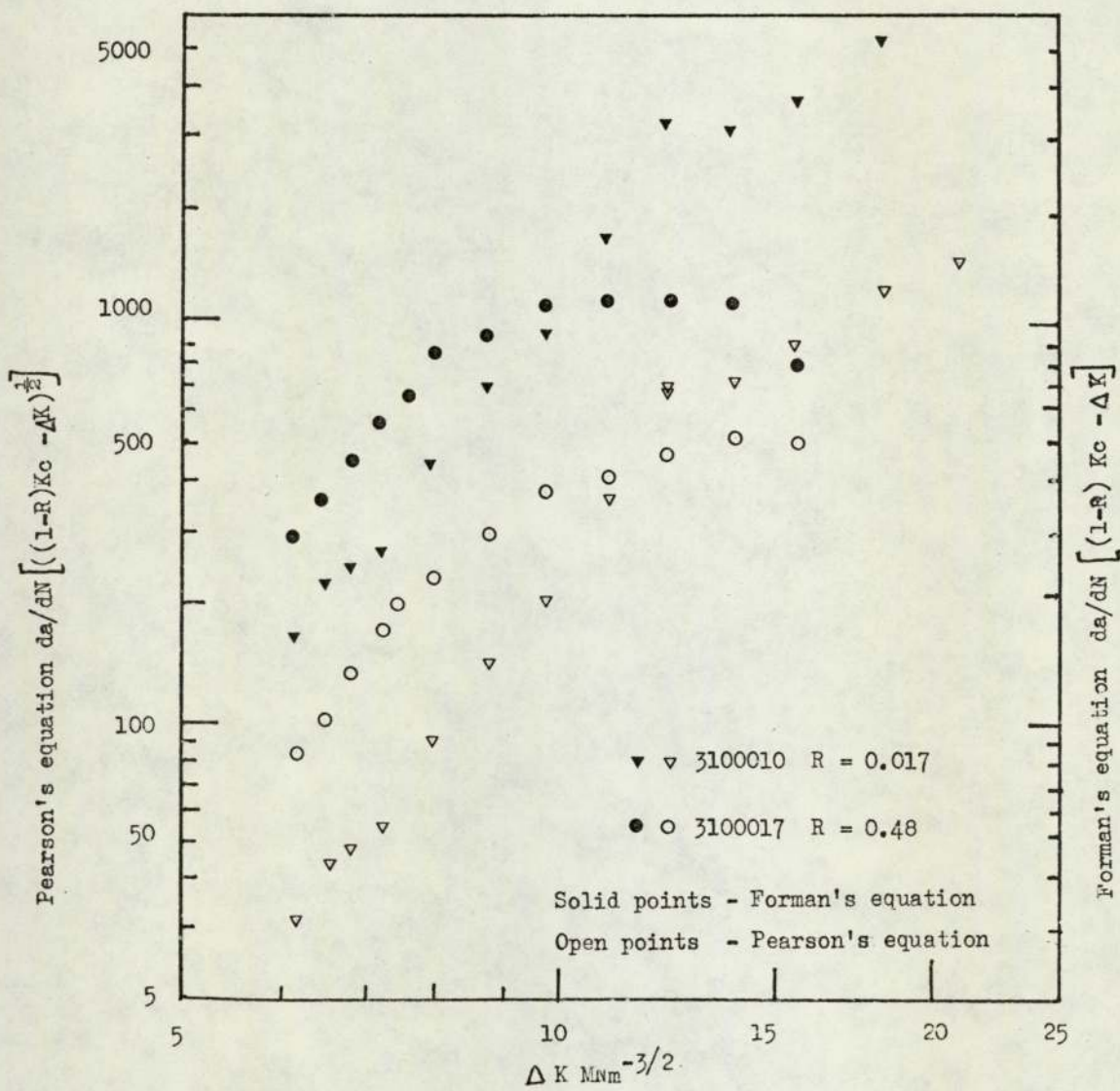
Fig. 6.2 Comparison of Forman's and
Pearson's equations

not clearly defined in the present results since the increase

in gradient of the curve occurs at very high crack growths which

are difficult to measure.

The change in slope from region 1 to region 2 has been

attributed to change in fracture mode from flat to shear

fracture, no such change was observed in Hiduminium 48 - at

either stress ratio. The slope change has also been attributed

to change in the micromechanism of the fatigue process; this

factor is considered later. However, the actual values of the

ΔK transition, more accurately the ΔK transition range,

depend on the mechanical properties of the material. Whilst

the transition in the parent material (σ_{ys} = 499 MN/m$^{3/2}$), at

a stress ratio of 0.48 occurs at ΔK = 8.5MN/m$^{3/2}$, at ΔK =

10 MN/m$^{3/2}$ in the harder part of the HAZ (σ_{ys} = 235 MN/m$^{3/2}$)

and ΔK =11.5MN/m$^{3/2}$ in the soft HAZ (σ_{ys} = 210MN/m$^{3/2}$). There-

fore the transition from region 1 to region 2 crack growth is

controlled by the proof stress; the higher the proof stress

the lower the transition in the slope of the crack growth rate -

ΔK curve. Transitions at a stress ratio of 0.13 were not

measured since they are not clearly defined in the HAZ material.

The large differences in crack growth rate with stress

ratio in the HAZ material (Figures 5.3 and 5.4) and also the

great differences between the parent and HAZ materials have

more practical significance than the change in slope of the

crack growth curve. The reduction in crack growth rate in the

HAZ could have resulted from residual welding stresses. The most

significant of these stresses influencing crack growth would

be the through plate thickness stresses. The presence of

- 94 -

compressive residual stresses in the centre of the plate which can be of yield stress magnitude would retard crack growth rate. However the compressive stresses in the centre of the plate need to be balanced by residual tensile stresses towards the surface of the specimen. These stresses would not increase crack growth rate significantly because crack growth is mainly dependent on the range of stress intensity. However had this residual stress pattern been effective, bowing of the fatigue crack front would have been observed[112], with the central part of the crack front being retarded with respect to the flanks. Since a uniform crack front was observed, any influence of residual stresses must have been small. Although yield magnitude residual stresses would have been generated in the HAZ after welding, these would have been relieved during the subsequent cutting and machining of the specimens; it will be recalled that the original welded plate thickness was 15mm. and the specimen thickness is 12.5mm.

The combination of low strength and high toughness in the HAZ means that the material can absorb more energy during fatigue cycling before crack extension can occur. In other words at a specific ΔK the cyclic plastic zone size in the HAZ is larger than that of the parent material. Therefore for the same fatigue input energy, i.e. the same loading conditions, the energy available for fracture is smaller because a greater proportion is used in deformation. For example the plastic zone radius of the 21140XX material at $\Delta K = 10 MN/m^{3/2}$ is 6.4×10^{-2} mm. whilst that of the parent material is an order of magnitude smaller at 5.3×10^{-3} mm.

Bradshaw and Wheeler[58] have reported that in an overaged aluminium alloy crack growth rates obtained were faster than in the peaked aged, higher strength material. Pearson[48] has compared crack growth rate of an aluminium alloy (2.5Cu, 1.5Mg, 1.2Ni) in the artificial and naturally aged conditions. The naturally aged, lower strength material gave faster crack growth than the higher strength artificially aged material.

The present results indicate that in the partially reverted and natrually aged region of the HAZ a reduction of crack growth rate occurs. Therefore the behaviour of a reverted structure is significantly different to an overaged structure even though both have strengths lower than the peak aged material.

Maddox[113] has measured tha fatigue behaviour of simulated HAZ in carbon manganese steels and only found a slight reduction in crack growth compared with the parent materials. The behaviour could be attributed to the presence of residual compressive stresses in the HAZ.

Dover[53] and Donahue[46] have interpreted crack growth rate in conjunction with crack tip opening displacement, δ, and concluded that as δ increased so did crack growth rate. The alternating δ was found to be proportional to $\Delta K^2/2\sigma_{ys}E$ therefore a decrease in yield strength should result in an increase in crack growth rate. In view of these factors it appears that another material parameter is required in order to account for the decrease in crack growth rate in the HAZ. Forman's and Pearson's equations do consider the stress ratio and fracture toughness of the material, but previously

in this section it was observed that neither equation was
able to account for the effect of stress ratio. When these
equations were applied to the HAZ data, the difference between
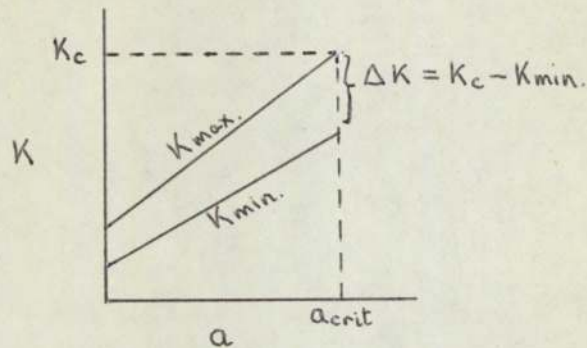high and low stress ratio crack growth rates were still
evident.

Figure 6.3

In order to take into account variations in crack growth
between the parent material and HAZ regions some material
parameter needs to be considered. The common material para-
meter characterising fracture is K_{1c} or Kc. Kc is the limit-
ing maximum value of stress intensity in the fatigue cycle
before failure occurs. Under constant load amplitude conditions
the stress intensity range increases with increase in fatigue
crack length. With positive stress ratios this results in
both the minimum and maximum values of stress intensity in the
fatigue cycle increasing with increase in crack length. This
situation is shown schematically in Figure 6.3. When the
value of Kmax reaches the critical stress intensity Kc, failure
occurs, in other words, when Kc-Kmin = Kmax-Kmin or ΔK = Kc-Kmin.
Therefore as the ratio of ΔK to Kc-Kmin approaches unity
the closer the crack length becomes to the critical length for
final failure to occur.

Since both ΔK (Kc-Kmin) and crack growth rate are proportional to crack length, crack growth rate can be correlated with the ratio of ΔK to (Kc - Kmin). Therefore for a particular value of ΔK the higher Kc becomes, due to higher material toughness, the lower the ratio ΔK/Kc - Kmin which results in a reduction of crack growth rate. The general equation which describes this behaviour can be expressed as:

$$\log \ da/dN \ = \ A \left[\frac{\Delta K}{Kc - Kmin} \right] + B$$

or $\log \ da/dN \ = \ A \ (Q) + B$

where A and B are experimental constants.

In addition to taking into accouht the fracture toughness the equation considers the role of stress ratio. An increase in the stress ratio results in an increase in Kmin which results in an increase in crack growth rate.

In order to test the applicability of the Q factor to the crack growth data for the HAZ and parent material in Hiduminium 48 the previous ΔK/da/dN data were recalculated in terms of Q and da/dN. A graph of the conversion of ΔK to Q for the stress ratios and fracture toughnesses used is given in Figure 6.4. Initially the correlation between the high and low stress ratio fatigue data for the HAZ 21140XX material was tried. Figure 6.5 shows that an encouraging trend is obtained. The large differences in crack growth rate with stress ratio obtained when the data was plotted conventionally is diminished. Therefore one fatigue equation can be used to express the crack growth rate behaviour of the HAZ subject to different stress ratios.
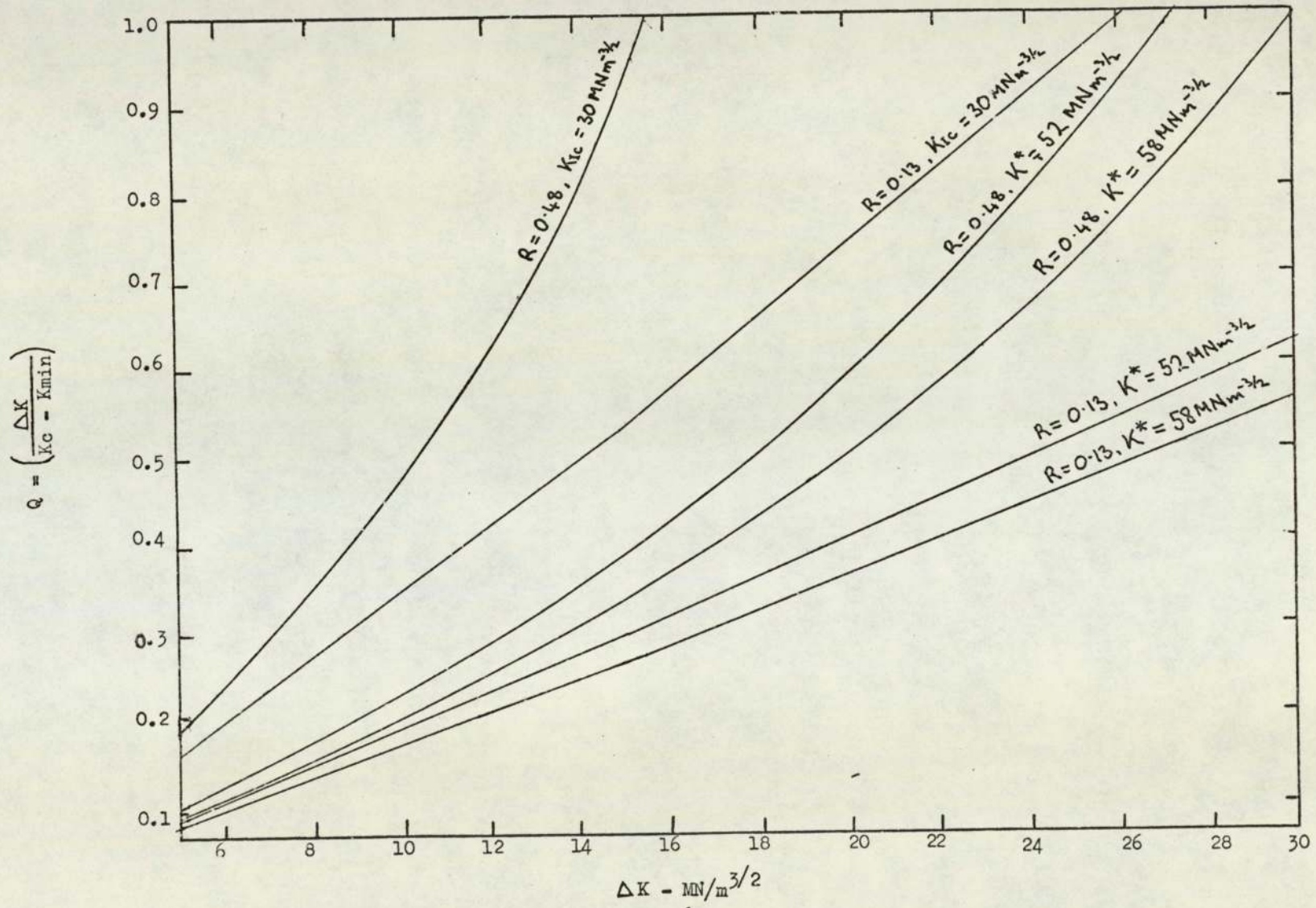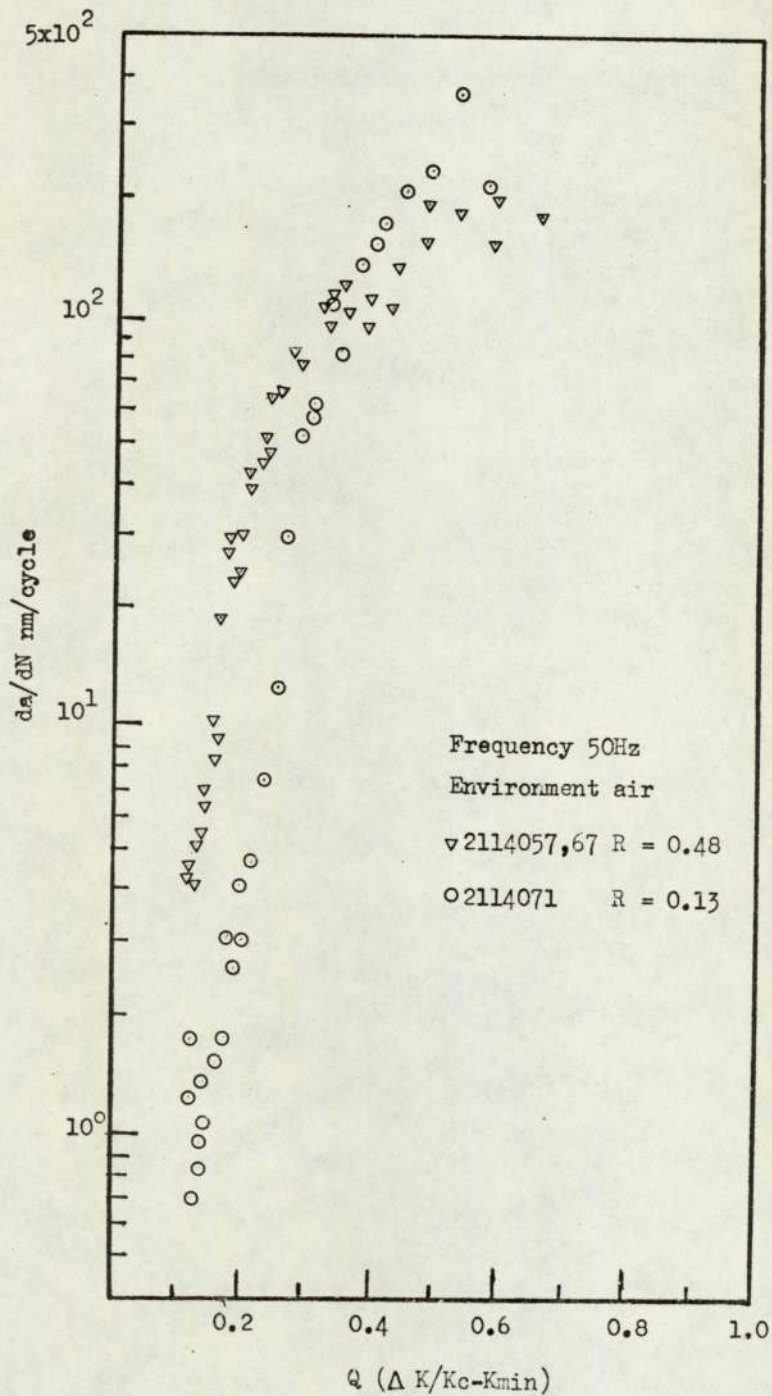
Fig. 6.4 Conversion graph of ΔK to Q

Fig. 6.5 Crack propagation rate as a
function of Q for two stress ratios

As a further check on the applicability of Q the effect of variations in fracture toughness between the two HAZ regions and the parent material were tested. Figure 6.6 demonstrates the ability of the Q factor to normalize the crack growth rates to a single curve. The relationship between Q and crack growth rate still shows the same two stage growth behaviour which was characteristic of the da/dN /ΔK curves. Therefore two fatigue equations are required to express the whole range of crack growth exhibited by the material. However a relationship based only on stage I crack growth would lead to a conservative estimate of fatigue life.

These results show that the Q concept in which crack growth rate is expressed as a function of the ratio of stress intensity range to the remaining available stress intensity (Kc - Kmin) is useful in accounting not only for stress ratio, but also for the fracture properties of the material. To use a design curve based on these principles it is still necessary to know the initial defect size in a structure and the loading conditions, in order that ΔK, Kmin and hence Q can be calculated. The life of the structure, that is the number of cycles required before the crack reaches a critical length for fast fracture to occur, can be found by integrating the design curve.

Fatigue fracture mechanisms in the parent material

In order to consider in further detail the mechanisms involved in the crack growth behaviour of the alloy the results from the fracture surface examination are discussed. In the parent material the change in slope of the crack growth rate - ΔK curve at about $12MN/m^{3/2}$ (when R = 0.13) indicates that
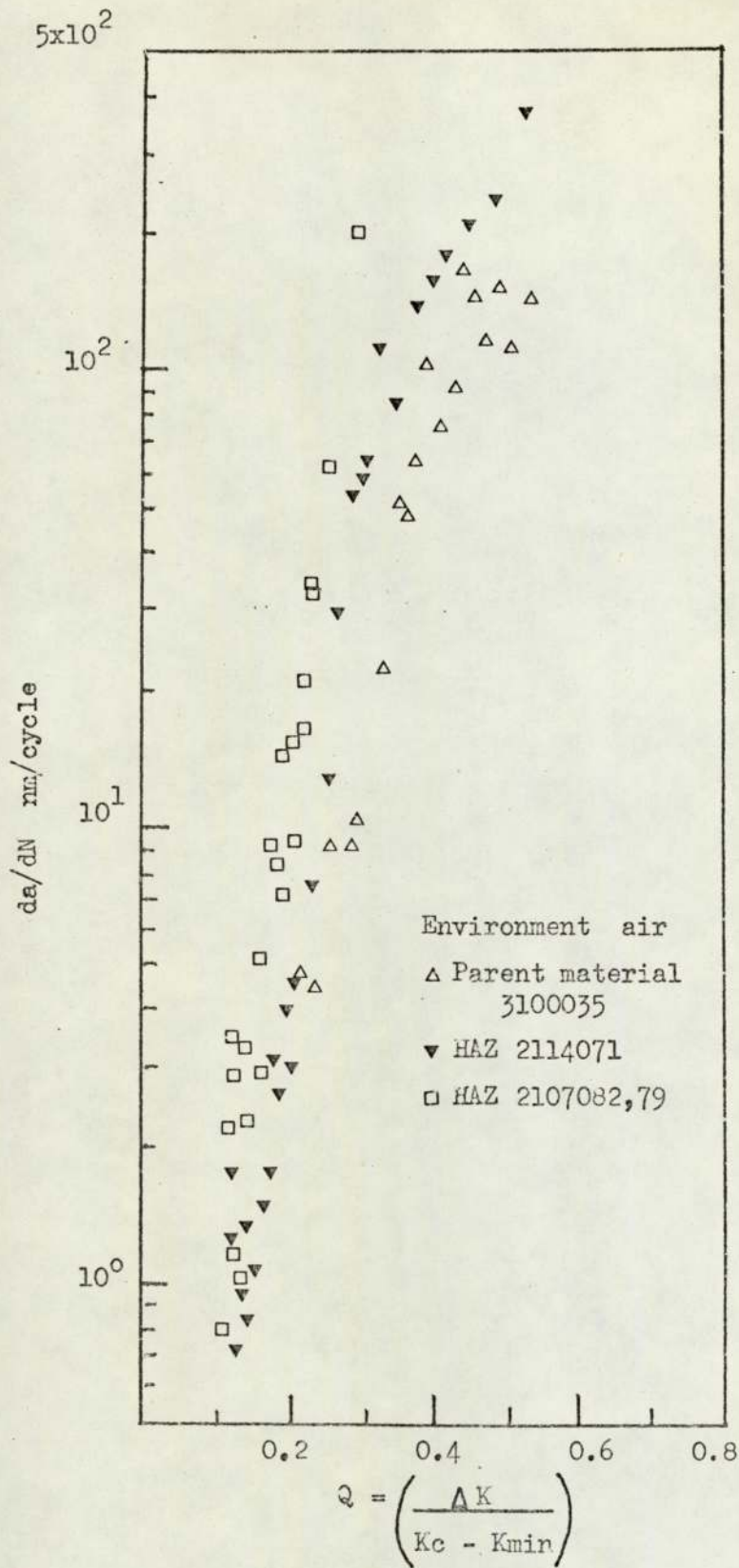
Fig. 6.6 Crack propagation rate as a
function of Q for parent material and HAZ
(stress ratio = 0.13)

there may be a change in mechanism controlling crack growth.
Examination of the fracture surfaces show that at low ΔK's
the fracture appearance is complex being composed of furrows
and facets (Figures 6.7 and 6.8). Some faceted areas have
associated with them steps and resemble microcleavage.
Similar stepped fracture has been reported by Feeney et al[66]
in 7075 aluminium alloy, who termed it "step-wise growth".
The step spacings do not bear any direct relationship to the
macro fatigue crack growth rate, but are about two orders
of magnitude larger than indicated by the latter. The
cleavage like appearance of the steps indicates that their
formation must have resulted suddenly after a build of strain
energy ahead of the crack tip. Adjacent to some of these
regions are areas of flat regions which under higher magnifica-
tion are covered with ductile striations. The striation

spacing was measured and, assuming that each striation was
produced by a load cycle, this distance would give the micro
crack growth rate. Comparisons of micro growth rates measured
in this way with the macro crack growth rate show good agree-
ment at medium ΔK's; Figures 6.9 and 6.10.

It should be noted that the ability to see striations
depends on their spacing and the resolution of the microscope.
For the instrument used striation spacings less than 400 $\overset{\text{o}}{\text{A}}$
are unresolvable. This means that the limit on measuring
micro crack growth is 40nm/cycle, and this equivalent to ΔK
of about $7MN/m^{3/2}$ for low stress ratios.

The 1 : 1 correlation between micro and macro crack growth
rates suggest that the controlling fatigue crack growth
mechanism is one of striation formation. Therefore fracture

Figure 6.7   X 52

Air fatigue fracture surface showing furrowing.

$\Delta K \approx 8MN/m^{3/2}$
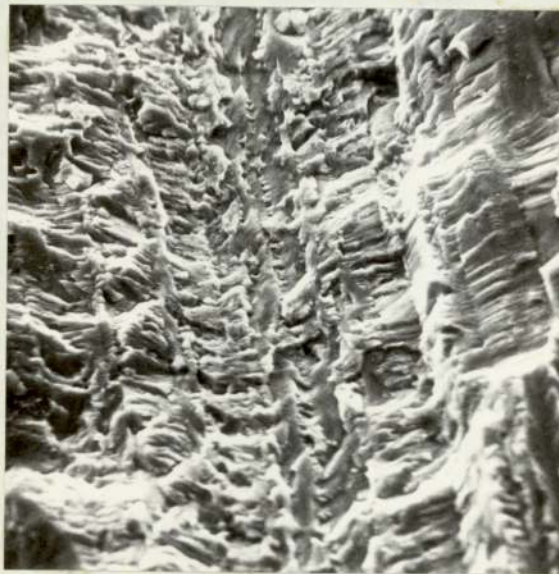

Figure 6.8   X 490

As Figure 6.7 but showing details of stepwise growth.

Figure 6.9   X 9000

Ductile striation crack growth in an
air environment, with striation spacing
equivalent to observed crack growth
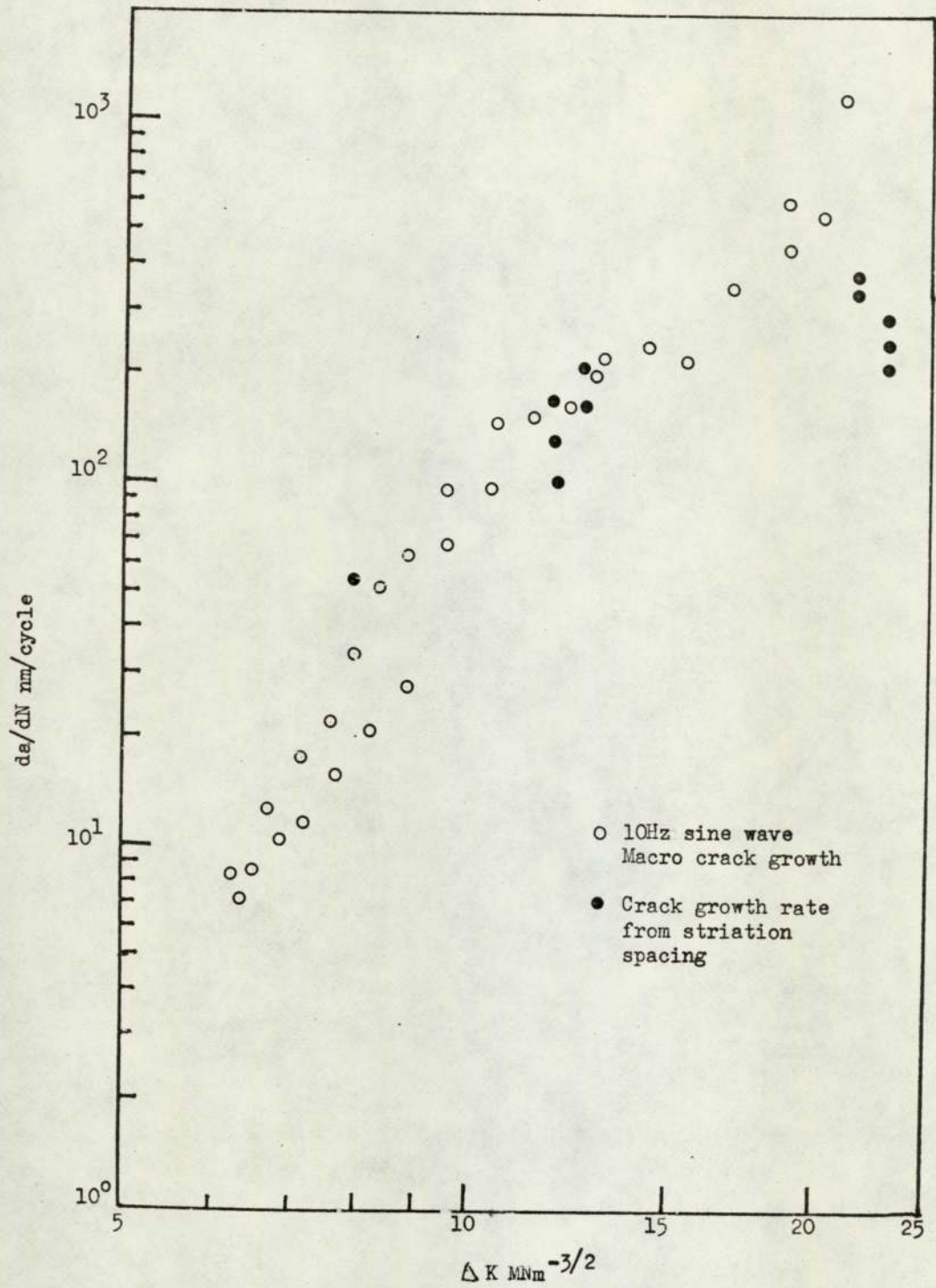rate.
$\Delta K = 12 MN/m^{3/2}$

Fig. 6.10 Comparison of macro and micro (striation
spacing) crack growth rates in air

surface details other than striations are minor variables in terms of crack growth. However the evidence for this mechanism is only for medium ΔK's. Figure 6.10 indicates that about $\Delta K = 8MN/m^{3/2}$ striation spacings are longer than the macro fatigue crack growth rate. Therefore striation formation may not be the controlling mechanism below this value of ΔK. A similar observation to this was made by Heiser and Hertzberg[111] on steel plate and by Bates and Clark[43] on 7079-T6 aluminium alloy. They concluded that each load cycle was not resulting in a formation of a striation and that other mechanisms were influencing crack growth.

Although Hiduminium 48 does not show a pronounced grain structure, evidence of a 'grain like' structure is shown by the low ΔK fracture surfaces. It is suggested that some form of grain orientation controlled crack growth, as suggested by Robinson[75], coupled with the cleavage like stepwise growth features are the controlling fatigue mechanisms at low ΔK's. The appearance of large spaced striations occurs in local regions of the crack front which initially lag the main front, since these regions must finally propagate faster than the loading fronts in order to catch up with them.

At high ΔK's the striations are more easily resolvable (Figures 6.11, 6.12) but their spacings are equivalent to crack growth rates less than the macro crack growth rate. Under these conditions a new mechanism of fracture occurs and this is by microvoid coalescence (Figure 6.13). Therefore the measured crack growth rate is the sum of the slower striation formation mechanism and the faster void coalescence mechanism.

Figure 6.11   X 1350

Ductile striation crack growth together
with evidence of void coalescence.
Striation spacings less than observed
crack growth rate.

$\Delta K = 22 \, MN/m^{3/2}$

Figure 6.12   X 3300

As Figure 6.11 showing striation
details.

The fracture surfaces show that the result of increasing ΔK and stress ratio is an increase in the volume fraction of microvoids. Since the primary mechanism of fracture in the fracture toughness test was by microvoid coalescence (Figure 6.14) the incidence of this mechanism during fatigue crack growth results from the Kmax component of the fatigue cycle. The amount of microvoid coalescence also depends on the volume of precipitates present in the matrix, and El-Soudani and Pelloux[70] found that increases in precipitate volume in 7075 aluminium caused an increase in the amount of void formation. Increases in the occurrence of microvoid coalescence resulted in increased crack growth rate; this confirms the present observations.

A further feature observed on the fracture surfaces was the presence of furrows (Figure 6.7). These are related to the microstructure of the alloy since they follow the inclusion and fibrous flow of the material. This relationship is indicated by the similarity of the inclusion stringer spacings, 0.05mm., and the furrow spacing, 0.02mm. However, since the stringer spacings were rather irregular, only a general order relationship is implied. The occurrence of furrows is related to environmental conditions and this factor is considered in more detail later.

Influence of corrosive environment

The influence of frequency of cycling in an air environment on the parent material is small. Figures 5.9 and 5.10 show that for both specimen orientations the lower frequency results in faster crack growth rate. It has been suggested that frequency effects in precipitation hardened aluminium alloys

- 102 -

Figure 6.13   X 410

Complete void coalescence during
fatigue at high ΔK's,

$\Delta K = 22MN/m^{3/2}$
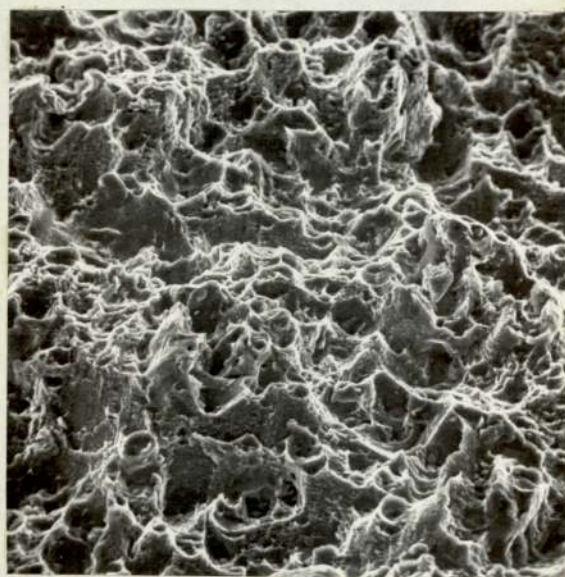

Figure 6.14   X 380

Void coalescence mode of fracture
during fast fracture after static
loading, i.e. fracture toughness
test,

are a result of overageing or reversion occurring at the crack tip[58]. In Hiduminium 48 reversion occurs more easily than overageing since ageing hardening occurs sluggishly. Reversion or resolution of the coherent G.P. zones is supposed to occur more readily at low cycling frequencies and results in a faster crack growth rate. Figures 5.9 and 5.10 show that higher crack growth rates are obtained at 10Hz. However, the HAZ tests, (Figures 5.12 and 5.13) show that reversion results in slower crack growth than the peak aged material. The increased crack growth rate is consistent with observations that this results from the increasing influence of water vapour in the atmosphere becoming apparent at low fatigue frequencies[77, 79].

An interesting point emerges from the test results given in Figures 5.9 and 5.10 in which the crack growth rates for two specimen orientations, notched at right angles to the primary plate rolling direction (21000XX and 31000XX respectively, are compared. These tests show that there is no influence of orientation. Nordmark and Kaufman[110] found that the rate of propagation was higher in the transverse than in the longitudinal specimens taken from extruded panels of aluminium 7075 (equivalent to 31000XX and 21000XX specimens respectively). These observations were consistent with the fracture toughness rating of the material. In the current plate material used the differences in metallographic and mechanical properties between the longitudinal and transverse directions were not sufficient to affect crack growth.

Although there is a frequency dependency on crack growth rate the influence of changes in wave shape, i.e. sine, triangular and square waves, show no such effect (Figure 5.11).

Bradshaw et al.[102] observed a similar independency of crack growth with waveform shape in a DTD 5070A aluminium alloy, in which more extreme types of waveform were used, i.e. pulsed spike and sine waveform.

The crack growth rates for the three waveforms in the de-ionized water environment are shown in Figures 5.14, 5.15 and 5.16. For comparison the scatter bands of the tests done in air from Figure 5.11 are also given. These tests show that environmental influences are not apparent for all the waveforms below $\Delta K = 10 MN/m^{3/2}$. At higher ΔK's environmental influences are greater but there is no influence of waveform. The value of $\Delta K = 10 MN/m^{3/2}$ indicates a threshold stress intensity range below which environment does not influence fatigue crack growth rate. However according to Speidel[97] the threshold ΔK in aluminium is about $2 MN/m^{3/2}$. The threshold behaviour is consistent with the rate of passivation mechanism put forward by Ford[98]. If the rate of passivation is greater than the film rupture rate at the crack tip, which is controlled by the ΔK level, the influence of environment is not apparent. Above $\Delta K = 10 MN/m^{3/2}$ the rate of film rupture exceeds the passivation rate, therefore fatigue crack growth rate increases.

It is interesting to note that the threshold stress intensity very nearly coincides with the change in slope of the crack growth rate curve. Region 1 is therefore insensitive to water environments while region 2 is sensitive.

The data from the tests in $3\frac{1}{2}\%$ NaCl solution are shown in Figures 5.14, 5.15 and 5.16. In this environment no threshold value of stress intensity range is apparent but crack growth

rates are increased by a factor of five times over the values obtained in air. The influence of $3\frac{1}{2}\%$ NaCl solution apart from increasing crack growth rate also reduces the inflexion in the crack growth rate curve to eliminate region 1 growth. In terms of Ford's mechanism the introduction of the chloride ion into the water reduces the passivation rate at the crack tip resulting in an increase in crack growth rate.

The acceleration of crack growth in sodium chloride solution may be a result of stress corrosion mechanism. However the stress corrosion tests, Figure 5.8, result in crack growth rates of about 10^{-7}mm/sec at a stress intensity of $26MN/m^{3/2}$. Typical corrosion fatigue crack growth rates at this ΔK level (which is nearly equivalent to Kmax since the stress ratio was low) are of the order of 2×10^{-3}mm/cycle at a frequency of 10Hz. The difference between this rate and the air fatigue crack growth is about 10^{-3}mm/cycle. Converting this cyclic growth rate into the equivalent static rate results in growth rates of 2×10^{-2}mm/sec. Therefore the stress corrosion crack extension rate is about four orders of magnitude lower than the corrosion fatigue crack growth rate. This means that the time spent at maximum load during the fatigue cycle does not influence crack growth rate. Therefore the square waveform should not result in faster crack growth than the triangular waveform. However, comparison of the corrosion fatigue crack growth rates for these waveforms shows that these are not the same, Figures 5.14, 5.15 and 5.16. In fact the sawtooth wave produces faster growth than the square wave. Barsom[100] has observed similar behaviour in steels in $3\frac{1}{2}\%$ NaCl and found

that crack growth rate depended on the rate of rise of load.
A dependency of crack growth rate on rise time in a high
strength aluminium alloy in which the corrosive medium was
distilled water has, however, not been found (ref. 101).

To investigate further the influence of rise time the
results from tests in which the frequency of cycling was changed
by two orders of magnitude were examined. In these tests
sinusoidal waveforms cycling at 1Hz and 120Hz were used and
the results obtained are shown in Figure 5.17. A clear influence
of frequency is shown, but in order to compare these results
with those obtained using different waveforms a common parameter
must be used. This parameter was taken to be the time taken
for the stress intensity to rise from its minimum to its
maximum value. From the crack growth rate versus ΔK curves
obtained a series of crack growth rates were taken, at specific
ΔK's, and compared with the stress intensity rise time.
These results are given in Table 6.2 and are shown plotted in
Figure 6.15. Thus the behaviour of the square wave, compared
with the sine and triangular wave forms, in producing lower
crack growth rates can be explained. The dependency of crack
growth rate on K rise time is marked at low ΔK's, but its
effect decreases with increase in ΔK. Extrapolation of the
curves in Figure 6.15 to very low K rise times indicates that
crack growth rate would increase until at nearly static stress
intensities the stress corrosion growth rate would be predicted.
However the observed stress corrosion crack growth rates were
very much lower than those obtained under corrosion fatigue
conditions, therefore some limiting K rise time must exist below

Table 6.2

Table of K rise times showing the influence of
frequency and waveform on crack growth in $3\frac{1}{2}\%$ NaCl

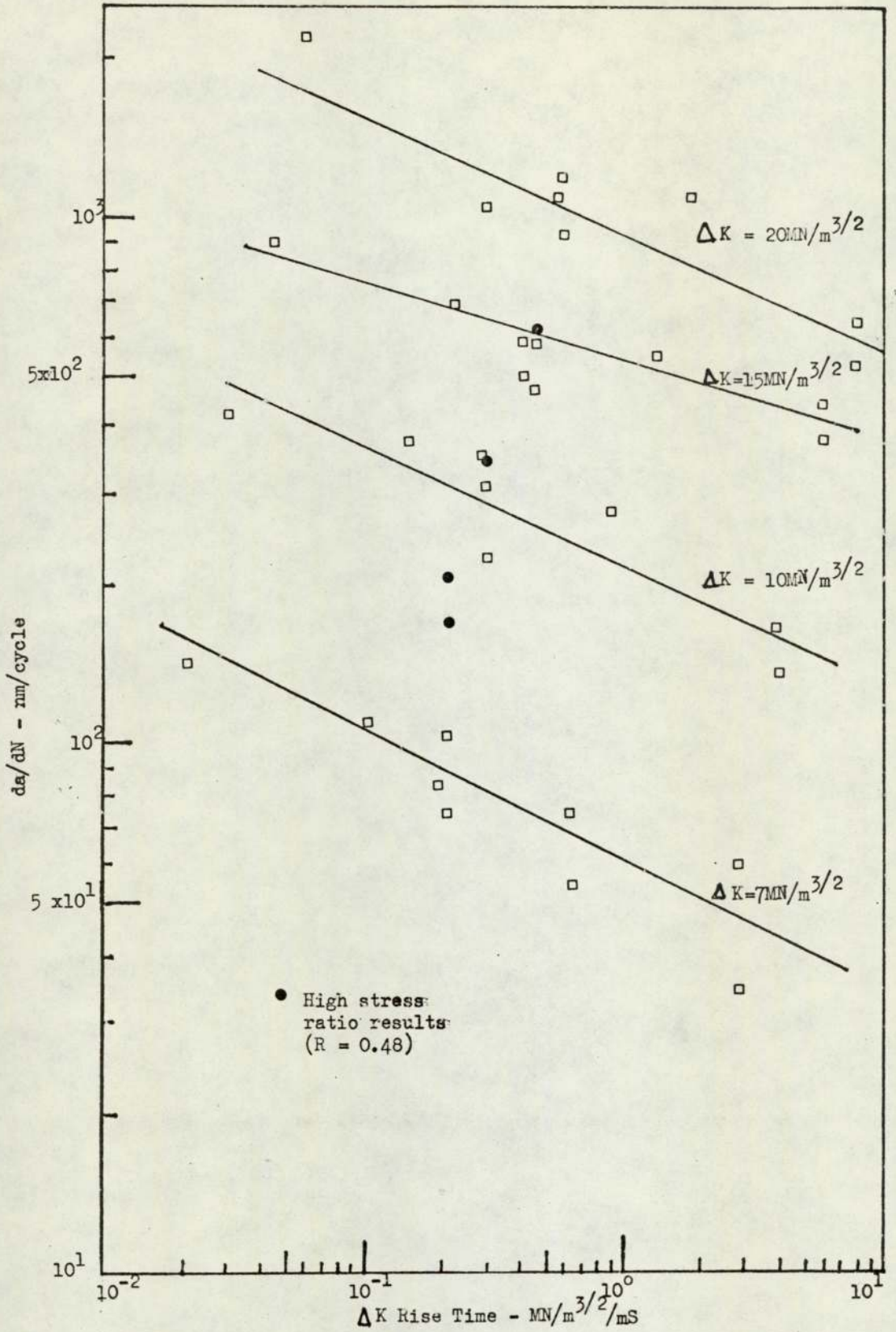| Waveform	Rise Time millisecs (ms)	Crack growth rate da/dN - nm/cycle - 1st line ΔK/rise time - $MN/m^{3/2}mS^{-1}$ 2nd line			
		$\Delta K = 7$	$\Delta K = 10$	$\Delta K = 15$	$\Delta K = 20$ $MN/m^{3/2}$
Sine 120Hz	2.48	35 - 50	140 - 170	380 - 350	550 - 640
		2.84	4.04	6.06	8.08
Sine 10Hz	32.3	75 -105	230 - 310	480 - 580	950 -1200
		0.22	0.31	0.47	0.62
Sine 5Hz	64.6	112	380	692	1047
		0.11	0.16	0.23	0.31
Sine 1Hz	323	144	430	910	2200
		0.022	0.031	0.046	0.062
Triangular 10Hz	34.6	85	360	500 - 560	1100
		0.20	0.29	0.43	0.58
Square 10Hz	10.8	56.75	280	550	1100
		0.65	0.93	1.39	1.86

Fig. 6.15 The influence of Δ K rise time on corrosion
fatigue crack growth behaviour

which crack growth rate falls to its stress corrosion value.
A similar observation was made by Barsom[93] on steel in $3\frac{1}{2}\%$
NaCl. This behaviour is peculiar since both very fast and
very slow K rise times result in decrease in environmental
sensitivity affecting crack growth.

These observations indicate that a definite amount of new
metal surface is required for environmental influence to
become apparent. With slow increases in stress intensity new
surface is not produced rapidly enough and crack growth is
governed by the slow, stress corrosion controlled, anodic
dissolution of material at the crack tip. In other words, the
rate of film formation at the crack tip, resulting in effectively
passivating the metal surface, is greater than the film
rupture rate due to the cycling load. At fast K rise times
the reverse occurs and the mechanical component of fatigue
crack extension exceeds environmental influences. Barsom[100]
found that the use of positive sawtooth waveforms in $3\frac{1}{2}\%$ NaCl
reduced environmental influences to such an extent that the
crack growth rates were the same as those observed in air. The
present results, however, do not show such a dramatic reduction
in crack growth rate with fast K rise times, e.g. a square
wave. A further factor that needs to be considered is the
reduction in crack growth rate with increase in frequency,
observed in air, on the K rise time effect. In Table 6.3
the difference between crack growth rates at 10 and 120Hz in
air and $3\frac{1}{2}\%$ NaCl are given, but it is apparent that a larger
frequency effect is observed in the $3\frac{1}{2}\%$ NaCl environment.

Therefore the K-rise time parameter takes environmental
influences into account more than any air frequency effect.

Table 6.3

Table showing the influence of environment on crack
growth at two frequencies

Test	da/dN (nm/cycle) in air at $\Delta K =$			
	7	10	15 $MN/m^{3/2}$	20
Air 10Hz	9 - 14	90 - 130	240 - 300	500 - 560
Air 120Hz	5 - 6	50 - 75	110 - 140	-
Δ da/dN	4 - 8	40 - 55	130 - 160	-
$3\frac{1}{2}\%$ NaCl 10Hz	75 - 105	230 - 310	480 - 580	950 - 1200
$3\frac{1}{2}\%$ NaCl 120Hz	35 - 50	140 - 170	380 - 450	550 - 640
Δ da/dN	40 - 55	90 - 140	100 - 130	400 - 560

The results discussed so far have been on tests done at low stress ratios (R = 0.13), however the influence of mean or maximum load can be determined by using higher stress ratios. The use of the high stress ratio results can therefore be used to test whether the K-rise time dependency of crack growth rate still occurs (Figure 5.5). Although the stress ratio was increased by a factor of approximately four times the effect on crack growth rate is small - only at ΔK's below $10MN/m^{3/2}$ is there a discernible effect. Therefore any stress corrosion effects are not sufficient to affect crack growth rate significantly since no increase in crack growth rate with R was observed at high ΔK's.

The crack growth rate obtained from these high stress ratio tests are plotted on the K rise time diagram and are indicated by the solid points, Figure 6.15. At ΔK's of 10 and $15MN/m^{3/2}$ the trend shown by the previous low stress ratio tests is followed. These results again show that the environmental effects in Hiduminium 48 are dependent not only on ΔK but more particularly on the K-rise time. The results for ΔK's below $10MN/m^{3/2}$ do not fall on the relationship produced at low stress ratios and reflect the influence of mean or maximum stress intensity.

The lack of correlation of the high stress ratio low ΔK in Figure 6.15 may result from differences in crack tip area exposed to the environment compared with the low stress ratio tests. Although under similar ΔK conditions the cyclic crack opening displacement is independent of stress ratio the actual minimum and maximum values are not. The influence of

stress ratio on the minimum cyclic value of crack tip displacement and its effect on crack tip area can be calculated as follows:

$$G = n \delta \sigma_{ys} \quad \text{, where} \quad \delta = \text{crack tip opening displacement}$$

and $K^2 = \dfrac{EG}{(1 - v^2)}$

therefore $\delta = \dfrac{K^2 (1 - v^2)}{n \sigma_{ys} E}$

At a ΔK level of $7 MN/m^{3/2}$, Kmin at R = 0.48 = 5.5 $MN/m^{3/2}$ and for R = 0.13 Kmin = 0.5 $MN/m^{3/2}$.

Therefore

$$\frac{\delta R = 0.48}{\delta R = 0.13} = \frac{(5.5)^2}{(0.5)^2} = 120$$

Therefore the increase in crack tip area due to an increase of R from 0.13 to 0.48 is 120 times (since area = δB, and B the specimen thickness is constant).

Such an increase in crack tip area may make the process of re-passivation more difficult, and sufficient, at low values of ΔK, to accelerate crack growth rate. Above $\Delta K = 10 MN/m^{3/2}$ the mechanical component of fatigue crack extension tends to outweigh environmental influences.

In the HAZ material the influence of cycling frequency from 50Hz to 120Hz in air, on fatigue crack growth was negligible, Figures 5.12 and 5.13. However in the $3\frac{1}{2}\%$ NaCl environment the soft HAZ material, 21140XX specimen (Figure 5.18) surprisingly shows no influence of cycling frequency over the range from 10Hz

to 120Hz. The 21070XX material, Figure 5.19, does exhibit an
influence of frequency but the effect is only small. Although
the effect of the salt water environment in increasing crack
growth rate is apparent at low and medium values of ΔK its
effect is almost independent of the range of cycling frequency
used. As a result of this observation and also because the
corrosion fatigue crack growth rates measured in the HAZ were
about one order of magnitude lower than the parent material
comparison of the HAZ and parent material in terms of stress
intensity rise time could not be made.

If the corrosion fatigue is considered to be due to the
relative imbalance between competing mechanisms of oxide rup-
ture and film passivation occurring at the crack tip, it appears
from the present data that an increase of cycling frequency
of over one order of magnitude is not sufficient to produce
an increase in oxide rupture rate which would raise crack growth
rate. However the oxide rupture rate is primarily dependent
on ΔK, but at sufficiently high values of ΔK the purely
mechanical component of fatigue can outpace corrosion influence.

This is observed in the 21140XX material where at high ΔK's
both corrosion and air fatigue crack growth rates attain the
same value.

Environmental fatigue mechanisms

Fracture surfaces at low ΔK's for the fast K-rise times
exhibit features that are common to those shown by the air
fatigue fracture surfaces. These are smooth flat areas and
V-shaped features pointing in the direction of crack propaga-
tion (Figure 6.16). Under high magnification the flat areas

have striations associtaed with them (Figure 6.17). However measurement of the striation spacings show that they are about one order of magnitude greater than the macro crack growth rate.

In contrast the slow K-rise time fracture surfaces, although partially covered by corrosion product, show cleavage-like features (Figure 6.18). These features contribute to the faster crack growth observed in the slow K-rise time tests.

At high ΔK's, the fast K-rise time fracture surfaces exhibit regions of relatively greater ductility in the form of void coalescence (Figure 6.19). These regions are adjacent to brittle striation pockets. Evidence of ductility in the slow K-rise times is shown by the presence of widely spaced voids, (Figure 6.20) however, this occurs only at very high ΔK's where the mechanical component of crack extension outpaces environmental influences.

These observations indicate that slow rise times result in high crack growth rates by promoting cleavage-like fracture. Further evidence for this behaviour is shown by comparing the square wave (fast K-rise time) with the sine wave tests (slow K-rise time) at the same frequency of cycling (Figure 6.21 and 6.22). The sine wave shows more cleavage-like fracture and step-wise growth than the square wave fracture surface.

At high ΔK's the use of both high and low stress ratios resulted in similar crack growth rates and this is reflected by the similar fracture surface features. Figures 6.23 and 6.24 show that fracture is by predominantly micro void coalescence. This implies a smaller contribution from the environment since micro void coalescence was the predominant

Figure 6.16   X 465

Fatigue fracture surface in a corrosive
environment ($3\frac{1}{2}\%$ NaCl). Cycling frequency 120Hz.

$\Delta K = 7.7$ MN/m$^{3/2}$

Figure 6.17   X 1900

As figure 6.16 but showing details
of brittle striations. Spacing $\approx$900nm.
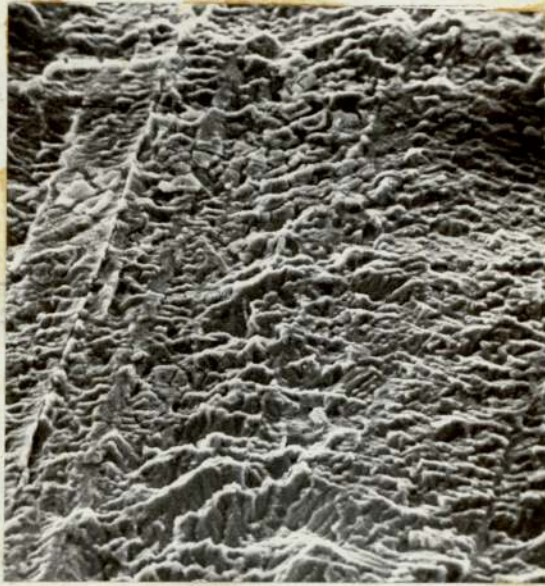crack growth rate = 64nm/cycle.

Figure 6.18   X 360

Corrosion fatigue fracture surface resulting
from 1Hz sine wave loading in $3\frac{1}{2}\%$ NaCl
showing presence of corrosion product
and evidence of cleavage.

$\Delta K = 7.2$ MN/m$^{3/2}$
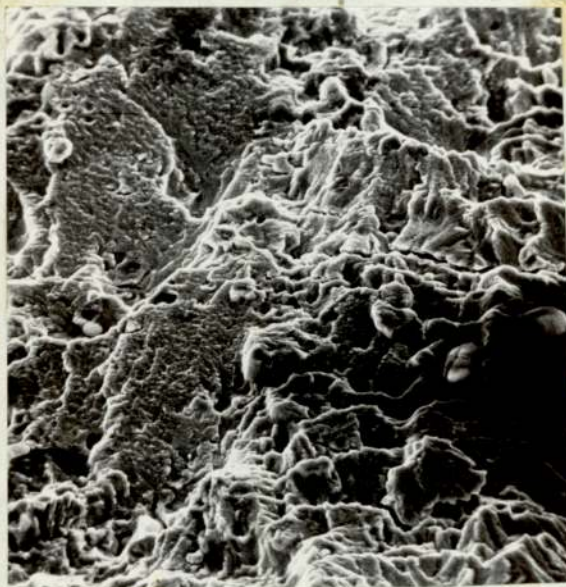
Figure 6.19   X 410

Mixed mode fracture, brittle striations
and void coalescence. 120 Hz.

$\Delta K = 19.5$ MN/m$^{3/2}$
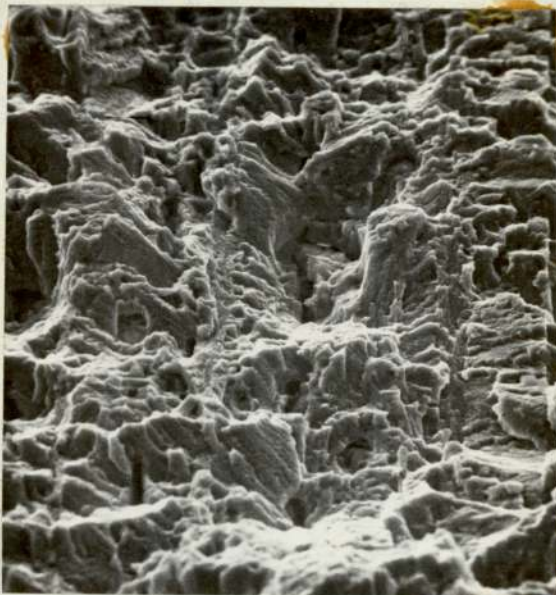
Figure 6.20   X 375

Similar to Figure 6.18 but at
$\Delta K = 22MN/m^{3/2}$, showing evidence
of void coalescence.

Figure 6.21   X 520

Corrosion fatigue ($3\frac{1}{2}\%$ NaCl) fracture
surface after sinusoidal loading at 10Hz,

$\Delta K = 7.2 \ MN/m^{3/2}$, da/dN 96 nm/cycle.

Figure 6.22   X 490

As Figure 6.21 but under square wave
loading.

$\Delta K = 7.0 \text{ MN/m}^{3/2}$, da/dN = 64nm/cycle,
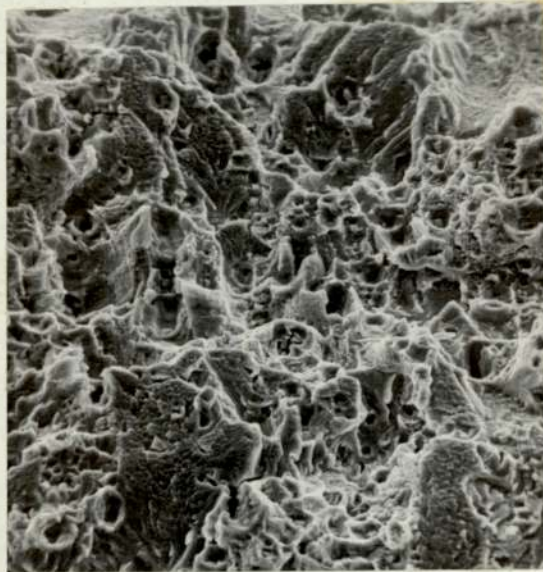
Figure 6.23   X380

Void coalescence under corrosion fatigue
at a high stress ratio (R = 0.48) and
high ΔK (= 19.2 MN/m$^{3/2}$) 10Hz sine
wave loading,

Figure 6.24   X 420

Void coalescence as in Figure 6.23
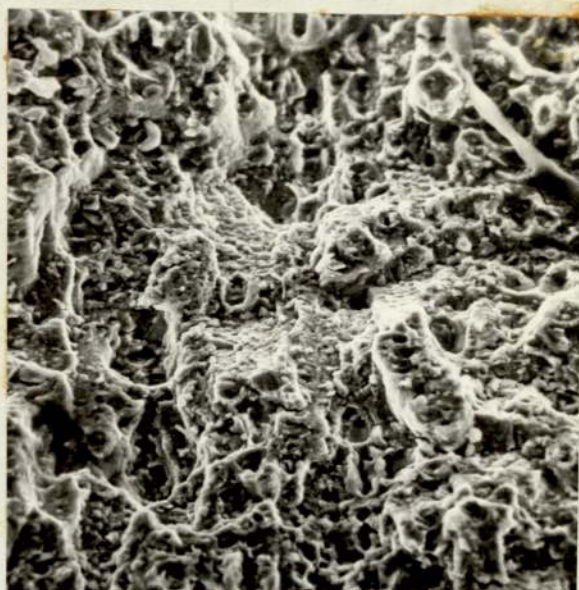but low stress ratio (R = 0.13).
$$\Delta K = 18MN/m^{3/2}$$

Figure 6.25   X 225

Stress corrosion (in $3\frac{1}{2}\%$ NaCl) fracture
surface showing gross furrowing.
$$K \approx 25MN/m^{3/2}$$

fracture mechanism in the high ΔK air fatigue tests.

A furrow type structure is present in most of the corrosion
fatigue fractures; however, furrowing appears to be more
frequent under slow K-rise time, e.g. when sine waveforms
are used. Furrowing also occurs in the high stress ratio cor-
rosion fatigue tests at low ΔK's. Furrowing was also observed
on the stress corrosion fracture surfaces where very slow
crack growth rates were measured (Figure 6.25).

Furrowing

In Al-Zn-Mg alloys annealing following the ingot casting
stage results in precipitation of transition elements present;
these are principally of the Al (Fe, Mn) type. During sub-
sequent rolling of the ingot the precipitates elongate and
result in the formation of a striated structure. Evidence for
this is shown in the micrographs of the etched surface of
Hiduminium 48 in which a fibrous structure with dark striations
in the direction of rolling is visible (Figures 5.23, 5.24 and
5.25). If the ingot annealing temperature is high the pre-
cipitate is coarse; this results in a decrease in the
re-crystallisation inhibiting property of the transition elements
present, i.e. manganese, chromium and zirconium. This further
results in an increase in the stress corrosion susceptibility
since corrosion can then proceed in an intergranular manner.

A low temperature anneal, on the other hand, results in the
precipitation of fine particles. This gives rise to a greater
resistance to recrystallization and leads to a lowering of
stress corrosion susceptibility. The stress corrosion sus-
ceptibility arises from the fact that the precipitates are

cathodic with respect to the matrix; therefore under corrosion conditions, preferential (anodic) dissolution of the matrix occurs. The conditions lead to the occurrence of exfoliation corrosion.

Metallographic examination of the Hiduminium 48 plate has shown that the precipitates are arranged in a planar manner. The crack orientations used in the stress corrosion and fatigue corrosion tests are, however, at right angles to the precipitate planes. Therefore the stress corrosion susceptible path, or rather, exfoliation corrosion path, was not tested. For this reason low stress corrosion crack growth rates are obtained in this alloy. The furrowing present on the stress corrosion and fatigue corrosion fracture surfaces therefore represent a form of stress corrosion down alóng the precipitates. The orientation of the precipitates, hence the furrows, are at right angles to the fracture plane. Therefore corrosion in this direction does not contribute to the fatigue or stress corrosion crack growth rate, but rather retards growth by effectively blunting the crack tip. The short transverse direction appears to be very susceptible to environmental influence while the longitudinal and transverse directions do not.

Fracture mechanisms in the HAZ

The two HAZ regions generally show similar fracture surface features as the parent material. However at low ΔK's, between 6 and $8MN/m^{3/2}$, and low stress ratio both HAZ regions exhibit unusual behaviour in that the crack growth rates do

not increase steadily with increase in ΔK, but show a
peculiar dip in the curve (Figure 5.3, 5.4, 5.12 and 5.13). A
similar effect has been observed in an aluminium alloy by
Mukherjee[114] and this was termed 'delayed retardation', but
this was noted to occur at about 10MN/m$^{3/2}$. Similar dips in
the da/dN/ΔK curve have been observed by El Soudani and Pelloux[70]
but at a much higher ΔK, i.e. 18MN/m$^{3/2}$. In this case
the dip was related to an increase in the amount of micro-void
coalescence occurring on the fracture surface. For the present
HAZ tests, fracture surfaces at low ΔK do not exhibit any
micro-void coalescence but only evidence of step-wise growth
and changes in micro fracture plane orientation (Figure 6.26).
At similar ΔK's, but at a higher stress ratio, R being
increased from 0.13 to 0.48, no such undulations in fracture
surface occur (Figure 6.28) and the crack growth rate continuously
increases with increase in ΔK, (Figure 5.3). Therefore the low
stress ratio fracture surface shows that the crack front must

have changed plane many times before more stable conditions
were attained and crack growth occurred more uniformly. The
crack growth rates measured are extremely low, 0.5 to 1nm/cycle
for the 21140XX material, and are the same order of magnitude
as the aluminium lattice spacing, (2.86 $\overset{o}{A}$, i.e. 0.286nm).
Therefore crack growth would be extremely sensitive to changes
in microstructure and some form of grain orientation control as
proposed by Robinson and Beevers[75] may be occurring. In this
mechanism crack extension is controlled by the orientation of
grains when the reversed plastic zone size is less than the
grain size. For 21140XX material at ΔK = 7.1MN/m$^{3/2}$ the

reversed plastic zone diameter ($2r_p$) is 0.066mm. while the sizes of the undulations on the fracture surface shown in Figure 6.26 are about 0.07mm. Therefore some dependency of microstructure on fatigue ~~en~~ crack growth is implied.

Striations in the form of step-wise growth are apparent in both air and salt water environments at low stress ratios (Figures 6.26 and 6.27). However on increasing the stress ratio from 0.13 to 0.48 the prominence of the step-wise growth mechanism decreases in both environments (Figures 6.28 and 6.29). Apart from promoting the cleavage-like fracture of step-wise growth the salt water environment also promotes furrowing, Figures 6.27 and 6.29. It will be recalled that furrowing was a result of a corrosion mechanism occurring along the inclusion stringer/matrix interface at right angles to the plane of fracture.

Figures ~~Feirues~~ 6.30 and 6.21 show that in both environments at high ΔK's a change in the fracture mode to one of microvoid coalescence takes place. This mechanism is associated with high ΔK's of region 2 in the crack growth rate/ΔK curve. This is the same fracture mechanism as observed in the parent material.

The harder region of the HAZ, as tested by the 21070XX series of specimens, show fracture surfaces similar to the 21140XX series, Figures 6.32 - 6.35. Although the dip in the air da/dN/ΔK curve in Region 1 growth is less prominent than in the soft HAZ, the fracture mechanism is similar since fracture at right angles to the fracture plane takes place, Figures 6.32 and 6.34. At high ΔK's void coalescence again occurs

- 115 -

but in some regions crack growth is by a ductile striation mechanism. Measurement of these striation spacings show them to be equivalent to the cyclic fatigue crack growth increment (Figure 6.33). This behaviour contrasts with that observed in the parent material where at similar ΔK's the micro striation mode crack growth rate was less than the overall macro crack growth rate.

In the salt water environment at low ΔK (R = 0.13) there is no evidence of furrowing, Figure 6.34. The reason for this is not clear, but it could be a result of crack growth through an inclusion depleted region of the material. A further factor could be the presence of corrosion product covering any furrows. At a similar ΔK but higher stress ratio (R = 0.48) furrows are once again evident (Figure 6.35). An increase in ΔK to 21.3 $MN/m^{3/2}$ results in the occurrence of a microvoid coalescence mode of fracture, Figure 6.36. Brittle striations are also evident but their spacing indicates a micro crack growth rate of over twice the observed macro crack growth rate. This is evidence showing that two competing crack growth mechanisms are taking place: the microvoid coalescence mechanism tending to hold up crack propagation and the brittle striation mechanism tending to accelerate growth. The observed crack growth rate is the sum of these two mechanisms.

The effect of stress ratio

Although the influence of stress ratio on the corrosion fatigue behaviour of the two HAZ materials is apparent at low and medium values of ΔK, at high ΔK the high and low stress

Figure 6.26   X 195

Fracture surface of soft HAZ (2114058) in an
air environment showing stepwise growth and
changes in fracture plane. R = 0.13,
$\Delta K = 7.1$ MN/m$^{3/2}$, da/dN = 0.8nm/cycle.

Figure 6.27   X 170

As Figure 6.26 but fatigue in $3\frac{1}{2}\%$ NaCl
and cycling at 10Hz.
$\Delta K = 8.3$ MN/m$^{3/2}$, da/dN = 10nm/cycle.

Figure 6.28   X 490

Similar to Figure 6.26 but at a higher
stress ratio. R = 0.48,

$\Delta K = 7MN/m^{3/2}$, da/dN = 9.2nm/cycle,

Figure 6.29   X 490

Furrowing under corrosion $(3\frac{1}{2}\%$ NaCl) fatigue
in soft HAZ (2114069), R = 0.48.

$\Delta K = 7.6 \ MN/m^{3/2}$

Figure 6.30   X 375

Microvoid coalescence in soft HAZ (2114069)
at high ΔK (20MN/m$^{3/2}$) in $3\frac{1}{2}\%$ NaCl, R=0.48.

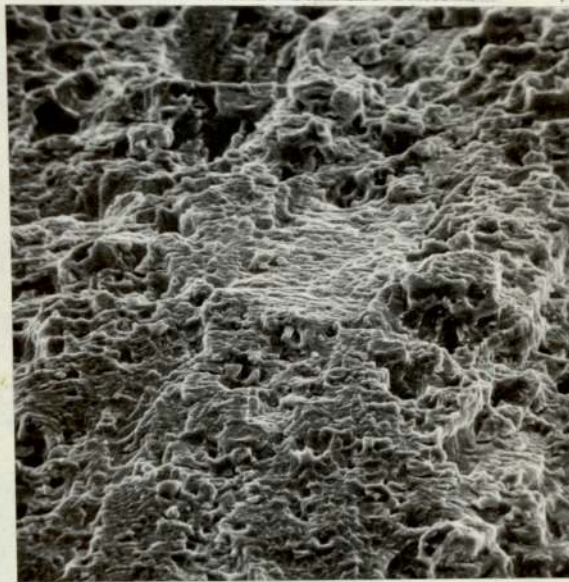Figure 6.31   X 375

Similar to Figure 6.30 (2114067) but
in an air environment.

$\Delta K = 21$ MN/m$^{3/2}$,   R = 0.48.

Figure 6.32　　　　　　　　　X 450

Fatigue fracture of hard HAZ (2107081)
at low ΔK ($= 7MN/m^{3/2}$) in an air
environment, R = 0.13.
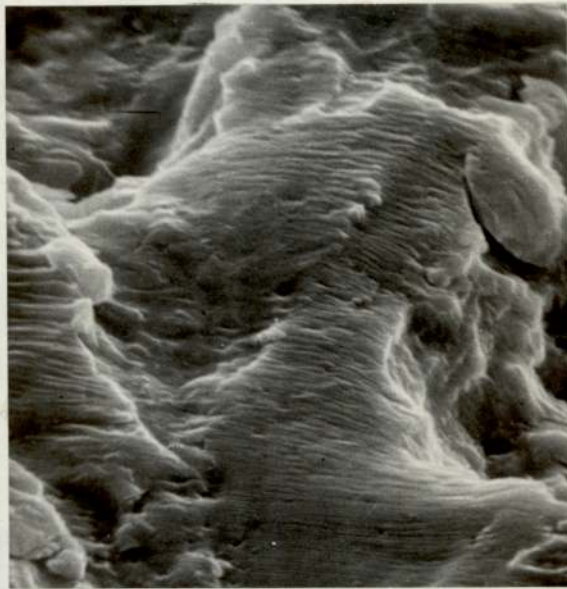
Figure 6.33　　　　　　　　　X 3800

Ductile striation formation in hard
HAZ, as Figure 6.32 but at
$\Delta K = 24MN/m^{3/2}$.
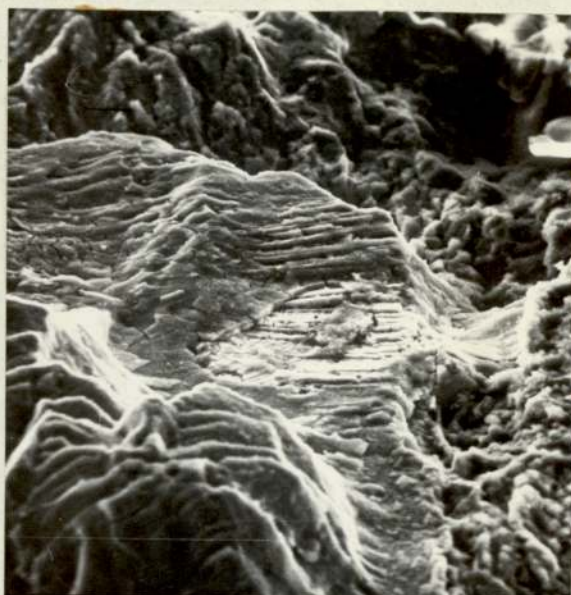
Figure 6.34   X 470

Stepwise growth in hard HAZ (2107085)
in $3\frac{1}{2}\%$ NaCl at 10Hz. R = 0.13,
$\Delta K = 7.4MN/m^{3/2}$.

Figure 6.35   X 450

Slight furrowing in hard HAZ (2007076)
in $3\frac{1}{2}\%$ NaCl at 10Hz. R = 0.48,
$\Delta K = 7.7MN/m^{3/2}$.

Figure 6.36   X 390

Microvoid coalescence in hard HAZ
(2107076) together with brittle
striations (spacing $\simeq$ 2000nm) in $3\frac{1}{2}$%NaCl,
R = 0.48, ΔK = 21.3, da/dN = 600nm/cycle.

ratio curves merge together. Thus the influence of mean stress on crack extension is reduced. This also indicates that crack extension cannot be occurring by a stress corrosion mechanism.
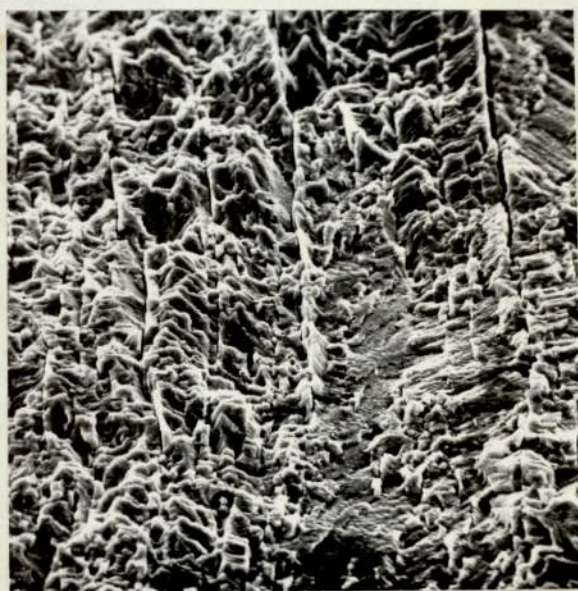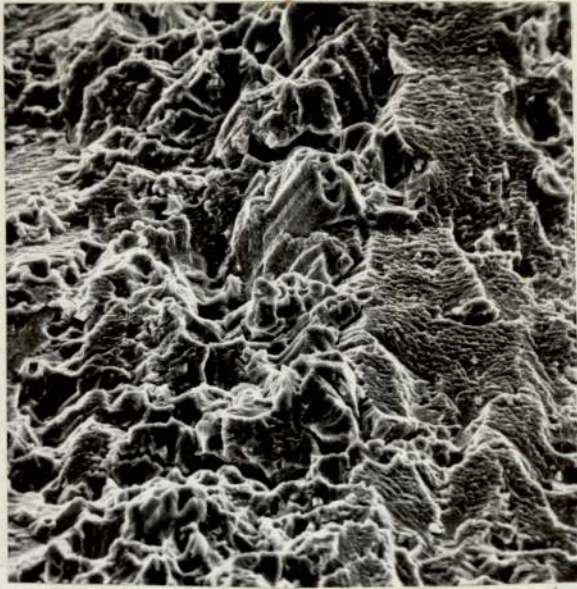
Since the value of the Q factor proved to be successful in normalizing the crack growth rates for different stress ratios its use in the present circumstances can be adopted to separate the observed crack growth into contributions from the mechanical and environmental components. The re-interpretation of the data in terms of Q (i.e. $\frac{\Delta K}{Kc - Kmin}$) is given in Figures 6.37, 6.38 and 6.39. These graphs have been plotted directly from the average crack growth rate from data given in Figures 5.5, 5.6 and 5.7. Good correlation between high and low stress ratios is obtained, in both HAZ and parent material, up to the transition where the high and low stress ratio curves merge on the normal ΔK plot. However the most important factor shown by using Q, in the region below transition, is that the environmental influence is independent of the size of the stress ratio. In other words the environmental component of corrosion fatigue depends only on ΔK. This pattern of behaviour is common to both regions of the HAZ investigated and also to the parent material. Therefore the stress ratio only influences the purely mechanical component of fatigue crack propagation while the salt water environmental influence is constant. If part of the fatigue cycle were above K_{Iscc} then crack growth would be highly dependent on stress ratio, cf. Wei-Landes hypothesis[81].
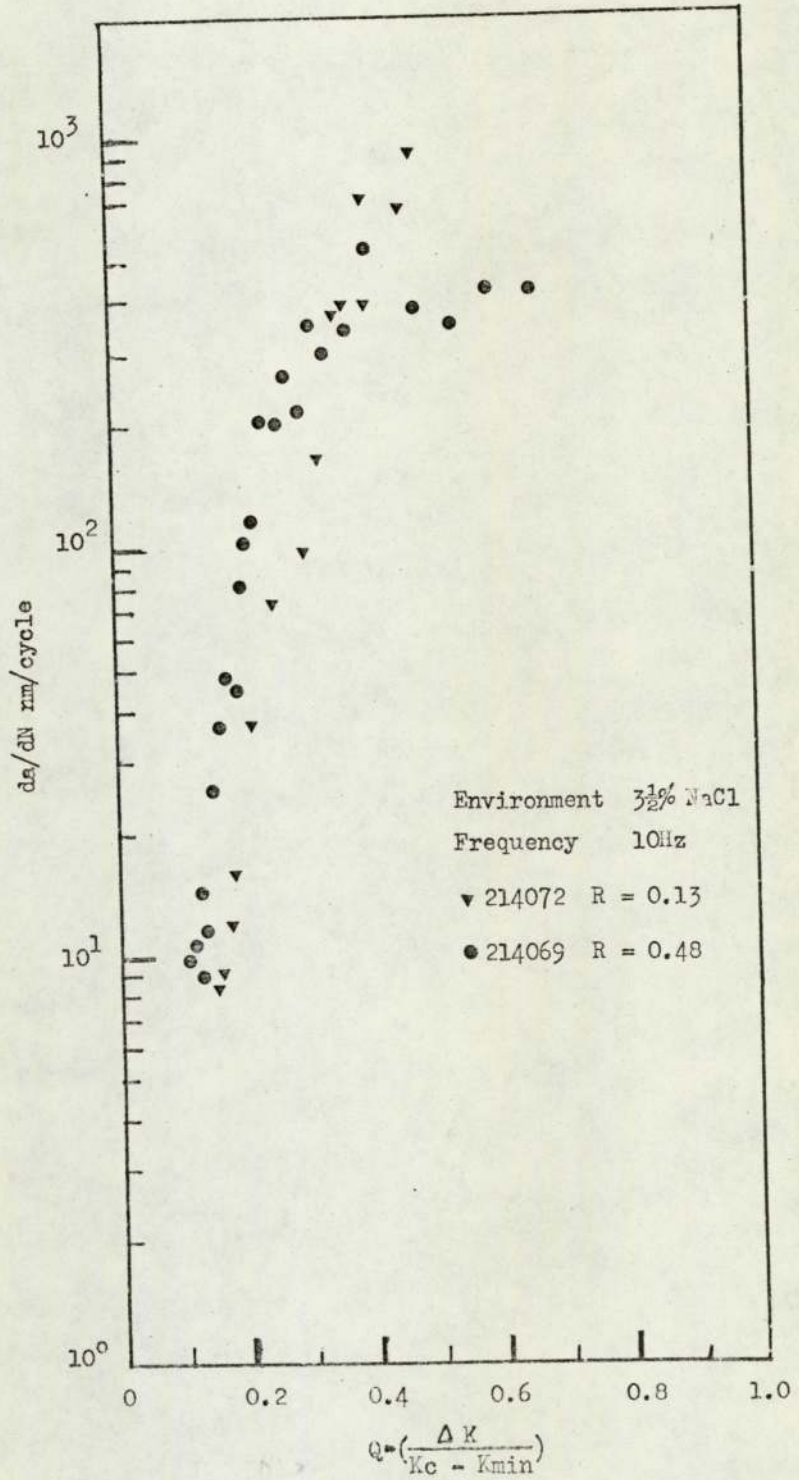
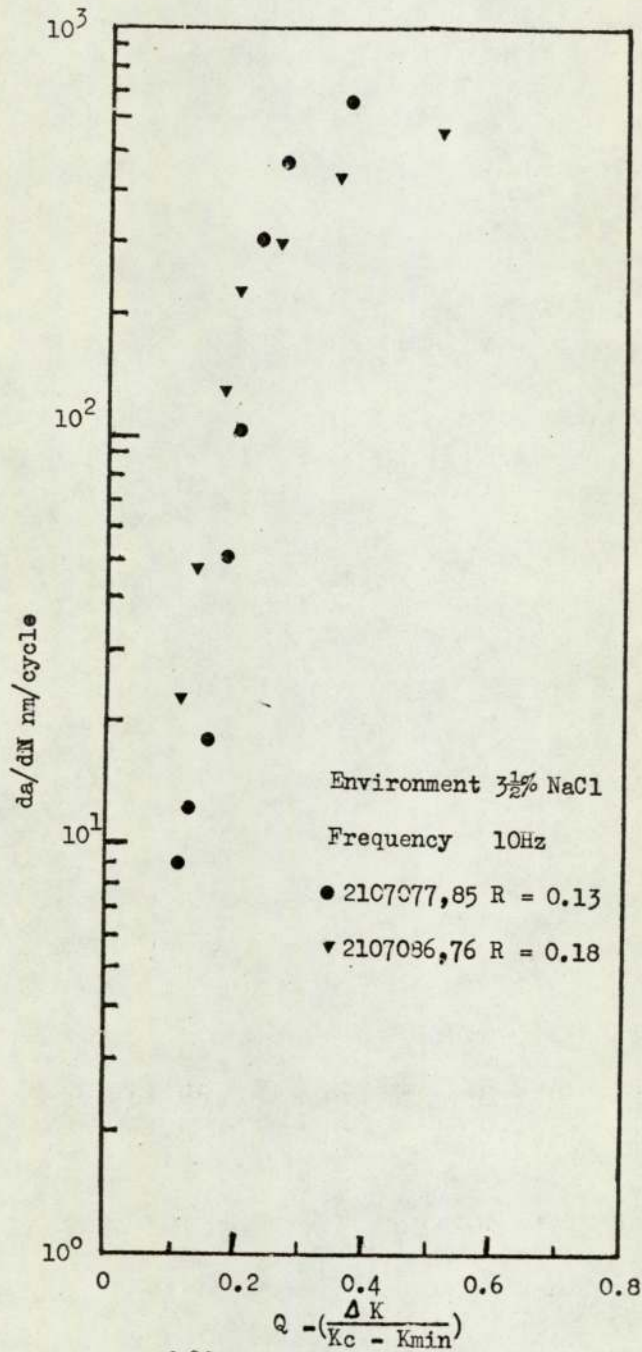Fig. 6.37 Crack propagation in salt water as a function of Q in the soft HAZ

Fig. 6.38 Crack propagation in salt water
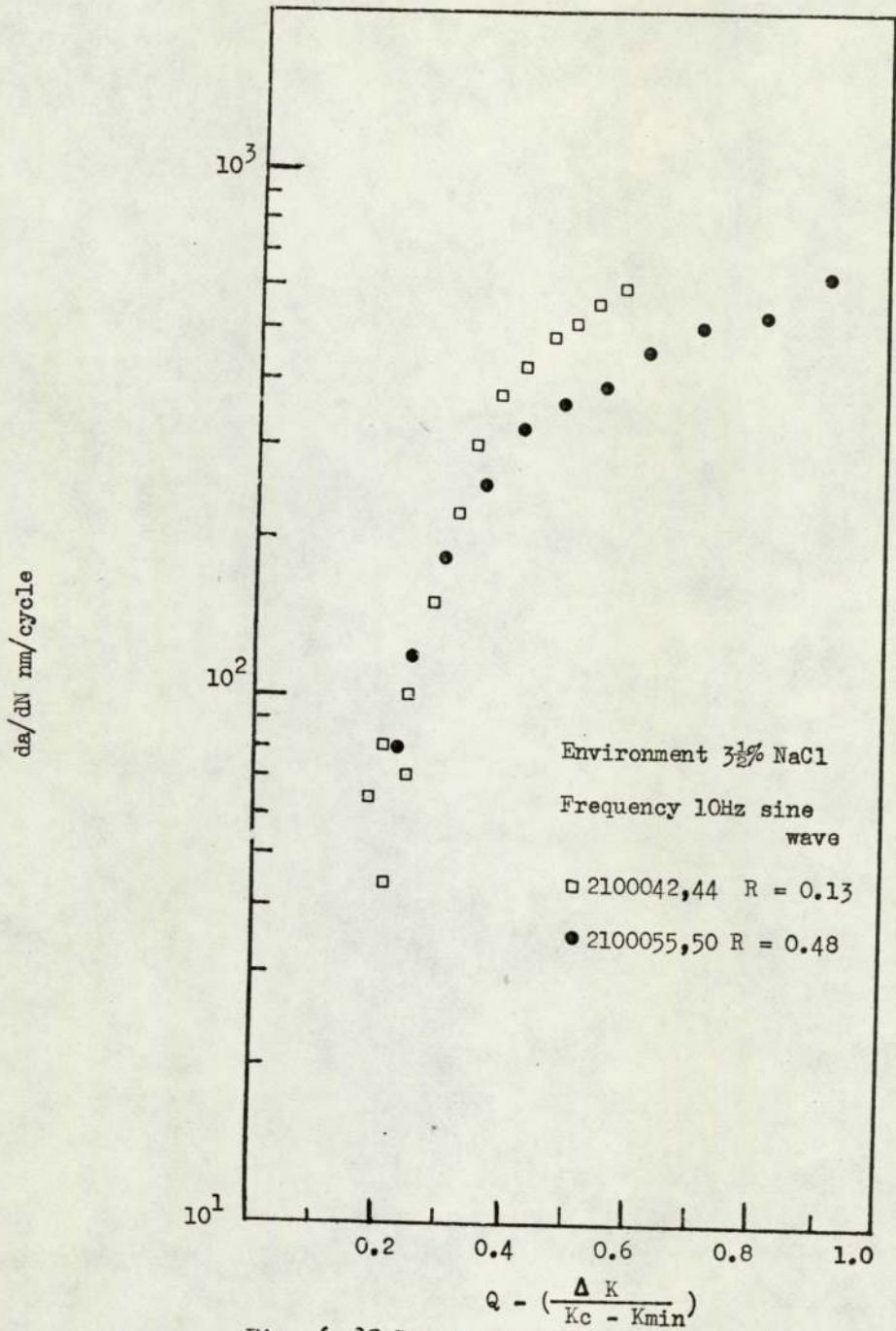as a function of Q in the hard HAZ

Fig. 6.39 Crack propagation in salt water as a function of Q in the parent material

Previously using the conventional ΔK plots of the crack growth data the precise dependancy of corrosive environment effects on stress ratio could not be determined, the main reason for this being that the dependancy of fatigue crack propagation on stress ratio in an ~~inert,~~ air environment could not be rationalized. Therefore in a corrosive environment the separation of stress ratio and corrosion fatigue influence was not possible. However the use of the Q factor has shown that stress ratio effects can be normalized and hence allowed the separation of environmental and mechanical components of fatigue.

Use of fatigue data in design

Although a number of variables affecting fatigue crack growth have been discussed, their significance with respect to engineering design is not the same. The most important variables affecting fatigue crack propagation have been shown to be, apart from stress intensity range, material fracture toughness, stress ratio and environment. The influence of testing variables such as frequency and waveshape, under corrosive conditions, are relatively minor, especially in the two regions of the heat affected zone investigated. Of the three environmental conditions investigated, air, water and salt water, the latter was found to have the greatest influence on crack growth rate, while pure water environments had relatively little.

Even though crack propagation is, primarily, dependent on ΔK, for a given material, the influence of stress ratio could only be accounted for by using the factor Q ($\Delta K/Kc - Kmax$).

The use of this factor enables the number of parameters used to describe crack propagation in a welded structure to be reduced to a single equation, since both material toughness of the parent material and the HAZ and stress ratio effects are taken into account. This simplifies the design of structures against fatigue failure.

As an example of how the Q factor concept can be used in a design situation the growth of defects in a welded structure is considered. For the purposes of the exercise the structure will be regarded as two flat plates of Hiduminium 48 butt welded together, in which the excess metal from the weld has been machined off. The plate is loaded transverse to the weld in tension; however it is also subject to a fatigue load.

The design static working stress is $65MN/m^2$ whilst superimposed on this is a fatigue loading of $\pm 70MN/m^2$, i.e. a maximum stress of $135MN/m^2$. In CP118:1969[115] the design stresses and lives for aluminium structures are recommended. The weld considered in this exercise is classified as a Class 2 weld. For the stress conditions used the life of such a structure is given as 2×10^6 cycles. We now consider the influence of a marine environment on the life of a structure in which there are pre-existing defects in the weldment and parent material. If inspection by non-destructive testing methods has discovered defects 2mm. deep and 10mm. long in the parent material and HAZ, then knowing the stressing conditions and the fatigue characteristics of the material, the growth of these defects can be calculated. For an infinite plate containing a through

thickness defect the stress intensity at the crack tip is
given by:

$$K = \sigma_w \sqrt{\pi a} \qquad (1)$$

However for a plate containing a semi-elliptical surface defect
the expression is modified to the following:

$$K = \frac{Mp \; Ms \; \sigma_w \sqrt{\pi a}}{\phi} \qquad (2)$$

where Ms is a magnification factor taking into account the
increase in K due to opening of the defect. Mp is the crack
tip plasticity correction factor which increases K by effectively
increasing the crack length. In fatigue this factor is small
and is usually neglected. ϕ is an elliptical integral which
takes into account flaw shape.

In the fatigue situation equation (2), neglecting the
influence of plasticity, becomes:

$$\Delta K = \frac{Ms}{\phi} \Delta \sigma_w \sqrt{\pi a} \qquad (3)$$

Fatigue crack growth rate is given by:

$$da/dN = A \; (Q)^B$$

where $\quad Q = \dfrac{\Delta K}{Kc - Kmin} \qquad (4)$

Assuming that the flaw shape does not change significantly
with crack growth, Equation 4 can be integrated to obtain the
number of cycles required for a defect to grow from a detectable
size to a critical size for fast fracture to occur, i.e. the
life of the structure. Since the lowest toughness region is
the parent material it is this region which controls the
integrity of the structure. Using equation 2 the critical flaw

- 120 -

size can be calculated from the fracture toughness and
maximum stress in the fatigue cycle, i.e.

$$K_{1c} = 30MN/m^{3/2}$$

$$\sigma_{max} \text{ in fatigue} = 135MN/m^2 = \sigma_w$$

Ratio of depth to length of the semi-elliptical defect,
$a/2b = 0.2$

then from (2)

$$a \text{ crit} = \frac{\phi^2}{Mp^2 \ Ms^2 \ \pi} \left[\frac{K_{1c}}{\sigma_w}\right]^2 \tag{5}$$

a crit = 17mm.

The number of cycles for the defect to grow from 2mm. to 17mm.
in the parent material and HAZ can now be calculated. It should
be noted that 17mm. is not the critical defect size for the HAZ
since the toughness of this region is very much higher than
the parent material. However, for comparison purposes the
growth of defects in this region will be calculated.

The integration of equation (4) can be made using computer
procedures, but a graphical integration method can also be
used. In conjunction with the relationships between Q and
crack growth rate and Q and ΔK, Figures 6.37, 6.38 and 6.39
respectively, a graphical integration is carried out by cal-
culating ΔK, using equation (3), over small intervals of crack
length increments from an initial to a critical crack length.
Using figure 6.4, the ΔK's are converted to Q and from the
relationship between Q and crack growth rate (Figures 6.37,
6.38 and 6.39) crack growth is obtained. The number of cycles
for growth over chosen crack length intervals is calculated

from the average crack growth rate over that interval. Finally, fatigue life is given by the summation of the cycles. This method is illustrated in Table 6.4. By repeating these calculations using data for the soft and hard HAZ the number of cycles required for a defect to grow to the critical size for the parent material can be found, Table 6.5. The resulting crack length versus cycle curves are shown in Figure 6.40. The integration has been terminated at 14mm. since above this length the crack propagation rate in the parent material is very fast and does not significantly influence life.

A further crack growth curve for the parent material in an air environment is given in Figure 6.40. This contrasts with the deleterious influence of the salt water environment on the parent material.

These results clearly show that the fatigue life of the structure is controlled by the behaviour of the parent material. It is important therefore that the size of defects present in a structure are known in order that premature failure is prevented. Figure 6.40 shows that even in air the life of the structure, calculated using recommended design methods, i.e. CP117:1969, can be reduced by over an order of magnitude, is sufficiently large defects are present.

In the vast majority of welded structures the weld profiles are not dressed to remove the excess metal from the weld bead. Under such situations the region of the weld toe has to be considered as a possible site of fatigue crack initiation. (For the behaviour of fatigue in the design of welded structures the reader is referred elsewhere (ref.118)). Factors such as

undercutting around the toe can further magnify the stress concentration factor so that fatigue crack initiation can readily occur in a small number of cycles. The presence of tensile weld residual stresses will not only help to promote initiation but will also aid propagation by effectively increasing the stress ratio. Entrapment of corrosive environments at the weld toe or undercut region will exacerbate both the initiation and propagation stages. The influence of the stress concentration factors diminishes rapidly as the crack grows through the plate thickness away from its initiation site. This results in a fall in the mean stress intensity factor at the crack which leads to a reduction in crack propagation rate.

All these factors reduce the fatigue initiation time so that the life of a welded structure will be controlled mainly by the rate of crack propagation. Therefore the crack propagation results described are valid for the analysis of crack growth in real welded structures. The technique could be further refined with knowledge of both the stress concentration gradient associated with the weld toe, and the manner in which the crack profile changes during growth.

Table 6.4

Calculation of fatigue life for parent

material in salt water (21000XX series)

R = 0.48

á mm.	ΔK MN/m$^{3/2}$	Q	da/dN mm/cycle	da/dN average mm/cycle	Δa mm.	ΔN cycles	ΣN cycles
2	5.28	0.204	6.1×10^{-5}	–	–	–	0
3	6.50	0.270	1.3×10^{-4}	9.3×10^{-5}	1	10,800	10,800
4	7.46	0.322	2.3×10^{-4}	1.8×10^{-4}	1	5,600	16,400
6	9.15	0.420	3.3×10^{-4}	2.8×10^{-4}	2	7,100	23,500
8	10.55	0.510	4.2×10^{-4}	3.8×10^{-4}	2	5,400	28,900
10	11.88	0.610	5.6×10^{-4}	4.9×10^{-4}	2	4,100	33,000
12	12.94	0.705	7.3×10^{-4}	6.5×10^{-4}	2	3,100	36,100
14	14.00	0.805	9.5×10^{-4}	8.4×10^{-4}	2	2,300	38,400

Note lnm = 10^{-6}mm.

Table 6.5

Growth of semi-elliptical surface defects

in a salt water environment

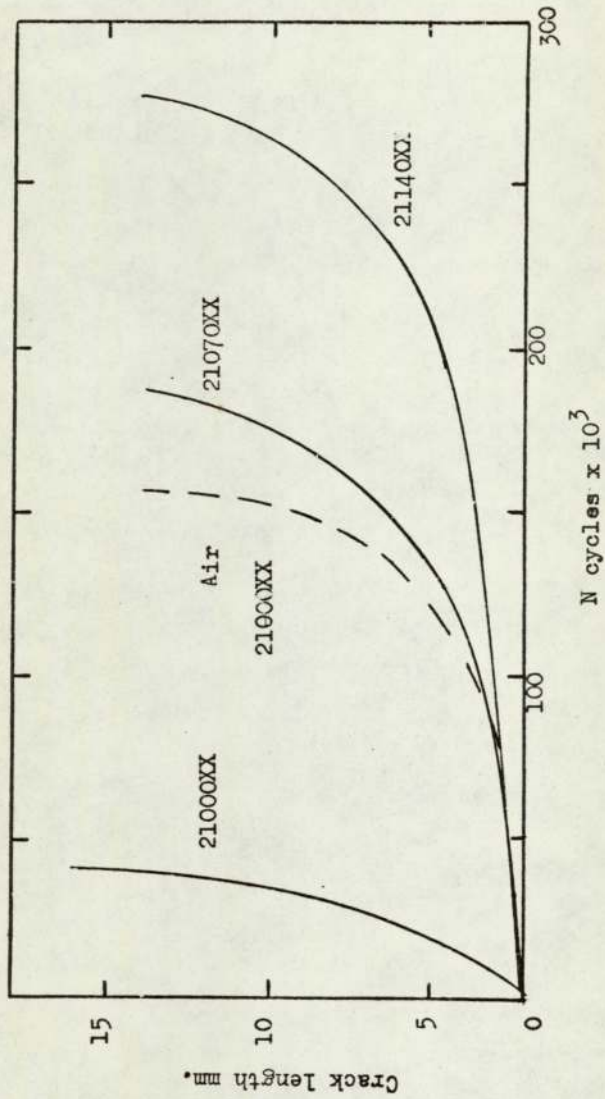| Specimen	K_{Ic} $MN/m^{3/2}$	a crit mm.	Cycles to grow from 2 to 14mm.	Change in Q
21000XX (Parent material)	30	17	38,400	0.204 − 0.805
21070XX ('Hard' HAZ)	58	65	187,000	0.100 − 0.280
21140XX ('Soft' HAZ)	52	52	276,800	0.110 − 0.355

Fig. 6 .40 Corrosion fatigue ($3\frac{1}{2}\%$ NaCl) crack growth

characteristics of semi elliptical surface defects in the

HAZ and parent material

7. CONCLUDING REMARKS

The present investigation into the corrosion fatigue behaviour of Hiduminium 48 has shown the value and usefulness of characterizing crack growth with the amplitude of stress intensity factor (ΔK). However this was possible only when constant load amplitude conditions were used. The influence of load shedding showed that load interaction effects modified the relationship between ΔK and crack growth rate.

Generally the crack growth rate/ΔK relationship was not linear, but divided into two regions in which the position of the transition was related to yield strength and environment. Under corrosion fatigue conditions in simple environments it was found that ionized water did not significantly influence crack growth. The greatest influence resulted from the presence of the chloride ion in salt water environments. Variations in frequency of cycling, from 1Hz to 120Hz, and also changes in wave form, from triangular to square waves, although not affecting air fatigue crack growth did affect the corrosion fatigue behaviour. The effect of all these loading parameters could however be explained in terms of the time for the stress intensity factor (K) to rise from its minimum to its maximum value within a fatigue cycle. It was found that the faster the K-rise time became, the smaller was the influence of the environment on crack growth rate.

The time spent at maximum load during the fatigue cycle was not an important factor since crack growth due to stress corrosion was very small in comparison with the increase in crack growth resulting from corrosion fatigue.

The influence of welding on the parent material properties was investigated. In the heat affected zone (HAZ) a reduction in strength occurred and two distinct regions were identified: one close to the weld fusion boundary where age hardening occurred after welding and the second adjacent to the first where no significant age hardening occurred. In both these regions crack propagation rate was reduced by about one order of magnitude compared with the parent material. The reduction in crack growth was not caused by compressive stresses in the HAZ but was related to the fracture toughness of the region. Since valid plane strain fracture toughness could not be measured in the region an estimate was derived from equivalent energy methods. The influence of stress ratio in both parent material and HAZ could not be accounted for by relationships proposed by Forman and Pearson. However by using the ratio of Kmax-Kmin to Kc-Kmin (Q), both the influence of stress ratio and material toughness on crack growth rate could be normalized to one curve.

Use of the Q concept allowed the environmental component of fatigue crack growth to be separated from the purely mechanical component of fatigue. It was found that this environmental component was substantially independent of stress ratio.

The Q concept also proved to be a useful design parameter in assessing the growth of fatigue cracks in a welded structure. The mechanism of fatigue crack growth was mainly dependent on ΔK, but stress ratio also had an influence at low ΔK's. At

low ΔK propagation by step wise growth occurred and this mechanism became significant in salt water environments.

Crack growth was controlled by a ductile striation mechanism only at medium values of ΔK when the striation spacings were equivalent to the observed crack growth rate. At low ΔK striation spacings were equivalent to the crack propagation rates greater than the macro growth rate, while at high ΔK's they were less than the macro crack growth rate. At high ΔK's with high and low stress ratios and in both the parent material and HAZ, the primary crack growth mechanism was by micro void coalescence.

In salt water at low ΔK's furrowing of the fracture surface occurred, but this did not accelerate fatigue crack growth. Furrowing was caused by a corrosion mechanism occurring at the interface between the matrix and precipitate rich areas parallel to the direction of crack propagation.

Appendix 1a

Calculation of the equivalent energy stress intensity factor (K*)
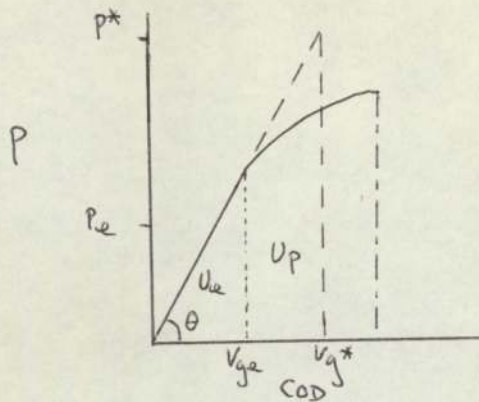
An estimate of the fracture toughness of a material having a load/clip gauge opening displacement relationship shown in the above figure, in which yielding before fracture occurs can be made by calculating the work to fracture. The work to fracture consists of the elastic and plastic energy (Ue and Up) i.e. the area under the load deflection curve. However since COD is proportional to deflection, the load-COD curve can be used directly. (This relationship is derived in Appendix 1b). The actual work to fracture is equated to the equivalent elastic work to fracture, i.e. the area under the equivalent elastic load P*. P* is calculated in the following way:

Ue + Up is proportional to the area under the curve, A.

A = A*, the area under the equivalent linear elastic

energy curve

1) $\therefore$ Ue + Up = k'A = k'A*

Ue' = k'Ae $\quad \therefore$ Ae = area under elastic part of the curve

k' = constant of proportionality

2) $\Delta* = $ Vg* k'' From appendix 1b

Δe = Vge k''

3) Substituting 2 into 3

$$\tan \theta = \frac{Pe}{Vge} = \frac{P*}{Vg*}$$

$$\therefore \quad \frac{Pe \; k''}{\Delta e} = \frac{P* \; k''}{\Delta *}$$

4) $\therefore \quad P* = \dfrac{\Delta * \; Pe}{\Delta e}$

5) $\quad Ue + Up = \frac{1}{2} P* \; \Delta *$ and $Ue' = \frac{1}{2} Pe \; \Delta e$

Substituting for Δ in 4 from 5:

6) $\quad (P*)^2 = \dfrac{(Ue + Up) \; Pe^2}{Ue'}$

Substituting for U from 1 into 6:

7) $\quad P* = Pe \sqrt{\dfrac{A}{Ae}}$

$$K = \frac{YP}{Bw^{\frac{1}{2}}}$$

$$\therefore \quad K* = \frac{Y \; P*}{Bw^{\frac{1}{2}}}$$

Appendix 1b

Calculation of centre point deflection from COD
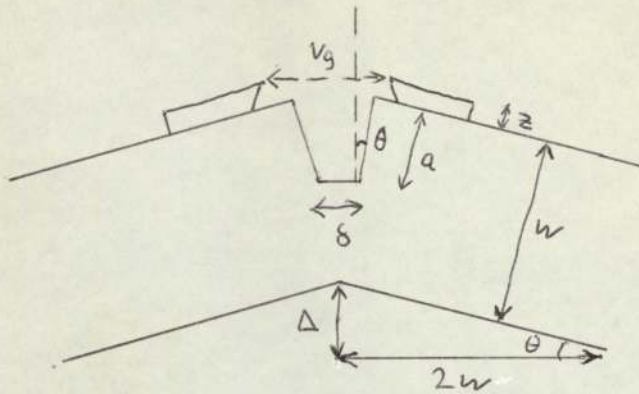
The deflection (Δ) of a rectangular section edge notch specimen under three point loading can be calculated from measurements of the crack opening displacement at the mouth of the notch. The crack tip opening displacement, δ, can also be calculated from Vg using the relationship given in DD19.[105].

    a = crack length

    z = high of knife edges

    W = specimen width

    2W = half span

$$\tan \theta = \Delta/2W$$

$$\sin \theta = \frac{(Vg/2 - \delta/2)}{a + z}$$

For small deflections $\tan \theta \simeq \sin \theta$

$$\therefore \quad \Delta = \frac{W}{a+z} (Vg - \delta)$$

Appendix 2

Determination of crack length of beam loaded under 3 point

loading from deflection.

    The deflection of a centrally cracked beam loaded under
three point bending is determined by considering the separate
contribution due to (i) deflection of beam without a crack
and (ii) deflection due to the notch.

Deflection of unnotched beam:

1) $\quad\quad \Delta_o = \dfrac{PL^3}{EI\ 48}$

2) Compliance, $Co = \Delta o/P$

3) $\therefore$ from equations 1 and 2:

$$Co = \dfrac{L^3}{EI\ 48}$$

For notched beam the compliance, C, is given in terms of the
strain energy release rate, G.

4) $\quad\quad G = \dfrac{P^2}{2B}\ \dfrac{dc}{da}$

5) $\quad\quad K^2 = EG/(1 - v^2)$

6) $\therefore\ K^2 = \dfrac{E}{(1 + v^2)}\ \dfrac{P^2}{2B}\ \dfrac{dc}{da}$

7) $\quad\quad K = \dfrac{Y\ 6\ Ma^{\frac{1}{2}}}{B\ W^2}$

8) $\quad\quad M = PL/4$

Squaring equation (7), equating to equation 6 and also

substituting for M (equation (8)), the compliance function

Y is given by:

$$9) \qquad Y = \sqrt{\frac{2}{9} \frac{EW^4 B}{L^2} \frac{1}{(1-v^2)da} \frac{dc}{} \frac{1}{a}}$$

10)

$$Let \quad F = \frac{2\ EW^4 B}{9\ L^2\ (1 - v^2)}$$

and substituting into equation (9):

$$11) \qquad \therefore\ Y^2 = F \frac{dc}{da} \frac{1}{a}$$

Integrating equation (11) with respect to a and c from zero

crack length (when compliance =Co, equation (3)) to some

specific length af and compliance Cf.

$$12) \qquad \int_{a = o}^{a = af} a\ Y^2\ da = F \int_{Co}^{Cf} dc$$

Y is a fourth degree polynomial in a/W. Let the result from

integrating the polynomial be X. Then equation (12) becomes:

$$13) \qquad X = F\ (Cf - Co)$$

$$\therefore Cf = \left(\frac{\Delta}{f}\right) + Co$$

$$14) \qquad Cf = measured\ deflection\ \Delta / P$$

$$\therefore\ equation\ (13)\ becomes:$$

$$15) \qquad \Delta = P \left[\left(\frac{X}{F}\right) + Co \right]$$

Crack length can be found by first extracting a value for crack

length, a, substituting into X function of equation 15 and carry

out a reiteration procedure to balance the right hand side
of the equation with the measured specimen deflection Δ.
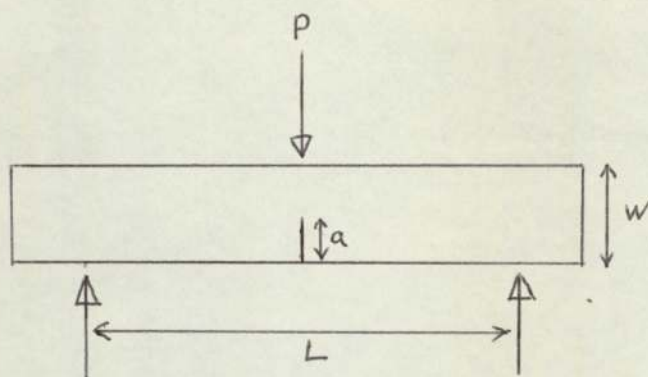
ACKNOWLEDGEMENTS

I would like to thank Dr. H.D. Williams for his assistance
in initiating the work and also Dr. J.T. Barnby for his
comments and encouragement, especially in the latter stages.
Thanks are also due to the Staff of the Metallurgy Department
for their co-operation and advice. Finally I would like to
thank my wife for her encouragement throughout the various stages
of the work.

ACKNOWLEDGEMENTS

REFERENCES

1. DONALDSON, D.R. and ANDERSON, W.E.

    Proc. Crack Propagation Symposium, Cranfield, vol. 2,

    375 (1961).

2. GRIFFITH, A.A.

    Phil. Trans Roy. Soc., vol. A-221, 163 (1920).

3. INGLIS, C.E.

    Trans. Roy. Instn. Naval Architects, vol. 60, 219 (1913).

4. IRWIN, G.R.

    Fracture Encyclopedia of Physics, Springer, Berlin,

    vol. 6, 551 (1958).

5. IRWIN, G.R.

    Jou. of Applied Mechanics, vol. 24, 361 (1957).

6. SNEDDON, I.N.

    Proc. Roy. Soc., vol. A-187, 229 (1946).

7. WESTERGAARD, H.M.

    Trans. ASME, vol. 61, A-49 (1939).

8. WILLIAMS, M.L.

    Jou. of Applied Mechanics, Trans. AMSE (1957).

9. PARIS, P.C. and SIH, G.C.

    'Fracture Toughness testing and its applications'
    ASTM STP 381, 30 (1964).

10. RICE, J.R.

    'Fatigue Crack Propagation' ASTM STP 415, 247 (1967).

11. WELLS, A.A.

    As ref. 1, 210.

12. WELLS, A.A.

    Eng. Fract. Mech., vol. 1, 3, 399 (1969).

13. SULIVAN, A.M.

    Mat. Res. and Stds., vol. 4, 20 (1964).

14. WINTERS, R.F.

    'The design and assessment of a linear compliance
    specimen for use in fatigue testing'. M. Sc. Thesis,
    Dept. of Metallurgy, Aston University (1969).

15. BROWN, W.F. and SRAWLEY, J.E.

    'Plane strain crack toughness testing of high strength
    metallic materials'. ASTM STP 410 (1966).

16. CROOKER, T.W.

    Eng. Fract. Mech., vol. 5, 35 (1973).

17. SORKIN, G., POHLER, C.H., STAVOY, A.B., and BORRIELLO F.E.

    Eng. Fract. Mech., vol. 5, 307 (1973).

18. PARIS, P.C.

    Proc. of 10th Sagamore Army Materials Research Conf.,
    Syracuse University Press, 107 (1964).

19. RICE, J.R.

    ref. 10.

20. ELBER, W.

    'Damage Tolerance in Aircraft Structures', ASTM STP 486,
    240 (1971).

21. IRVING, P.E., ROBINSON, J.L. and BEEVERS C.J.

    'Fatigue Crack Closure in Titanium and Titanium Alloys'
    Research Report, Dept. of Physical Metallurgy and Science
    of Material, University of Birmingham (1972).

22. GROSSKREUTZ, J.C.

ref. 18.

23. GROSSKRENTZ, J.C. and SHAW, G.G.

Fracture, 2nd Brighton Conf., 620 (1969).

24. PLUMBRIDGE, W.J. and RYDER, D.A.

Metals and Materials Review 136, vol. 3, 119, (1969).

25. FORSYTH, P.J.E.

ref. 1, vol. 1, 76.

26. PARIS, P.C. and ERDOGAN, T.

Jou. of Basic Eng. Trans. ASME, vol. 85, 528 (1963).

27. LIU, H.W.

Discussion paper, ref. 18.

28. MILLER, G.A.

Trans. ASM, vol. 61, 442 (1968).

29. CROOKER, T.W.

N.R.L. Report 7347.

30. FORMAN, R.G., KEARNEY, V.E. and ENGLE, R.M.

Jou. of Basic Eng., Trans. ASME, vol. 89, 459 (1967).

31. HARTMAN, A. and SCHIJVE, J.

Eng. Fract. Mech., vol. 1, 615 (1970).

32. HUDSON, C.M. and SCARDINA, J.T.

Eng. Fract. Mech., vol 1, 429 (1969).

33. DUBENSKY, R.

'Mechanical behaviour of materials', vol. 11, 175,

The Society of Material's Science, Japan (1972).

34. PEARSON, S.

Eng. Fract. Mech., vol. 4, 19 (1972).

35. WILHEM, D.P.

Ref. 10, 363.

36. NEWAN, J.C.

Ref. 10, 380.

37. SWANSON, S.R., CICCI, F. and HOPPE, W.

Ref. 10, 312.

38. HEALD, P.T., LINDLEY, T.C. and RICHARDS, C.E.

Mat. Sci. Eng., vol. 10, 235 (1972).

39. WEERTMAN, J.

Int. Jou. Fract. Mech., vol. 5, 13 (1969).

40. RICHARDS, C.E. and LINDLEY, T.C.

Eng. Fract. Mech., vol. 4, 951 (1972).

41. CHEREPANOV, G.P. and HALMANOV, H.

Eng. Fract. Mech., vol. 4, 219 (1972).

42. PARIS, P.C., BUCCI, R.J., WESSEL, E.T., CLARK, W.G. and

MAGER, T.R.

Westinghouse Research Laboratory Scientific Paper

71-1E7-FMPWR-P7 (Dec. 1971).

43. BATES, B.C and CLARK, W.G.

Trans. ASM 62, 380 (1969).

44. COOKE, R.J. and BEEVERS C.J.

'The effect of load ratio on the stresses for fatigue

crack growth in a medium carbon steel' - Research report

Dept. of Physical Metallurgy, Birmingham University.

45. FROST, N.E., HOLDEN, J. and PHILLIPS, C.E.

Ref. 1, vol 1., 166.

46. DONAHUE, R.J., CLARK H. Mc. I, ATANMO, P., KUMBLE, R. and

MCEVILY, A.J.

Int. Jou. of Fract. Mech., vol. 8, 2, 209 (1972).

47. KLESNIL, M. and LUKAS, P.

Eng. Fract. Mech., 4, 77 (1972).

48. PEARSON, S.

R.A.E. Technical Report 72236, Farnborough (Feb. 1973).

49. CLARK, W.G.

Eng. Fract. Mech., vol. 1, 385 (1968).

50. BARSOM, J.M.

"Damage Tolerance in Aircraft Structures"

ASTM STP 486 1 (1971).

51. BARSOM, J.M.

Trans. ASME Jou. of Eng. for Industry 1190 (Nov. 1971).

52. CROOKER, T.W.

Eng. Fract. Mech., vol. 5, 35 (1973).

53. DOVER, W.D.

Eng. Fract. Mech., vol. 5, 11 (1973).

54. VON EUW, E.F.J., HERTZBERG, R.W. and ROBERTS, R.

Stress analysis and growth of cracks, ASTM STP 513 230 (1972).

55. KHAIRUZZAMAN, M.

"The effects of programme loading on fatigue crack
propagation"; Ph. D. Thesis, Dept. of Metallurgy,
University of Aston (1973).

56. DOWSE, K.R. and RICHARDS, C.E.

Met. Trans., vol. 2, 599 (Feb. 1971).

57. FORSYTH, P.J.C., STUBBINGTON, C.A. and CLARK, D.

Jou. Inst. of Metals, vol. 90, 238 (1961 - 62).

58. BRADSHAW, F.J. and WHEELER, C.

Int. Jou. of Fract. Mech., vol. 5, 255 (1969).

59. KOTERAZAWA, R.

Ref. 33, 209.

60. BROEK, D.

Ref. 23, 754.

61. TOMKINS, B.

Phil. Mag., vol. 18, 1041 (1968).

62. LAIRD, C.

Ref. 10, 136.

63. MCMILLAN, J.C. and PELLOUX, R.M.N.

Ref. 10, 505.

64. PELLOUX, R.M.N.

Ref. 23, 731.

65. STUBBINGTON, C.A.

Metallurgia, vol. 68, 109 (1963).

66. FEENEY, J.H., MCMILLAN, J.C. and WEI, R.P.

Met. Trans., vol. 1, 1741 (1970).

67. PELLOUX, R.M.N.

Trans. ASM, vol. 57, 5, 11 (1964).

68. FORSYTH, P.J.E. and RYDER, D.A.

Metallurgia, 117, (1961).

69. GRIFFITHS, J.R., MOGFORD, I.L. and RICHARDS, C.E.

Metal Science Jou., vol. 5, 150 (1971).

70. EL-SOUDANI, S.M. and PELLOUX, R.M.N.

Met. Trans. vol. 4, 519 (1973).

71. CROOKER, T.W., COOLEY, L.A., LANGE, E.A. and FREED, C.N.

Trans. ASM, vol. 61, 568 (1968).

72. CLARK, W.G.

Eng. Fract. Mech., vol. 1, 385 (1968).

73. RITCHIE, R.O. and KNOTT, J.F.

"Mechanism of Fatigue crack growth in low alloy steels"

Dept. of Metallurgy, University of Cambridge, (Aug. 1972).

74. HOEPPNER, D.W.

Ref. 10, 486.

75. ROBINSON, J.L. and BEEVERS, C.J.

"The effects of load ratio, interstitial content and grain size on low stress fatigue crack propagation in α-titanium"; Research report, Dept. of Physical Met. and Science of Materials, University of Birmingham (1973).

76. ACHTER, M.R.

Scripta Met., vol. 2, 525 (1968).

77. HARTMAN, A.

Int. Jou. of Fract. Mech., vol. 1, 167 (1965).

78. WEI, R.P.

Int. Jou. of Fract. Mech., vol. 4, 633 (1970).

79. WEI, R.P.

Eng. Fract. Mech., vol. 1, 4, 633 (1970).

80. WALKER, K., PENDLEBERRY, S. and MCELWEE, R.

"Effects of environment and complex load history on fatigue life". ASTM STP 462, 234 (1970).

81. WEI, R.P. and LANDES, J.D.

Int. Jou. of Fract. Mech., vol. 5, 69 (1969).

82. BROOM, T. and NICHOLSON, A.J.

Jou. Inst. Metals, vol. 89, 183 (1960).

83. MCEVILY, A.J. and WEI, R.P.

Corrosion Fatigue: Chemistry, Mechanisms and Microstructure; University of Connecticut, Storrs, NACE 2, pp. 381 (1971).

84. GERBERICH, W.W., BIRAT, J.P. and ZACKAY, V.F.

Ref. 83, pp. 396.

85. VAN DER SLUYS, W.A.

Eng. Fract. Mech., vol. 1, 44 (April 1969).

86. BROWN, B.F.

    Materials and Res. Stas., vol. 6, 129 (1966).

87. BEACHAM, C.D. and BROWN, B.F.

    ASTM STP, 425, 66 (1967).

88. JOHNSON, H.H. and PARIS, P.C.

    Eng. Fract. Mech., vol. 1, 3 (1968).

89. WEI, R.P. and LANDES, J.D.

    Material Res. and Stds., vol. 9, 7, 25 (1969).

90. GALLAGHER, J.P.

    Jou. of Materials JMSLA, vol. 6, 4, 941 (1971).

91. PARIS, P.C., BUCCI, R.J. and LITTLE C.D.

    Stress Analysis and Growth of Cracks, Part 1, ASTM STP 513,
    196 (1972).

92. CROOKER, T.W. and LANGE, E.A.

    ASTM STP 462, 258 (1970).

93. BARSOM, J.M.

    Eng. Fract. Mech., vol. 3, 15 (1971).

94. BARSOM, J.M.

    Int. Jou. of Fract. Mech., vol. 7, 163 (1971).

95. PETTIT, D.E., HOEPPNER, D.W. and HYLER, W.S.

    ASTM STP 462, 241 (1970).

96. STOLTZ, R.E., PELLOUX R.M.

    Met. Trans., vol. 3, 2433 (1972).

97. SPEIDEL, M.O., BLACKBURN, M.S., BECK, T.R. and FEENEY, S.A.

    As ref. 83, pp. 324.

98. GARRETT, G.G.

    "The practical implications of fracture mechanisms"

    Institute of Metallurgists, 157 (March 1973).

99. KRUPP, W.E., HOEPPNER, D.W. and WALKER, E.K.
As ref. 83, pp. 468.

100. BARSOM, J.M.
As ref. 83, pp. 424.

101. HUDAK, J.J. and WEI, R.P.
As ref. 83, discussion pp. 433.

102. BRADSHAW, F.J., GUNN, N.J.F. and WHEELER, C.
R.A.E. Tech. Memo. 93 (1970) Farnborough.

103. SELINES, P.J. and PELLOUX, R.M.
Met. Trans. vol. 3, 2525 (1972).

104. "Methods for plane strain Fracture Toughness (K_{1c})
Testing"; Draft for Development, DD 3, B.S.I., (1970).

105. "Methods for Crack Opening Displacement Testing"
DD 19, B.S.I. (1972).

106. LIU, H.W. and IINO, N. as reference 23, pp. 812.

107. JACK, A.R., YELDHAM, D.E.
CEGB Report SSD/MID/R/215/70 (1970).

108. DAVIES, K.B., FEDDERSON, C.E.
Int. Jou. of Fracture, vol. 9, 116 (1973).

109. McCARTNEY, L.N., COOPER, P.
NPL Report, Mat. App. 23 (October 1972).

110. NORDMARK, G.E., KAUFMAN J.G.
Eng. Fract. Mech., vol. 4 193 (1972).

111. HEISER, F.A., HERTZBERG R.W.
Jou. of Basic Eng. Trans ASME 211 (June 1971).

112. DAWES, M.G.
Metal Constr. (February 1971).

113. MADDOX, S.J.
Metal Constr. vol. 12 (7), 285 (1970).

114.   MUKHERJEE, B.

      Int. Jou. of Fracture, vol. 8, 449 (1972).

115.   THE STRUCTURAL USE OF ALUMINIUM

      CP 118 1969 British Standards Institute

116.   TIFFANY, C.F. and MASTERS, J.N.

      As reference 9, pp. 249

117.   GILBEY, D.M. and PEARSON , S.

      Royal Aircraft Establishment Tech. Rep. 66402 (1966).

118.   GURNEY, T.R.

      Fatigue of welded structures, Cambridge University
      Press, 1968.

119.   MERKLE, J.G.

      ASTM STP 536, pp. 264   1973